DEFINITION OF FORCES ON TURBOMACHINERY ROTORS
TASK B REPORT:
DYNAMIC ANALYSIS OF ROTORS

PREPARED FOR:
GEORGE C. MARSHALL SPACE FLIGHT CENTER

UNDER
CONTRACT NAS8-34505

BY
DARA W. CHILDS

RD-2-83, 1 MAY 1983

(NASA-CR-170763) DEFINITION OF FORCES ON TURBOMACHINERY ROTORS. TASK B REPORT: DYNAMIC ANALYSIS OF ROTORS (Texas A&M Univ.) 105 p HC A06/MF A01 CSCI 21E
N83-24507
Unclas
G3/07 03690

Turbomachinery Laboratories
Mechanical Engineering Department
Texas A&M University
College Station, Texas 77843

DEFINITION OF FORCES ON TURBOMACHINERY ROTORS
TASK B REPORT:
DYNAMIC ANALYSIS OF ROTORS

prepared for:
George C. Marshall Space
Flight Center
Alabama 35812

under

CONTRACT NAS8-34505

Principal Investigator:
Dara W. Childs
Mechanical Engineering Dept.
Texas A&M University
College Station, Texas 77843

Turbomachinery Laboratories Report
RD-2-83, 1 May 1983

DEFINITION OF FORCES ON TURBOMACHINERY ROTORS
TASK B REPORT: DYNAMIC ANALYSIS OF ROTORS

List of Figures

11(c). HPOTP preburner accelerometer amplitudes (g's) in the Y-Z plane for an acceleration from 30,200 to 35,000 rpm. The dead-band clearances and the destabilizing cross-coupling coefficients are zero.

12. HPOTP synchronous bearing 2 reaction amplitudes at 30,200 rpm for the bearing clearances of Eq.(11). The initial conditions used in this simulation run were generated from an earlier zero-bearing-clearance run.

13(a). HPOTP bearing 2 reaction amplitudes (lbs) for an acceleration from 30,200 to 32,500 rpm with the bearing clearances of Eq.(11), no external bearing damping, and no destabilizing force at the main impeller.

13(b). HPOTP preburner accelerometer amplitudes (g's) in the X-Z plane for an acceleration from 30,200 to 32,500 rpm with the bearing clearances of Eq.(11), no external bearing damping, and no destabilizing force at the main impeller.

13(c). HPOTP preburner accelerometer amplitudes (g's) in the Y-Z plane for an acceleration from 30,200 to 32,500 rpm with the bearing clearances of Eq.(11), no external bearing damping, and no destabilizing force at the main impeller.

14(a). HPOTP bearing reaction 1 from the transient, nominal, nonlinear model for a simulation of 30,000 rpm running speed.

14(b). HPOTP bearing reaction 2 from the transient, nominal, nonlinear model for a simulation of 30,000 rpm running speed.

14(c). HPOTP bearing reaction 3 from the transient, nominal, nonlinear model for a simulation of 30,000 rpm running speed.

14(d). HPOTP bearing reaction 4 from the transient, nominal, nonlinear model for a simulation of 30,000 rpm running speed.

14(e). HPOTP preburner accelerometer in the X-Z plane from the transient, nominal, nonlinear model for a simulation of 30,000 rpm running speed.

14(f). HPOTP preburner accelerometer in the Y-Z plane from the transient, nominal, nonlinear model for a simulation of 30,000 rpm running speed.

14(g). HPOTP turbine accelerometer in the X-Z plane from the transient, nominal, nonlinear, model for a simulation of 30,000 rpm running speed.

14(h). HPOTP turbine accelerometer in the Y-Z plane from the transient, nominal, nonlinear, model for a simulation of 30,000 rpm running speed.

15(a). HPOTP preburner accelerometer levels in the X-Z plane from the transient, nominal, nonlinear model at 30,000 rpm for an increase in the main impeller cross-coupling coefficient by the factor 1.57.

15(b). HPOTP preburner accelerometer levels in the Y-Z plane from the transient, nominal, nonlinear model at 30,000 rpm for an increase in the main impeller cross-coupling coefficient by the factor 1.57.

List of Tables

I. INTRODUCTION

The rotordynamic characteristics of turbomachinery are known to depend on the forces developed due to relative motion between the rotor and the housing. For example, the critical-speed locations generally depend on the bearing stiffnesses, seal damping influences rotor stability and bearing-reaction amplitudes near critical speeds, etc. A systematic examination of the influence of changes in the forces acting on rotors is the subject of this study. More specifically, the sensitivity of the rotordynamic characteristics to changes in rotor forces is the subject of this study and report.

Rotordynamic characteristics of the HPOTP (High Pressure Oxygen Turbopump) and HPFTP (High Pressure Fuel Turbopump) of the SSME (Space Shuttle Main Engine) are investigated in this study. Because of their markedly different rotordynamic characteristics, these units are considered to be representative of a range of possible future liquid-rocket-engine turbomachinery.

The following steps were used to examine the sensitivity of rotordynamic characteristics to changes in force parameters:

(a) A "nominal" rotordynamics model is analyzed based on best estimates of the parameters which are known to influence rotordynamic characteristics. The selection of "best estimates" is largely based on the TASK A report [1].

(b) A systematic and sequential change in the parameters which define the forces is carried out to establish the influence of these changes on the rotordynamic characteristics. The decision on the appropriate magnitude of changes to be undertaken from the nominal parameters was also largely based on [1].

The rotordynamic models used in this study resemble those employed by the author [2,3,4] and other rotordynamics investigators of the SSME turbopumps. Specifically, modal models are used to represent the structural dynamics models

of the rotor and housing. Free-free modes are used for the rotor, and the housing modes are developed from a general finite-element structural dynamics development. The forces which couple the housing and rotor depend on their relative motion and are generally modeled as linear elements. The dead-band clearances at the bearings provide the only known significant nonlinearity in the rotor-housing models.

Both linear and nonlinear analysis techniques are employed. The bearing clearances are neglected in models used for linear analysis. Linear analysis results yield (a) complex eigenvalues, which are used to predict onset speeds of instability and (b) synchronous-response due to imbalance excitation, which predict bearing reactions and housing accelerometer levels as a function of running speed. The nonlinear analysis is based on a transient time-integration approach and is only used to examine the combined effects of bearing dead-bands and fixed-direction side loads. Most of the results presented here are based on linear analysis and models.

Given that the bearings of turbopumps tend to be most vulnerable to failure due to excessive synchronous or subsynchronous vibration loads, synchronous bearing magnitudes due to imbalance are used as a relative measure of vibration quality for a given turbopump configuration. The term relative is underlined because bearing reaction predictions from linear models generally predict larger bearing loads than nonlinear models which include bearing dead-band clearances and sideloads. The second relative measure of the vibration quality of a turbopump configuration is the OSI (Onset Speed of Instability) as predicted by linear models.

The data and parameters which are required to define a rotordynamics model can be separated into those which are relatively well known, and assumed fixed, and those which are known only within limits and are to be varied. A discussion of these two types of data follows.

Specified Data

In this study, the following parameters are assumed to be known and fixed:

(a) rotor and case structural dynamic models,

(b) local radial case stiffness at bearing locations,

(c) speed-dependent stiffness and damping coefficients for the balance piston,

(d) speed-dependent hydrodynamic side load, and

(e) the imbalance distribution.

Varied Data

Data which are varied account for (a) uncertainties in force magnitudes, and (b) alternative configurations of force elements. Parameters which control the following force elements are varied:

(a) bearing stiffnesses,

(b) impeller cross-coupling forces,

(c) turbine clearance-excitation forces,

(d) liquid seals,

(e) turbine-interstage seals, and

(f) bearing "dead-band" clearances.

Appendix A provides most of the numbers required to define both the nominal and extremes for the forces to be varied.

II. ANALYSIS RESULTS FOR THE HPOTP

A. Introduction

With respect to the HPOTP, this study began as a "theoretical" investigation without any particular regard for rotordynamic problems being experienced by the HPOTP development program. However, as the study has progressed, concern has increased at MSFC and Rocketdyne over rotordynamic problems encountered with the HPOTP in achieving FPL (Full Power Level) conditions. Specifically, HPOTP units have developed subsynchronous vibration problems after sustained operation above RPL (Rated Power Level) conditions. Consequently, the scope of this study was broadened to address some aspects of the current subsynchronous vibration problems.

B. The Nominal Linear Model

The nominal linear model is based on best estimates of parameters and primarily differs from the corresponding nonlinear model in the following aspects:

(a) bearing dead-band clearances are assumed to be zero, and

(b) the linear model does not include axial motion of the rotor; hence, coupling at the balance piston is not accounted for.

The fixed data cited in Chapter I provide the basic structure of the nominal model. The remaining data used to define the nominal model are discussed below.

Bearing Stiffnesses

The four bearings are identified numerically, proceeding from the preburner impeller to the turbine. The nominal bearing stiffnesses used are

$$K_{bi} = 8.76 \times 10^7 \text{ N/m } (.5 \times 10^6 \text{ lb/in}); \; i = 1,2,...4 \qquad (1)$$

Impeller-Cross-Coupling Coefficients

Table B.11 defines the nominal coefficients.

Clearance-Excitation Forces

The nominal clearance-excitation force coefficient is based on the data of Table B.12. However, a β of 0.25 is used, which reduces the cited coefficient by a factor of four.

Seal Coefficients

The nominal rotor model accounts for the seal configurations which were in use at the outset of this study and does not account for either changes which have been made or proposed as remedies to current rotor-dynamic vibration problems. Nominal seal coefficients are provided in Table B.1. The "original" turbine interstage seal coefficients of these tables are used in the nominal model.

Damping

The nominal linear model without additional damping between the housing and rotor yields a predicted onset speed of instability at 25,810 rpm. Linear damping was added between the rotor and housing at the center of the main impeller and at the bearing supports. The damping coefficients C = 525 Ns/m (3 lb sec/in) elevated the predicted OSI to 30,430 rpm, with an associated whirl frequency of 540 Hz. This value of damping was used in the nominal linear model.

Imbalance Distribution

The imbalance distribution used in all cases consisted of the following aligned imbalances:

	Location	Magnitude
(a)	Boost Impeller	.1273 gm.cm
(b)	Main Impeller	10.18 gm.cm
(c)	Mid-turbine	12.73 gm.cm

Table 1. HPOTP imbalance distribution.

While considerable uncertainty exists concerning the particular imbalance distribution in a given turbopump, the distribution of Table 1 provides adequate excitation for the modes of interest. Appendix A provides the numbers used to define the remaining "fixed" data.

C. The Influence of Changes in Bearing Stiffnesses

Introduction

The principal direct influence of a change in bearing stiffnesses is the location of critical speeds. Results are presented in this section for the dynamic characteristics of the following configurations:

(a) nominal model,

(b) nominal model with bearing stiffneses reduced 50%,

(c) nominal model with bearing stiffnesses increased by 50%, and

(d) nominal model with a complete loss of stiffness at bearing 2.

The results presented are from a linear model which neglects bearing clearances and are useful for comparison purposes. However, as demonstated in section H of this chapter, the dead-band clearances markedly change the dynamic characteristics of the rotor with respect to stability characteristics and peak amplitudes.

Nominal Model

Figure 1 illustrates the local coordinate system used for definition of HPOTP rotor and housing motion. The frames of Figure 2 illustrate the synchronous response characteristics of the nominal model. The first and second critical speeds are at 12,500 and 32,500 rpm, respectively. The first critical speed primarily involves overhung motion of the turbine as illustrated in Figure 3. The second critical speed is a coupled housing-rotor mode similar to that of Figure 4.

By comparison to [3], the current model has fewer predicted resonant peaks in the operating range, and substantially less assymmetry between the X-Z and Y-Z plane response. Aside from the first and second critical peaks, only a few small resonant peaks are evident in the operating speed range. The fact that the peaks at the first and second critical speeds are not split is an additional indication of symmetry in the housing modes.

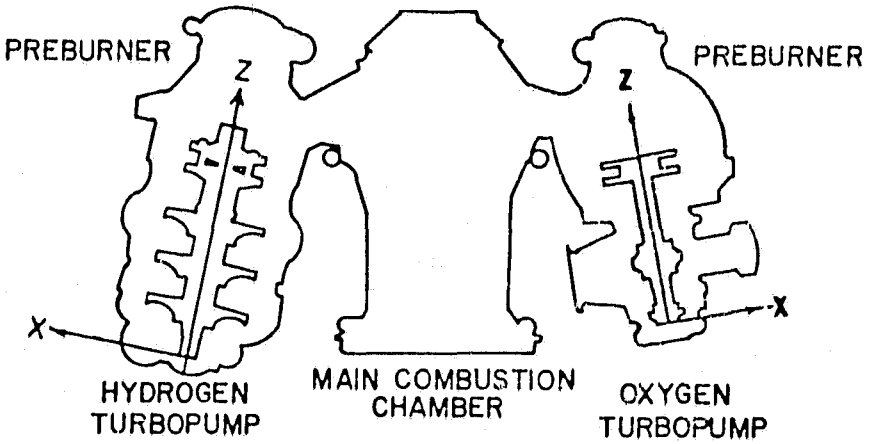

Figure 1. Local coordinate systems for SSME rotordynamic analyses.

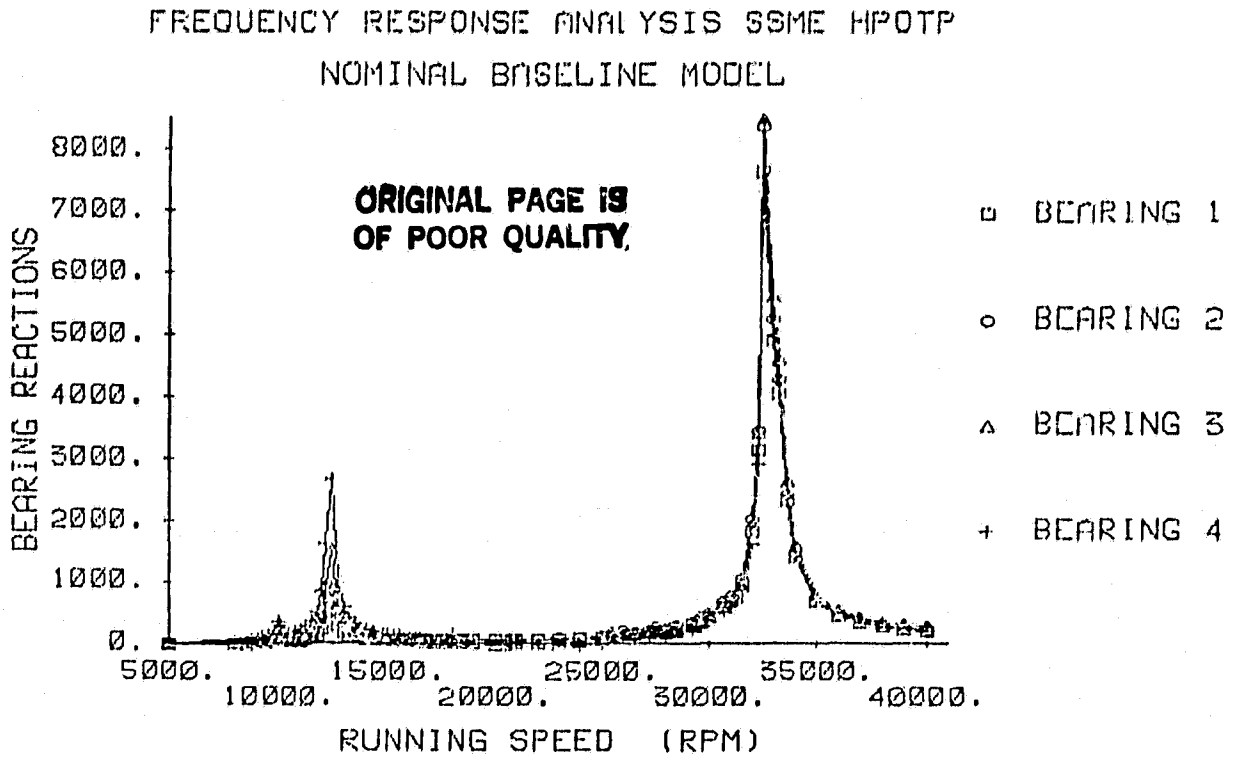

Figure 2(a). Synchronous response solutions for bearing reactions of the nominal model.

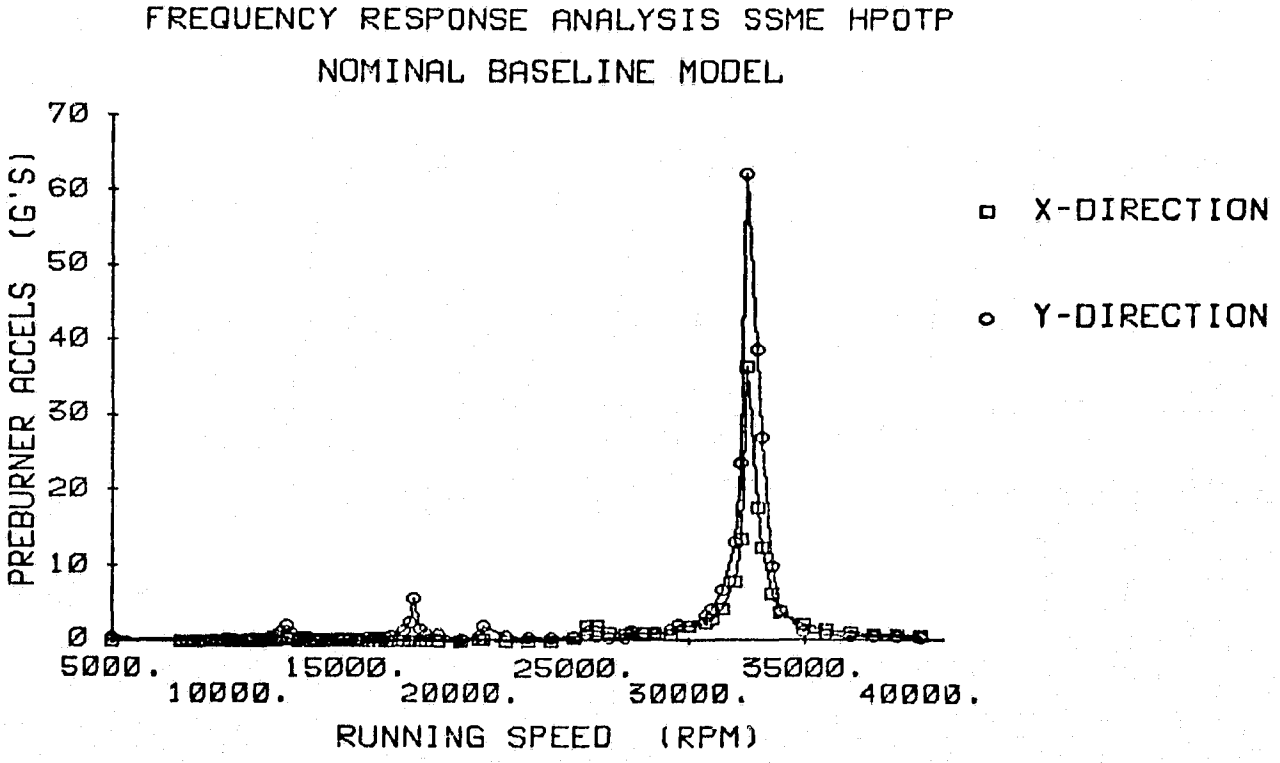

Figure 2(b). Synchronous response solutions for preburner accelerometer magnitudes of the nominal model.

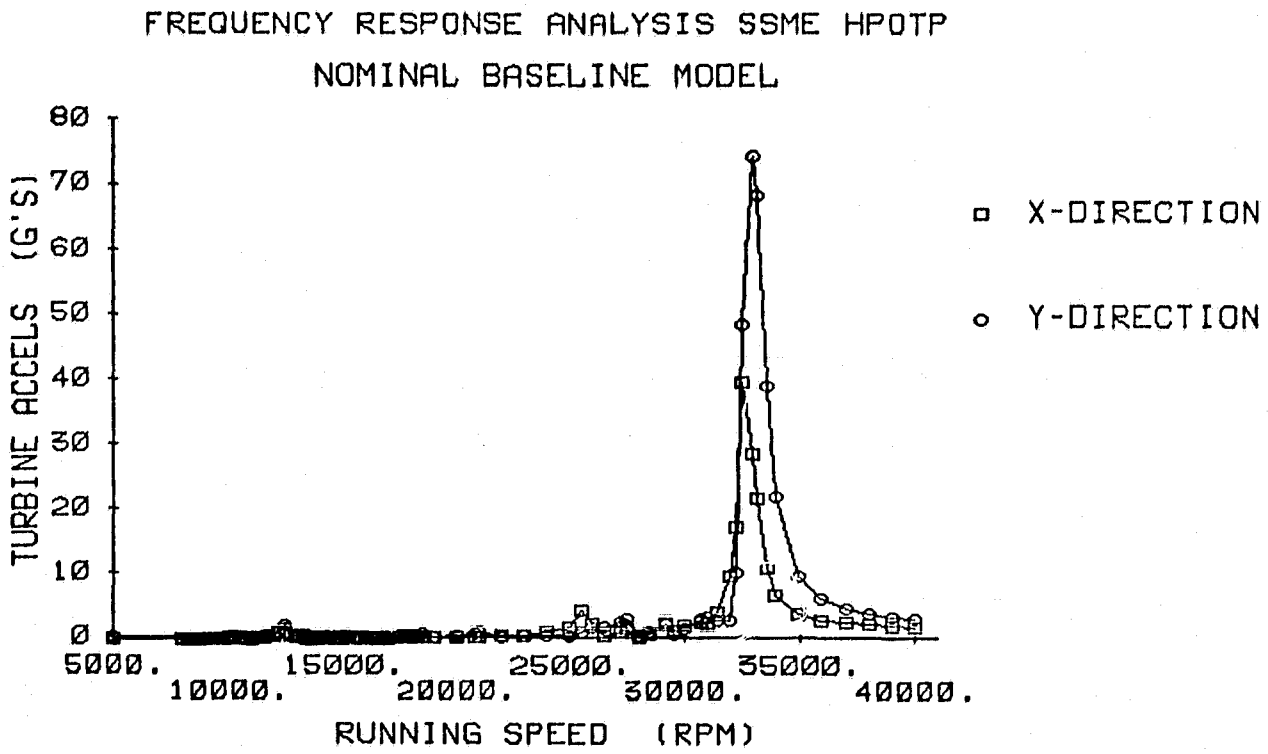

Figure 2(c). Synchronous response solutions for turbine accelerometer magnitudes of the nominal model.

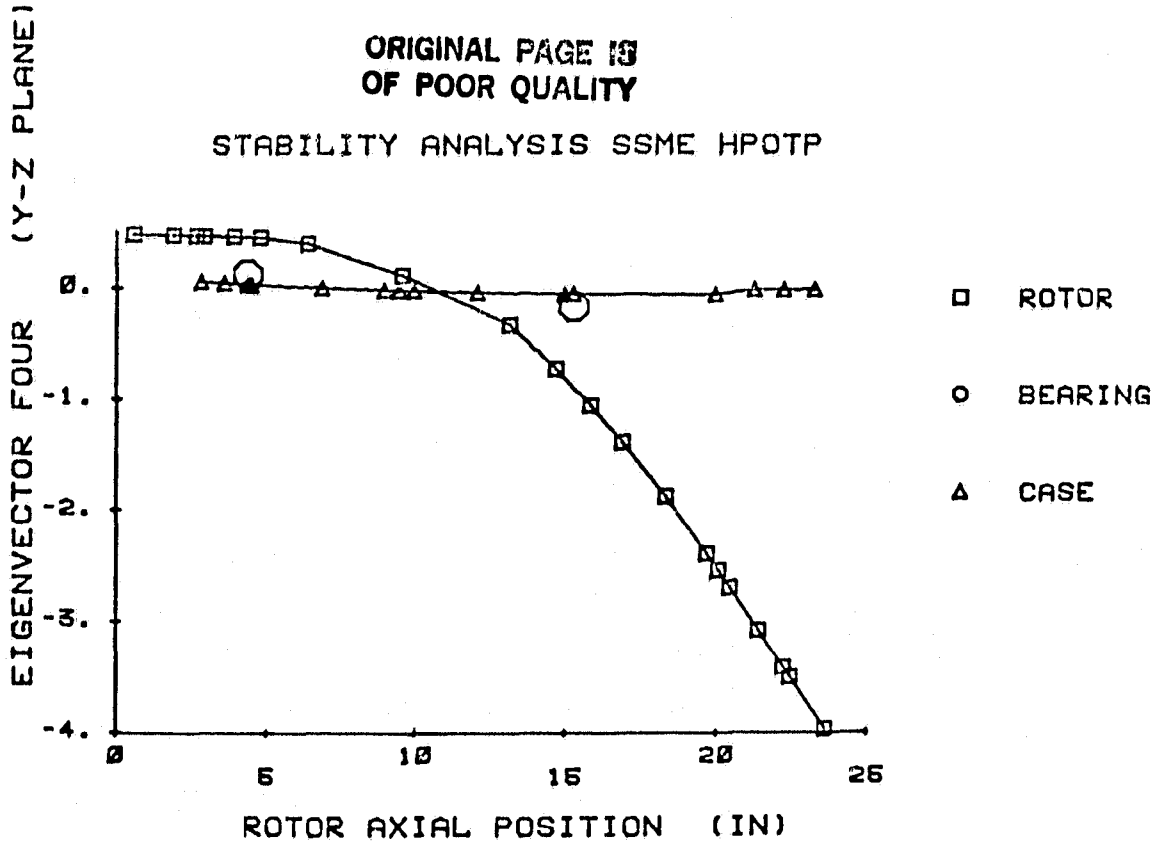

Figure 3. Coupled-rotor-housing mode for first critical speed.

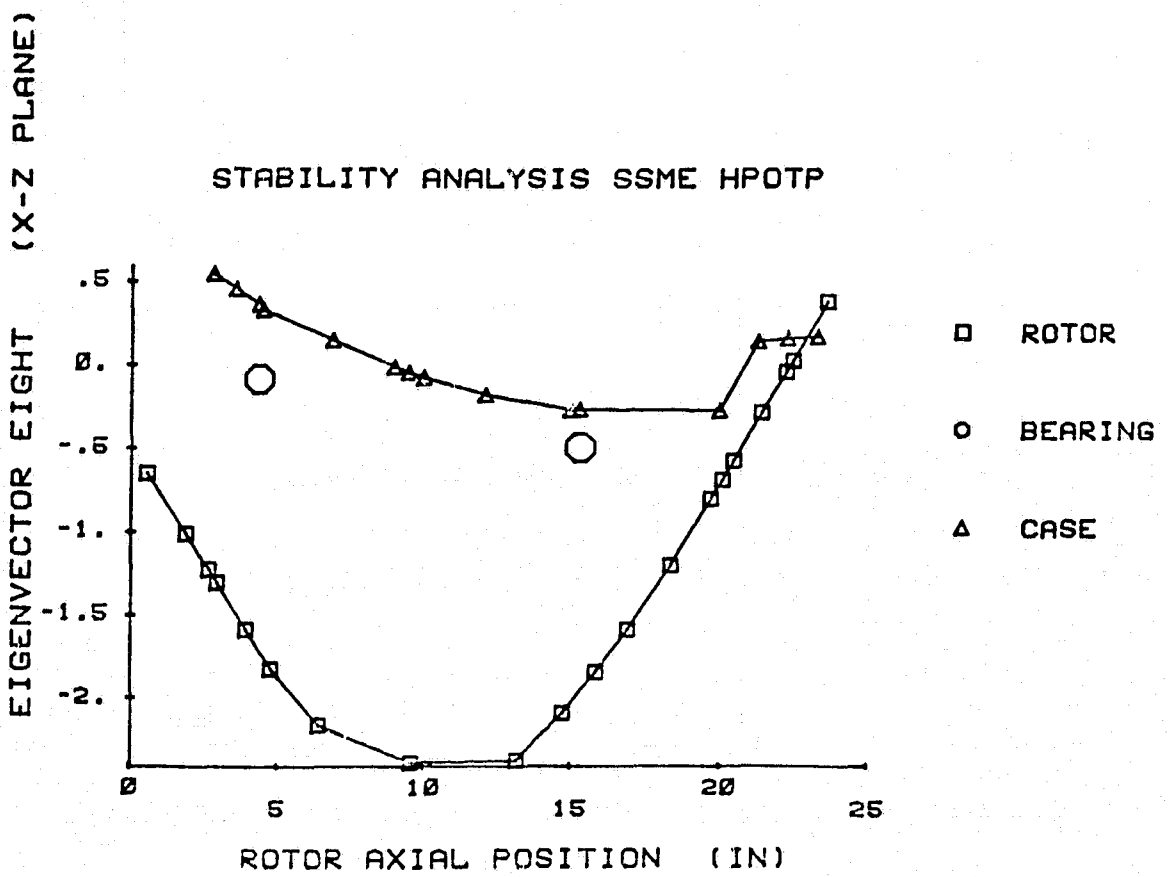

Figure 4. Coupled-rotor-housing mode for second critical speed.

The FPL running speed of the HPOTP is 30,900 which is 95% of the predicted second critical speed. Obviously, this is an undesirable situation, which is exacerbated by minimal damping. For comparison purposes, the predicted maximum bearing reactions of the nominal model at 30,500 rpm are

$$R_1 = 2527 \text{ N (568 lbs)}, \quad R_2 \ 2835 \text{ N (637 lbs)}$$
$$R_3 = 2780 \text{ N (625 lbs)}, \quad R_4 \ 2433 \text{ N (547 lbs)} \qquad (2)$$

Soft Bearings

Figure 5 illustrates the synchronous response solution for a 50% reduction in stiffness from the nominal model, i.e.,

$$K_{bi} = 4.38 \times 10^7 \text{ N/m } (.25 \times 10^6 \text{ lb/in}); \quad i = 1,2,...4 \qquad (3)$$

Only the bearing-reaction magnitudes are illustrated, and illustrate a reduction in the first and second critical speeds to 10,500 and 25,000 rpm, respectively. The following peak bearing reactions now occur in the operating range at the second critical speed.

$$R_1 = 22{,}820 \text{ N (5130 lbs)}, \quad R_2 = 23{,}950 \text{ N (5385 lbs)}$$
$$R_3 = 18{,}281 \text{ N (4110 lbs)}, \quad R_4 = 15{,}150 \text{ N (3407 lbs)} \qquad (4)$$

The associated onset speed of instability and whirl frequency are 21,950 rpm and 417 Hz., respectively.

Stiff Bearings

Figure 6 illustrates the synchronous response solution for a 50% increase in bearing stiffness in the nominal model to

$$K_{bi} = 1.31 \times 10^8 \text{ N/m } (.75 \times 10^6 \text{ lbs/in}); \quad i = 1,2,...4 \qquad (5)$$

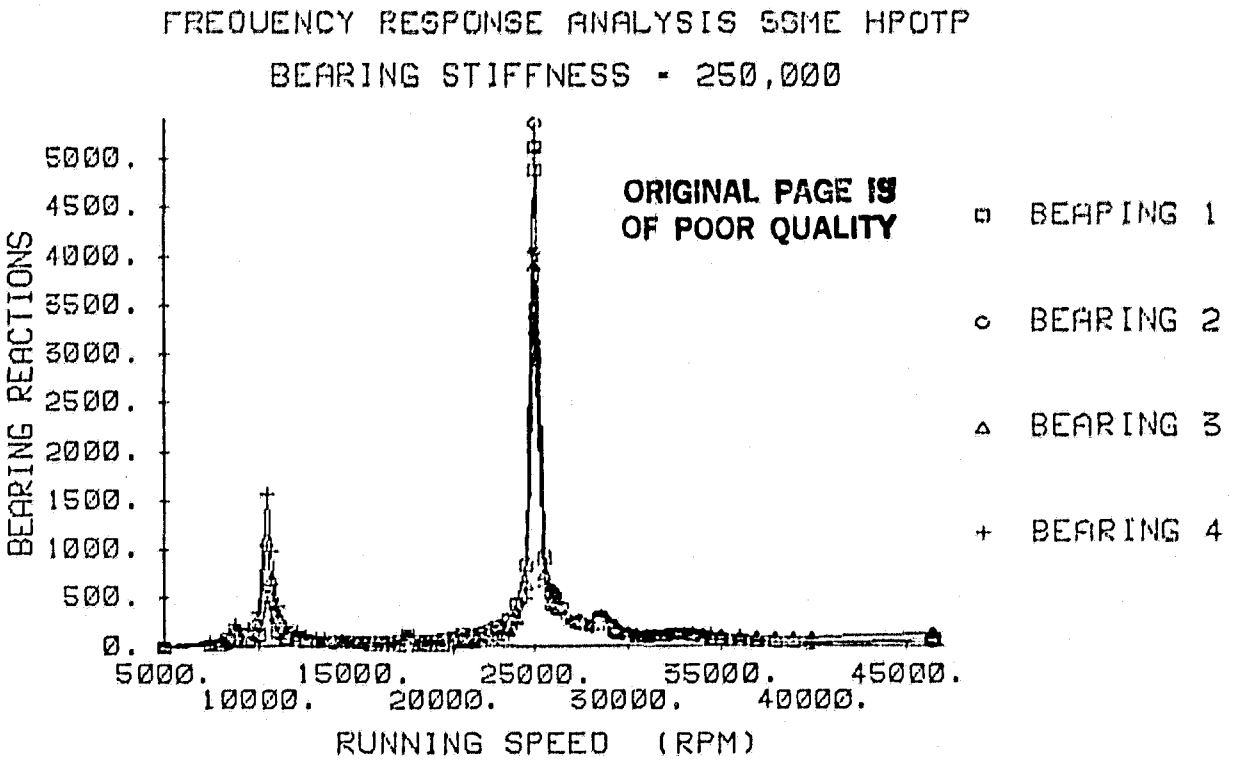

Figure 5. Synchronous response solutions for bearing reaction magnitudes with soft bearing stiffnesses (K_{b1} = 4.38 x 10^7 N/m = .25 x 10^6 lb/in).

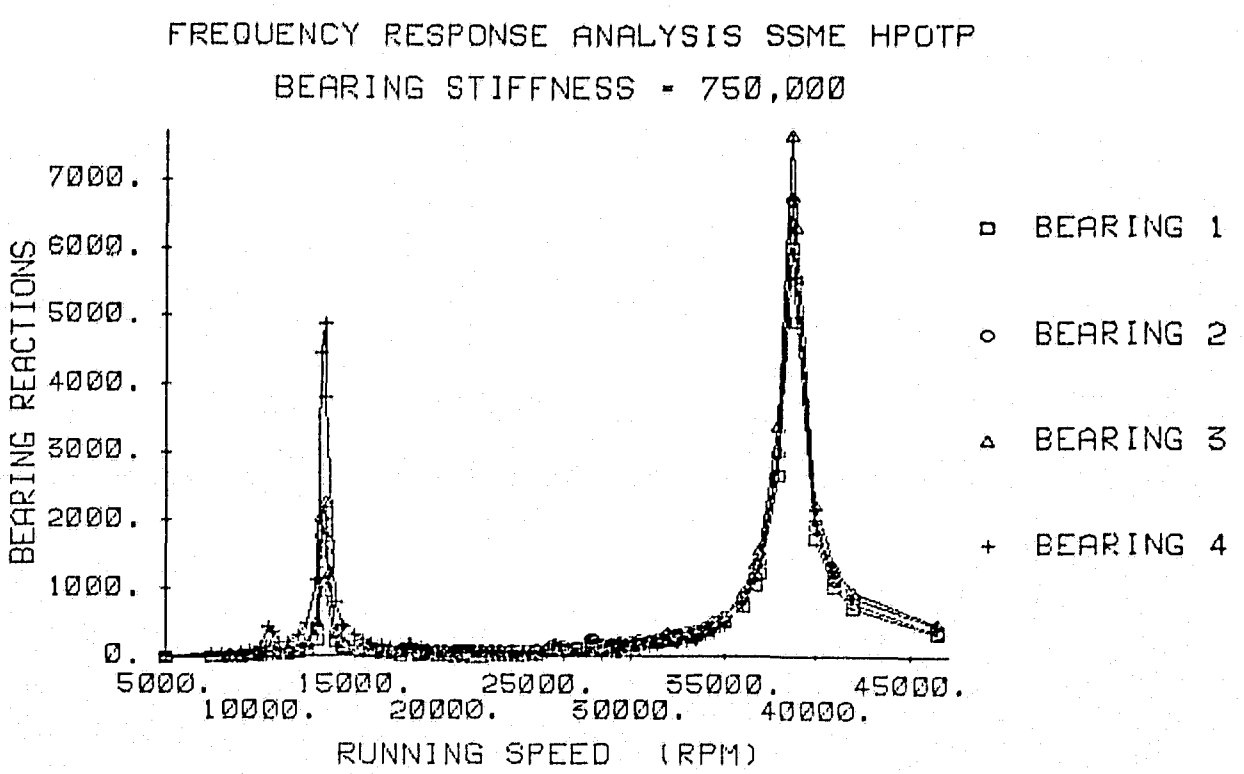

Figure 6. Synchronous response solutions for bearing reaction magnitudes with stiff bearing stiffnesses (K_{b1} = 1.31 x 10^8 N/m = .75 x 10^6 lb/in).

The illustrated bearing reactions show an increase in the first and second critical speeds to 13,460 and 38,750 rpm, respectively. The maximum bearing loads at 30,500 rpm are

$$R_1 = 934 \text{ N } (201 \text{ lbs}), \quad R_2 = 1090 \text{ N } (246 \text{ lbs})$$
$$R_3 = 867 \text{ N } (195 \text{ lbs}), \quad R_4 = 506 \text{ N } (114 \text{ lbs}) \qquad (6)$$

The associated onset speed of instability and whirl frequency are 25,300 rpm and 646 Hz., respectively.

Bearing Stiffness 2 Eliminated

Inspection of the balls in bearing 2, following subsynchronous vibration episodes, has revealed a loss of diameter on the order of .17 mm (6.5 mils). With this loss of diameter, bearing 2 might completely lose its stiffness, leaving bearing 1 to carry the load. Figure 7 illustrates the synchronous response characteristics for bearing-reaction magnitudes with a complete loss of stiffness in bearing 2. The single-peak critical speed at 32,500 rpm of the nominal model is replaced by a three-peak cluster of critical speeds within the operating range. The three new critical speeds are located as follows

26,420 rpm (440 Hz)
27,890 rpm (464 Hz)
29,370 rpm (496 Hz)

A small peak continues to be present at 32,500 rpm. Maximum bearing reactions generally occur at the 26,420 rpm, and are

$$R_1 = 15{,}710 \text{ N } (3531 \text{ lbs}), \quad R_2 = 0{,}0$$
$$R_3 = 10{,}680 \text{ N } (2400 \text{ lbs}), \quad R_4 = 8{,}820 \text{ N } (1980 \text{ lbs})$$

The onset speed of instability for this configuration is 32,640 rpm; however, the whirl frequency is at 444 Hz, which is in the range of subsynchronous frequencies experienced in practice.

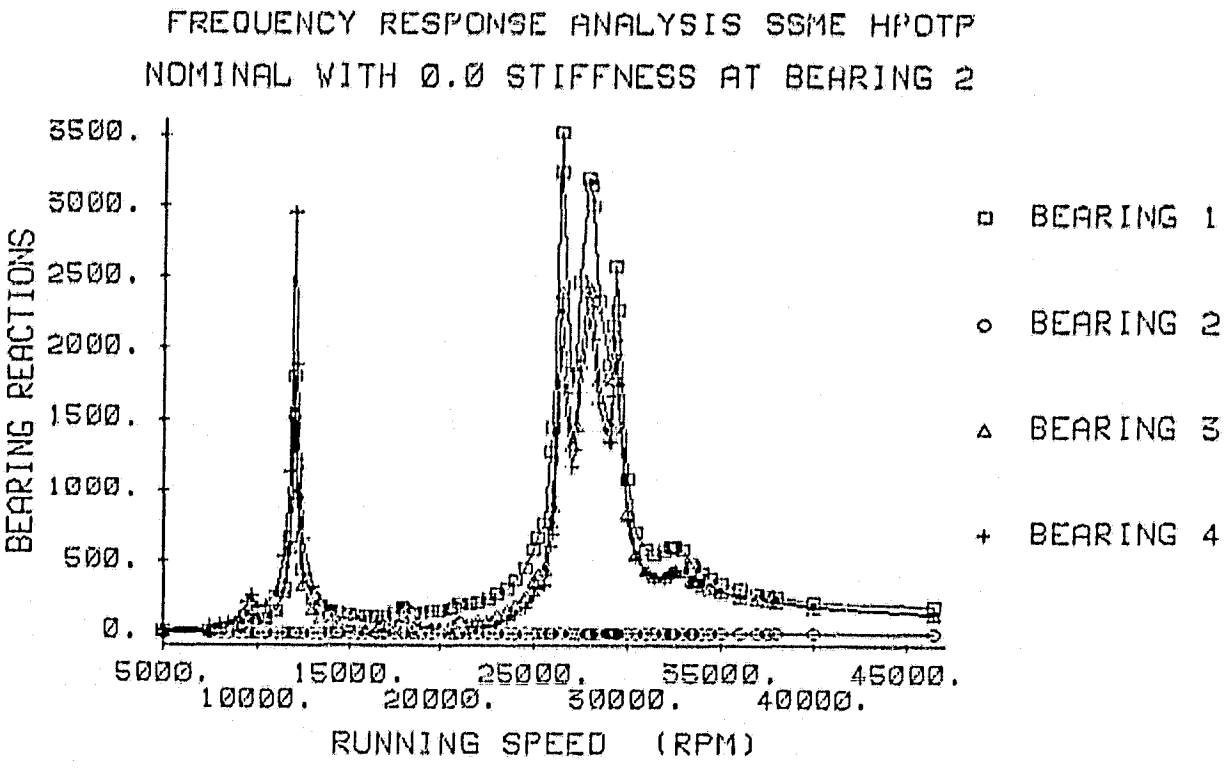

Figure 7. Synchronous response solutions for bearing reaction magnitudes with zero bearing stiffness for bearing 2.

Assessment

The HPOTP is potentially subject to severe problems due to both synchronous-response amplitudes and instability associated with the second critical speed. Both the onset speed of instability and critical-speed locations are sensitive to changes in bearing stiffnesses.

The following summary of the results of this section is helpful in understanding the dynamic characteristics of the HPOTP.

Configuration	2nd Criticals	Whirl Frequency at Instability
Nominal	32,500	540 Hz.
50% Stiffness	25,000	417 Hz.
150% Stiffness	38,750	646 Hz.
$K_{b2} = 0$	26,420 27,890 29,366	444 Hz.

The fact that the whirl frequencies experienced in practice range from 400 to 480 Hz. can only be explained by a loss in bearing stiffness. Specifically, the whirl frequency that would be expected for the nominal bearing stiffness would be 540 Hz. which is simply too high in comparison to the observed results. Further, given that most units only begin to whirl after sustained operation, bearing damage with an associated loss of stiffness is probably required to yield subsynchronous motion.

A summary of the onset speed of instabilities for the configurations examined follows.

Configuration	OSI
Nominal	30,429
50% Stiffness	21,946
150% Stiffness	25,299
$K_{b2} = 0$	32,636

The results for 150% of bearing stiffness are puzzling in that an increase in bearing stiffness would be expected to elevate the OSI. However, in this case, the increase in bearing stiffness reduces the effectiveness of the limited damping which is available. The result of eliminating K_{b2} is also surprising in that the OSI is increased. However, eliminating K_{b2} yields a marked change in the mode shape, which increases the effectiveness of the limited damping which is available.

The above numerical results emphasize the limitations of mathematical models, and linear models in particular, in reaching conclusions about specific turbomachinery units. On the basis of general experience with unstable turbomachinery units, the 150% stiffness configuration would be very much preferred, if such a configuration were available. The contrary predicted results arise because of ignorance concerning the forces acting on the rotor.

D. The Influence of Changes in Impeller Cross-Coupling Coefficients

The recent report by Jery and Franz [5] includes the nondimensional results of Eq.(A.8) for vaned-diffuser stiffness coefficients. These results supplement the earlier test data of Chamieh et al. [6] for a logarithmic volute. Test results are not as yet available for the damping and added-mass coefficients of impellers.

Changing the coefficients of Eq.(A.8) as follows

$$-\frac{1}{\rho A_2 V_2^2}\begin{Bmatrix} F_X \\ F_Y \end{Bmatrix} = \begin{bmatrix} -2.0 & 0.9 \\ -0.9 & -2.0 \end{bmatrix}\begin{Bmatrix} X/R_2 \\ Y/R_2 \end{Bmatrix}$$

in the nominal model yields an onset speed of instability and whirl frequency at 24,533 rpm and 544 Hz., respectively. The magnitude of increase in the cross-coupling coefficients from 0.7 to 0.9 is reasonable based on [5,6] and yields a marked reduction in OSI.

E. The Influence of Changes in Clearance Excitation Forces

The nominal model uses a $\beta = 0.25$ in Eq.(A.10) with the Table of B.12. Increasing β to 0.6 as suggested by the test results of [7] has no perceptible influence on the OSI associated with the second-critical-speed mode, because the mode shape associated with this motion has relatively small motion at the turbine. Conversely, the first-critical-speed mode shape has large motion at the turbine.

The nominal model predicts that the lowest critical speed motion would first become unstable at approximately 17,600 rpm and then become stable again at approximately 23,800 rpm. The whirl frequency increases rapidly with speed, but is approximately 250 Hz. Increasing β to 0.6, significantly extends the predicted speed range of instability to (14,400 - 27,200 rpm).

Hence, with respect to the HPOTP, the first-mode stability is sensitive to reasonable changes in the clearance-excitation force, while the second-mode is almost completely insensitive to changes in this force.

F. The Influence of Changes in Liquid Seals

Introduction

The liquid seals in the current flight hardware consist of the inlet and discharge wear rings for the boost impeller. Labyrinth configurations are used for both these seals and, on the basis of past experience and analysis, provide comparatively little stiffness or damping. In fact, the absence of damping through the main impeller and boost impeller portions of the turbopump is a major factor in both subsynchronous vibration problems and high synchronous bearing loads associated with the second critical speed. The following alternative configurations have been proposed to supply additional damping through this portion of the turbopump:

(a) Replace the boost-impeller inlet wear-ring seal with a smooth constant-clearance seal. Table B.9 contains the predicted seal coefficients for this configuration.

(b) Replace the boost-impeller inlet wear-ring seal with a "damper-seal". This configuration differs from the smooth seal in that a deliberately surface-roughened stator is employed. Table B.8 contains the predicted seal coefficients for this configuration.

(c) Replace the rear wear-ring seal with a smooth constant-clearance seal. Table B.5 contains predicted coefficients for this seal.

(d) Replace the current unshrouded main-impeller inducers with shrouded inducers to create new seals on the outside surfaces of the inducers. Table B.10 contains predicted coefficients for these seals.

The effectiveness of these proposed changes in reducing synchronous bearing loads and improving the predicted rotordynamic stability of the HPOTP is the subject of this section.

Smooth, Constant-Clearance Inlet Seal for the Boost Impeller

This change elevates the OSI to 34,580 rpm, an increase of 4150 rpm in comparison to the nominal model. The whirl frequency associated with this configuration is 550 Hz. as compared to the nominal model whirl frequency of 540 Hz. The bearing reactions at 30,500 rpm are

$$R_1 = 1780 \text{ N } (400 \text{ lbs}), \quad R_2 = 2120 \text{ N } (477 \text{ lbs})$$
$$R_3 = 2410 \text{ N } (542 \text{ lbs}), \quad R_4 = 1950 \text{ N } (443 \text{ lbs}) \tag{8}$$

Damper Inlet Seal for the Boost Impeller

This change elevates the OSI to 34,980 rpm which is an increase of 4550 and 400 rpm, respectively, over the nominal model and the smooth inlet seal result. The associated whirl frequency is approximately 550 Hz., and the bearing reactions at 30,500 rpm are

$$R_1 = 1830 \text{ N } (410 \text{ lbs}), \quad R_2 = 2160 \text{ N } (487 \text{ lbs})$$
$$R_3 = 2430 \text{ N } (547 \text{ lbs}), \quad R_4 = 1970 \text{ N } (443 \text{ lbs}) \tag{9}$$

By comparison to Eqs.(2), this represents a reduction in bearing loads on the order of 25% for bearings 1 and 2. The second critical speed is elevated slightly to 34,980 rpm from the nominal value of 32,500 rpm.

Figure 8 illustrates the synchronous bearing-reaction magnitudes for this configuration. By comparison to Figure 2(a), observe that the damper seal does not significantly modify the overall dynamic characteristics of the turbopump.

Smooth Discharge Seal for the Boost Impeller

This change would elevate the predicted OSI to 41,640 in comparison to 30,430 for the nominal. The associated whirl frequency is approximately 575 Hz., and the bearing reactions are

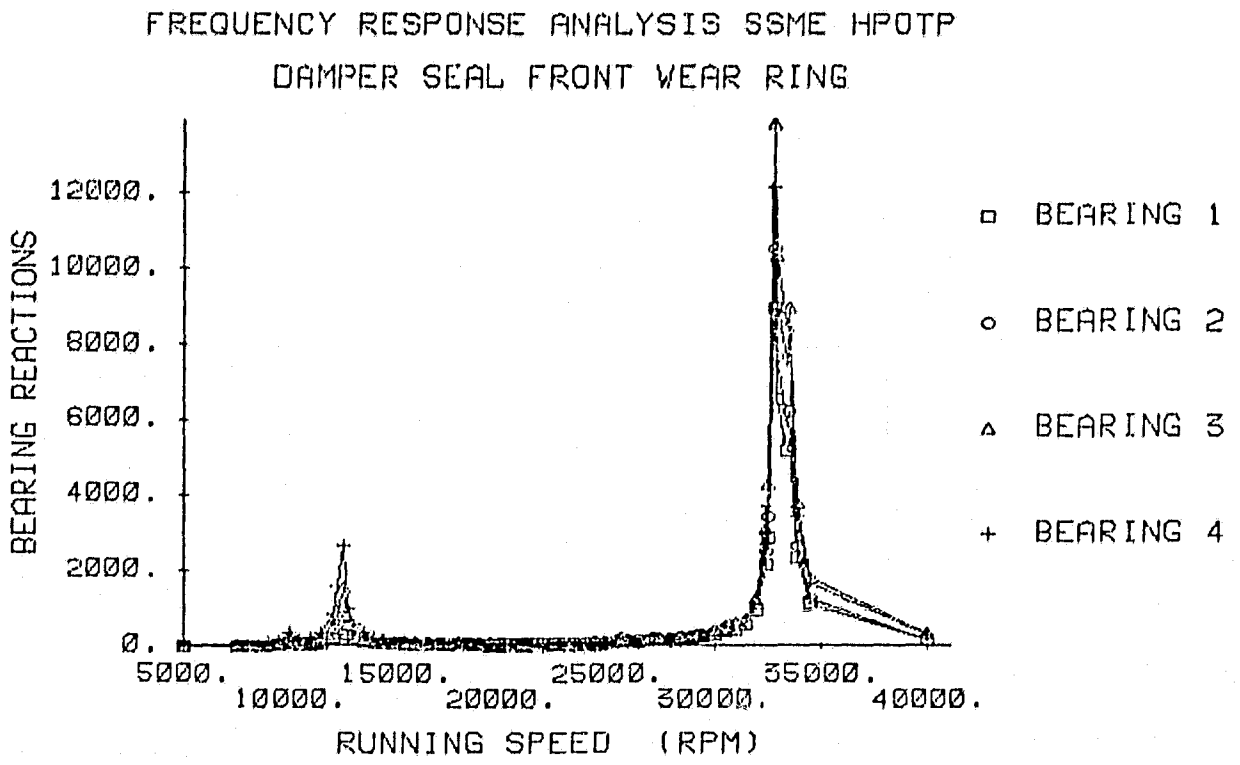

Figure 8. Synchronous response solutions for bearing reaction magnitudes with a damper-seal configuration at the inlet boost-impeller seal.

$$R_1 = 1130 \text{ N } (254 \text{ lbs}), \quad R_2 = 1430 \text{ N } (320 \text{ lbs})$$
$$R_3 = 1780 \text{ N } (400 \text{ lbs}), \quad R_4 = 1400 \text{ N } (316 \text{ lbs}) \qquad (10)$$

This change yields a reduction of approximately 50% in the nominal predictions for R_1 and R_2.

Figure 9 illustrates the synchronous response solution for the bearing reactions for this configuration. An elevation of the second critical speed to 34,500 rpm is the principal, predicted consequence of introducing a smooth constant-clearance configuration in the boost-impeller discharge seal.

Shrouded Inducer Seals

Introducing shrouded inducer seals yields OSI that are much greater than 40,000 rpm. The associated bearing reaction loads are

$$R_1 = 518 \text{ N } (117 \text{ lbs}), \quad R_2 = 540 \text{ N } (122 \text{ lbs})$$
$$R_3 = 410 \text{ N } (91.7 \text{ lbs}), \quad R_4 = 410 \text{ N } (92.8 \text{ lbs}) \qquad (11)$$

The current plans at Rocketdyne and MSFC are to modify the present configuration by implementing both a damper-seal configuration for the boost-impeller inlet and shrouded impeller seals. The frames of Figure 10 illustrate the predicted synchronous response amplitudes for this configuration and demonstrate that the bearing-reaction problem associated with the second critical speed is eliminated. A resonance continues to exist in the neighborhood of 33,000 rpm; however, the bearing reactions are no longer of a magnitude that elicits concern. The calculated bearing reactions at 30,500 rpm are

$$R_1 = 406 \text{ N } (91.3 \text{ lbs}), \quad R_2 = 464 \text{ N } (104. \text{ lbs})$$
$$R_3 = 406 \text{ N } (91.3 \text{ lbs}), \quad R_4 = 398 \text{ N } (89.5 \text{ lbs}) \qquad (12)$$

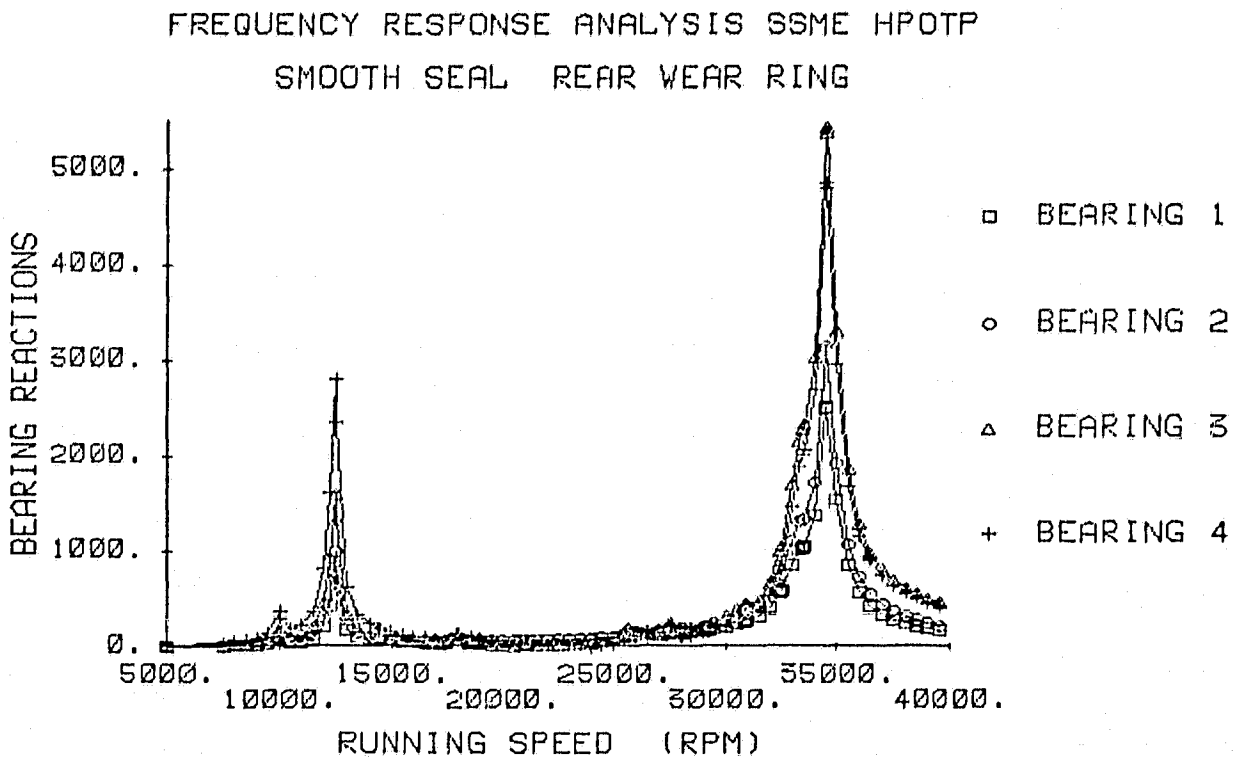

Figure 9. Synchronous response solutions for bearing reaction magnitudes with a smooth, constant-clearance configuration for the boost-impeller discharge seal.

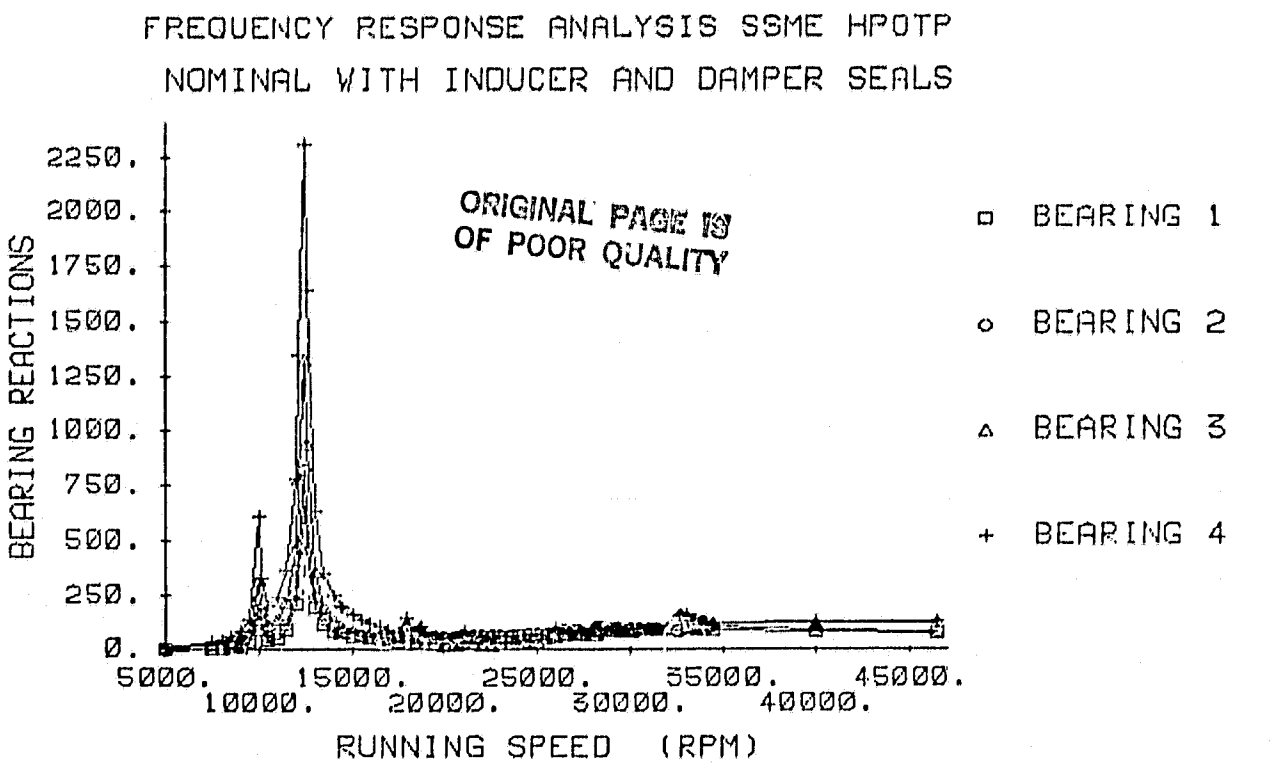

Figure 10(a). Synchronous response solutions for bearing reaction magnitudes with a damper seal for the preburner inlet and shrouded-inducer seals.

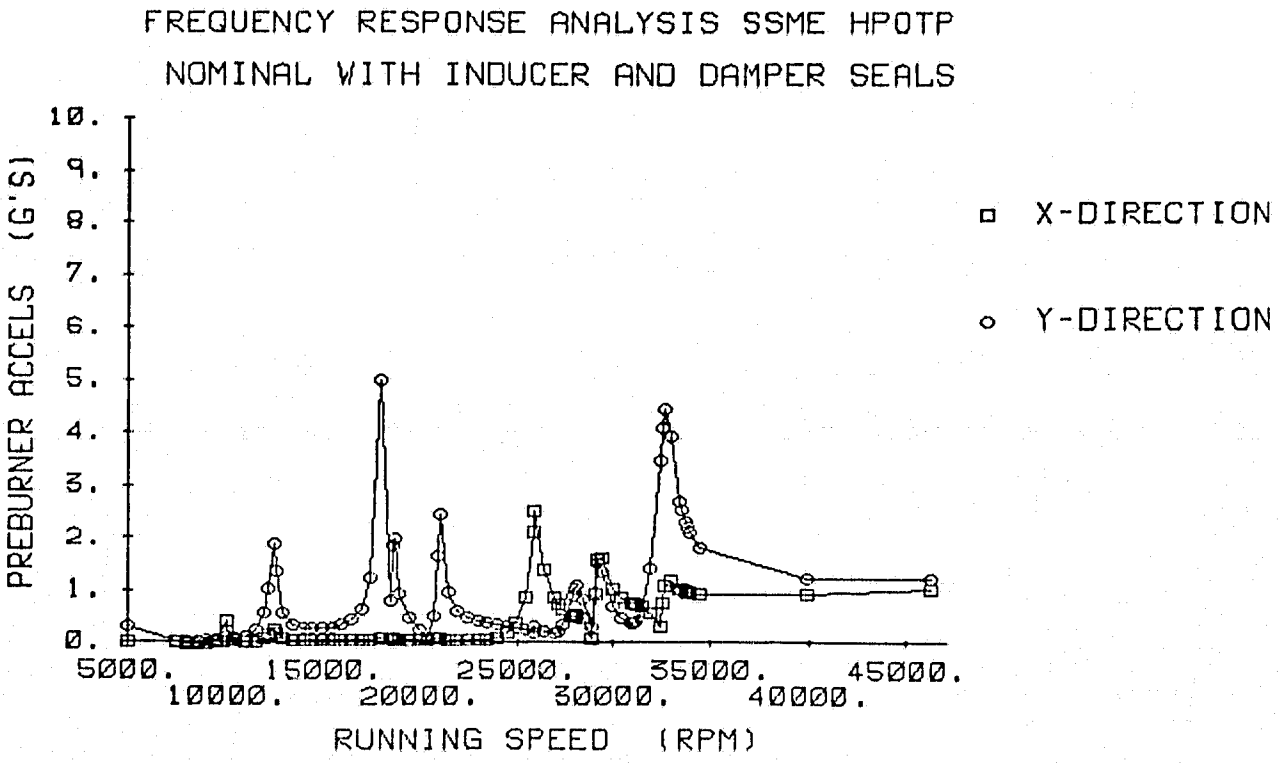

Figure 10(b). Synchronous response solutions for preburner accelerometer magnitudes with a damper seal for the preburner inlet and shrouded-inducer seals.

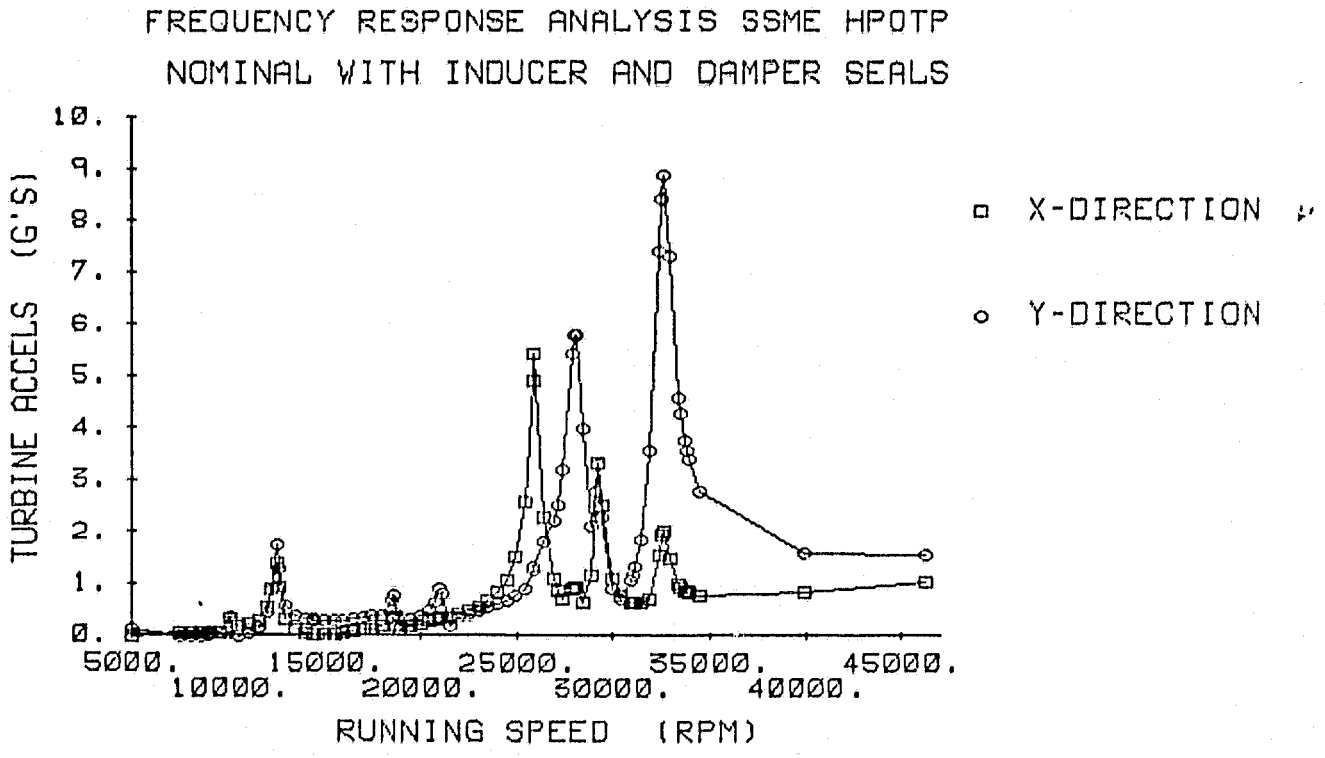

Figure 10(c). Synchronous response solutions for turbine accelerometer magnitudes with a damper seal for the preburner inlet and shrouded-inducer seals.

which are approximately one sixth of the predictions for the nominal case.

The predicted accelerometer results in Figures 10(b) and (c) suggest that new resonances have been introduced by incorporation of inducer and damper seals. However, most of these peaks are present in the nominal model results of Figures 2(b) and (c). They are simply suppressed by the scaling which was required to account for the huge predicted g-levels associated with the second critical speed.

Assessment

The results of this section support the following general conclusions with respect to seal modifications:

(a) The damper seal or smooth constant-clearance seal have the potential for elevating the OSI by approximately 14%. These seals do not significantly alter the critical speed location. They reduce the bearing reactions by approximately 25%.

(b) Introducing a constant-clearance configuration for the boost impeller discharge increases the predicted onset speed of instability by 37% and reduces the predicted bearing reactions by approximately 50%. This change elevates the second critical speed by approximately 6%.

(c) The inducer seals eliminate the bearing-reaction problem associated with the second critical speed, and elevates the OSI far beyond the top operating speed.

G. The Influence of Changes in the Turbine Interstage Seal

As noted in the preceding section E, linear analysis of the nominal model predicts that motion associated with the first critical speed would be unstable over the speed range (17,600 - 23,800 rpm). Use of the seal coefficients in Table B.1 for a tapered seal with anti-vortex ribs in the linear model eliminates this instability prediction. Those results are to be expected, since the first-critical-speed mode shape of Figure 3 involves large motion at the turbine.

Changing the turbine interstage seal coefficients causes a slight reduction in the OSI associated with the second critical speed from 30,430 to 30,290 rpm. The fact that changing the turbine interstage seal location has a minimal predicted influence on motion associated with the second critical speed is to be expected, given the nature of the mode illustrated in Figure 4. Specifically, the second-critical-speed mode shape involves very small motion in the turbine.

H. The Influence of Changes in Bearing "Dead-Band" Clearances

The influence of changes in dead-band bearing clearances are nonlinear and must be examined by means of a transient nonlinear program. From past experience, bearing clearances are known to yield the following deviations from the predictions of linear models:

(a) Peak amplitudes are smaller but may be experienced at lower speeds. This result is analytically predicted by Yamamoto [8] in the absence of side loads. A parametric study of this effect was examined at length in reference [3].

(b) The rotor is more stable with clearances than without them. This stability enhancement has been explained previously as resulting from bearing stiffness asymmetry resulting from the combined influence of bearing clearances and a fixed-direction side load.

The turbine and pump bearing clearances used in this study were

$$\delta_P = .0254 \text{ mm } (.001 \text{ in})$$
$$\delta_T = .0127 \text{ mm } (.0005 \text{ in}) \qquad (11)$$

In addition to the effect of bearing clearances, the transient model accounts for the axial rigid-body motion of the rotor. This motion is coupled to the housing model via the balance-piston coefficients.

The response characteristics of the transient model becomes linear when the dead-band clearances are eliminated, and transient simulation runs were made in this mode to verify that the transient program was functioning as expected with the following results:

(a) In the absence of external damping at the bearings or main impeller, the transient model is unstable as predicted.

(b) As predicted, the second critical speed is located between 32,000 and 32,500 rpm. The frames of Figure 11 illustrate the result of

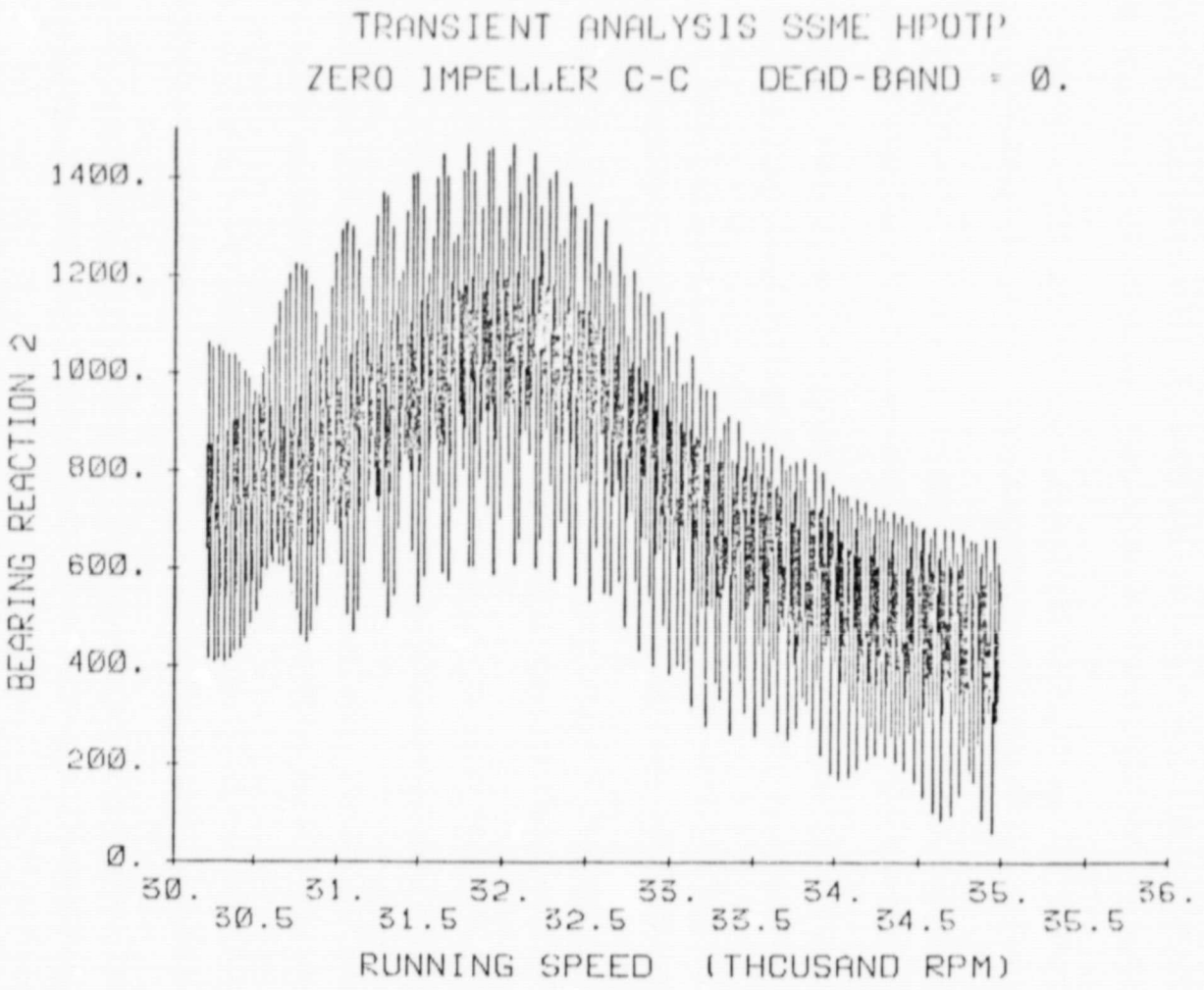

Figure 11(a). Bearing reaction 2 (lbs) for an acceleration from 30,200 to 35,000 rpm. The dead-band clearances and the destabilizing cross-coupling coefficients at the main impeller are zero.

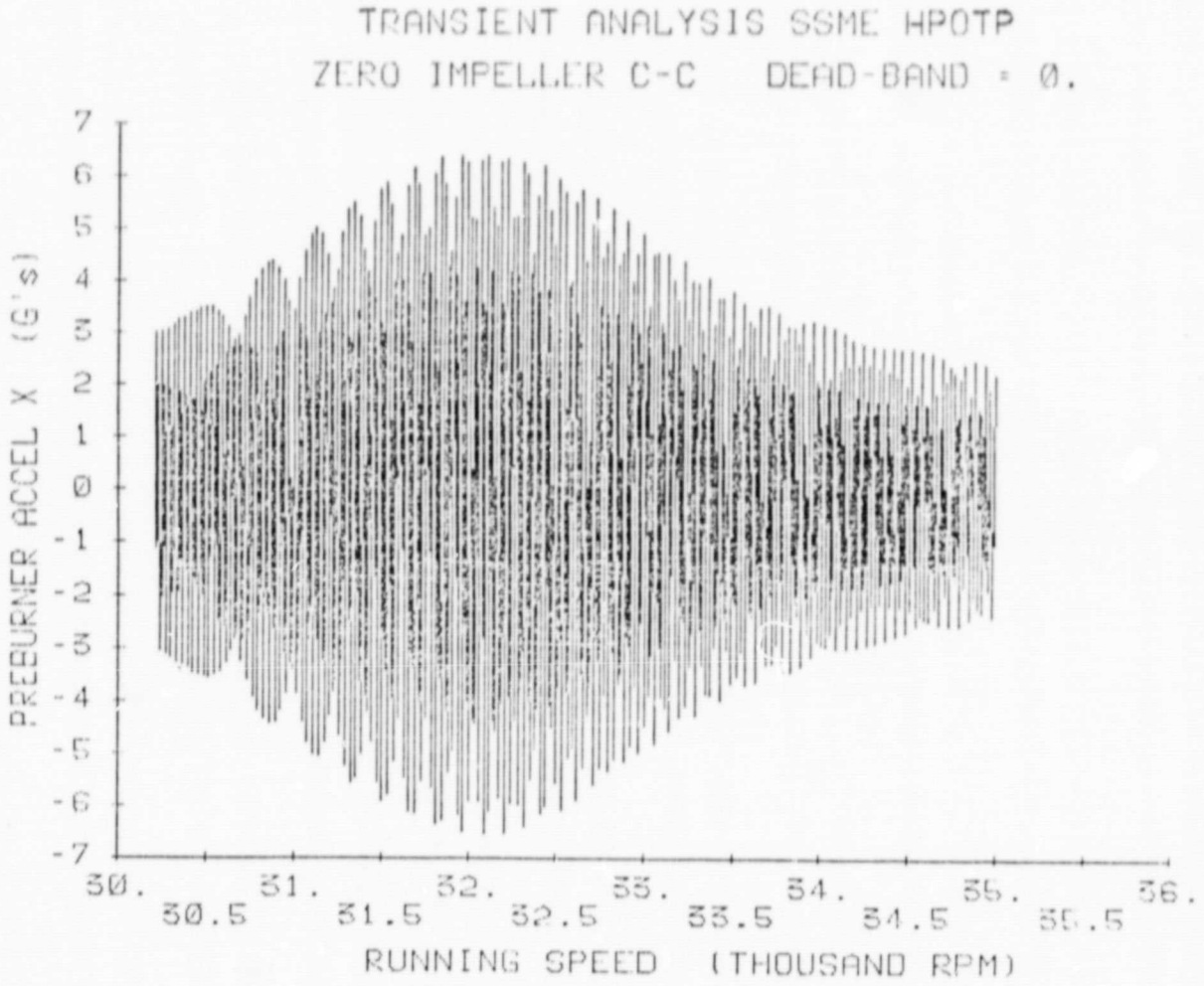

Figure 11(b). Preburner accelerometer amplitudes (g's) in the X-Z plane for an acceleration from 30,200 to 35,000 rpm. The dead-band clearances and the destabilizing cross-coupling coefficients at the main impeller are zero.

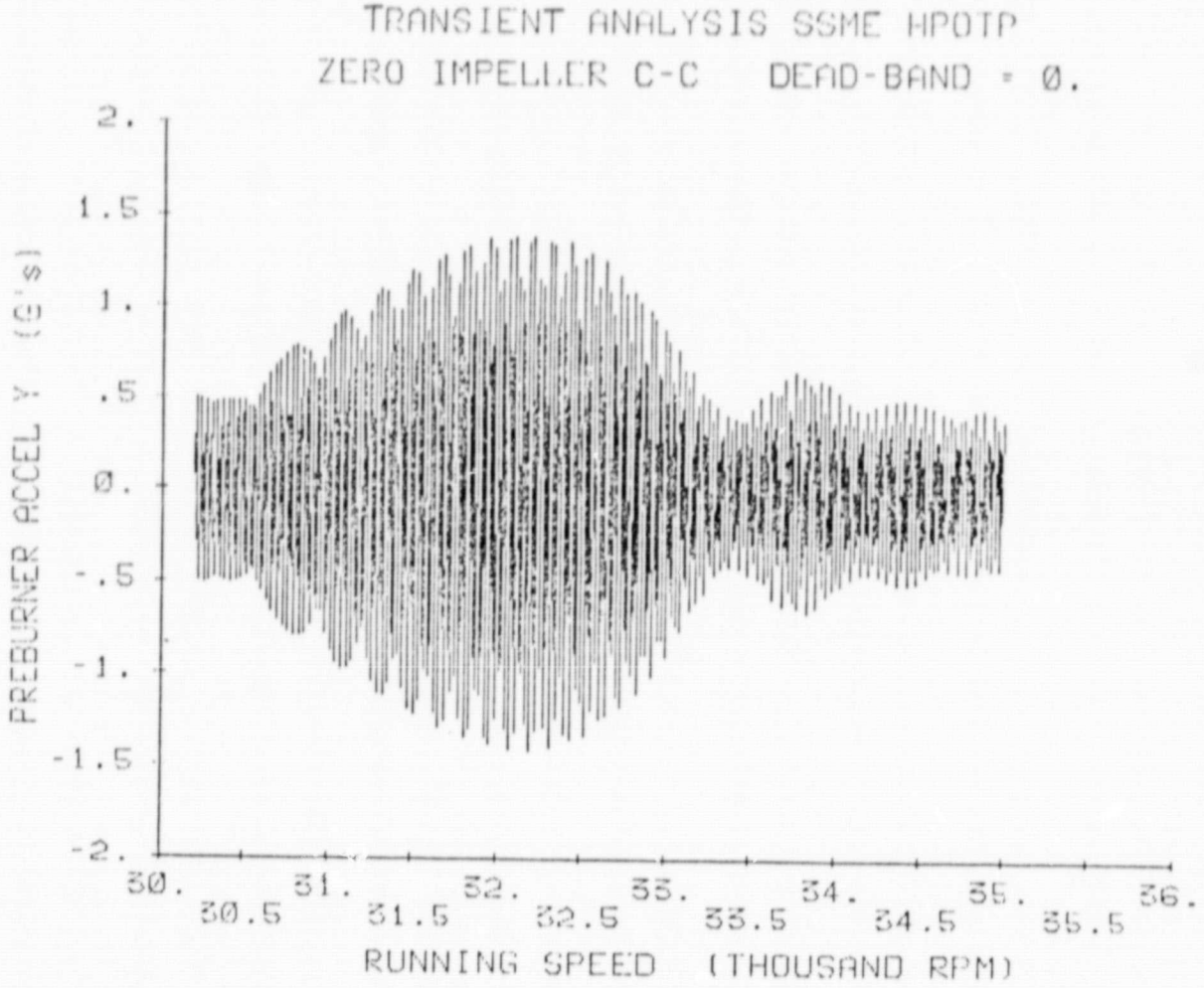

Figure 11(c). Preburner accelerometer amplitudes (g's) in the Y-Z plane for an acceleration from 30,200 to 35,000 rpm. The dead-band clearances and the destabilizing cross-coupling coefficients are zero.

an acceleration from 30,200 to 35,000 rpm. This motion is stable because the destabilizing forces at the main impeller has been eliminated.

Simulation runs including the influence of the bearing clearances of Eq.(11) confirm the general reduction of amplitudes. Figure 12 illustrates this result for bearing 2. This is a constant-speed run at 30,200 rpm; however, the initial conditions were obtained from a previous zero-bearing clearance run which included damping at the bearings of 1750 Ns/m (10 lb sec/in). The sharp initial reduction in amplitude is occasioned entirely by the introduction of bearing clearances, since the external damping at the bearings has been reduced to zero. The frames of Figure 13 illustrate an acceleration from 30,200 rpm to 35,000 rpm with bearing clearances, no external damping at the bearings, and no destabilizing forces at the main impeller. A comparison of these results to those of Figure 13 demonstrates the following:

(a) The peak amplitude in bearing loads associated with a 32,000~32,500 rpm critical speed has been eliminated.

(b) The distinct peak in the preburner accelerometer levels in the X-Z plane is substantially eliminated.

(c) The amplitudes of preburner accelerometer levels in the Y-Z plane is substantially reduced; however, an apparent resonance continues to be present at approximately 32,500 rpm.

The frames of Figure 14 illustrate simulation results for the nominal model with the bearing clearances of Eq.(11), no bearing damping, and the nominal impeller-cross-coupling coefficients of Table B.11 when running at 30,000 rpm. The results of Figures 14(a) and (b) show that bearing 1 and 2 are unloading periodically at a frequency of approximately 80 Hz.

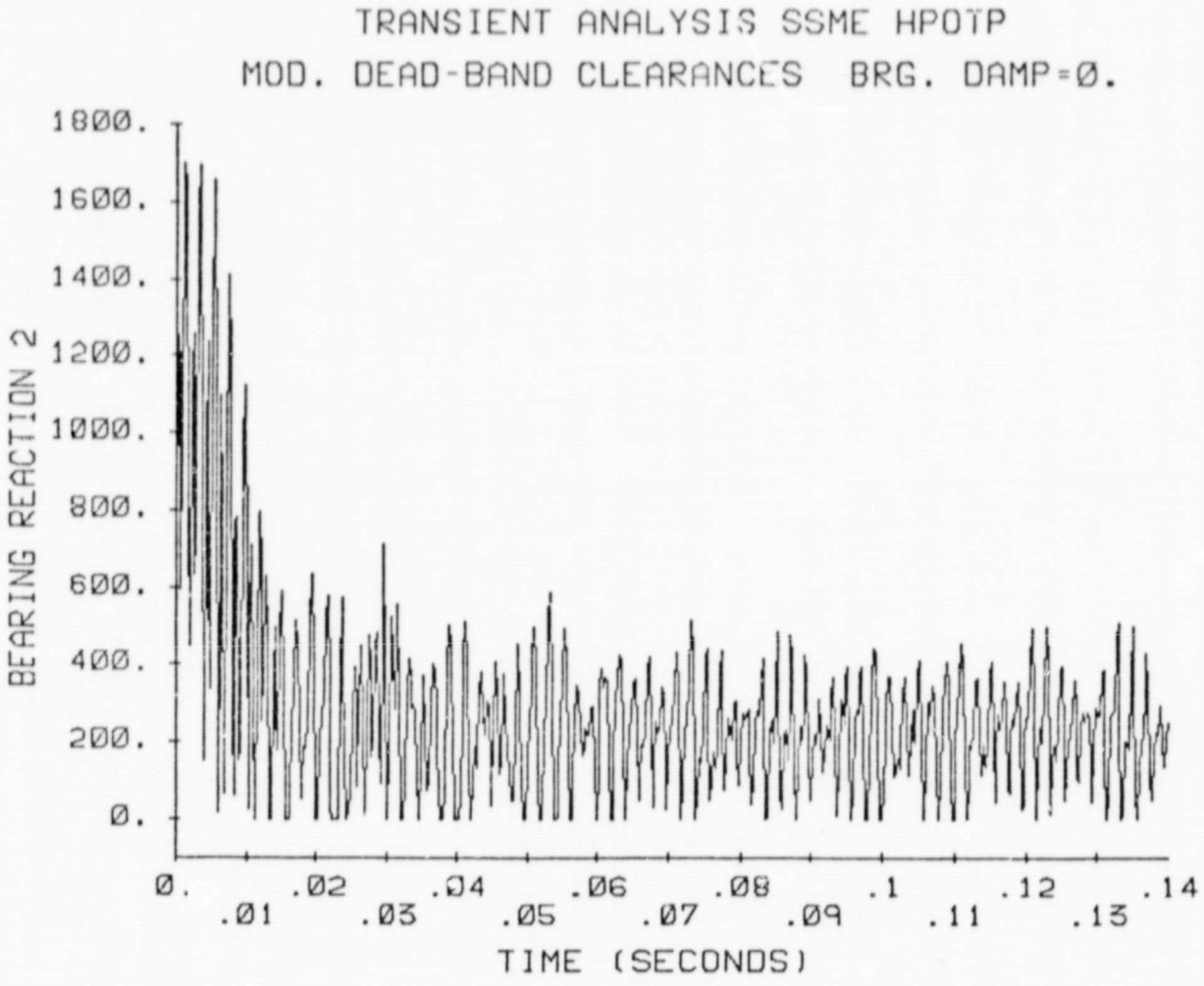

Figure 12. Synchronous bearing 2 reaction amplitudes at 30,200 rpm for the bearing clearances of Eq.(11). The initial conditions used in this simulation run were generated from an earlier zero-bearing-clearance run.

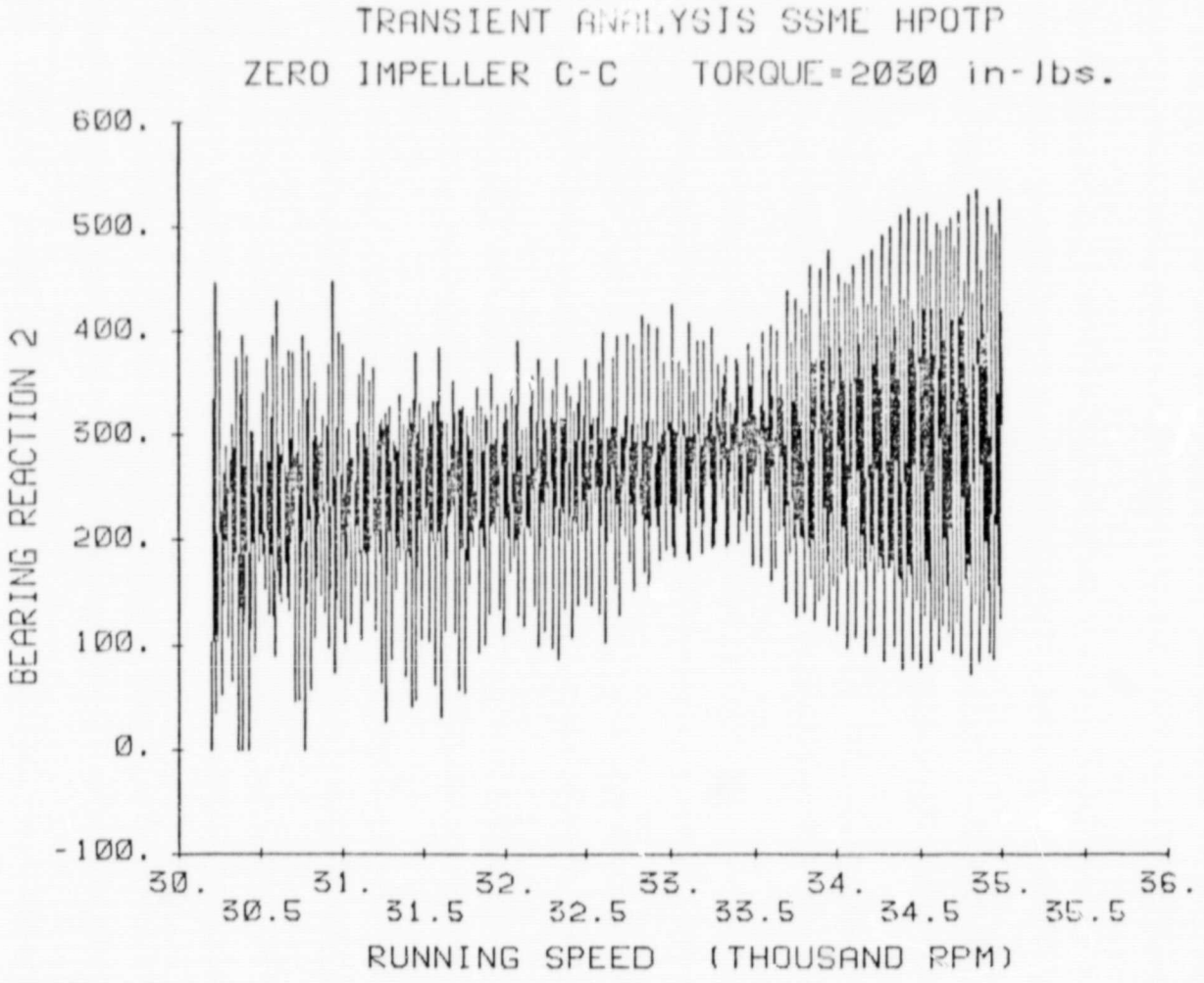

Figure 13(a). Bearing 2 reaction amplitudes (lbs) for an acceleration from 30,200 to 35,000 rpm with the bearing clearances of Eq.(11), no external bearing damping, and no destabilizing force at the main impeller.

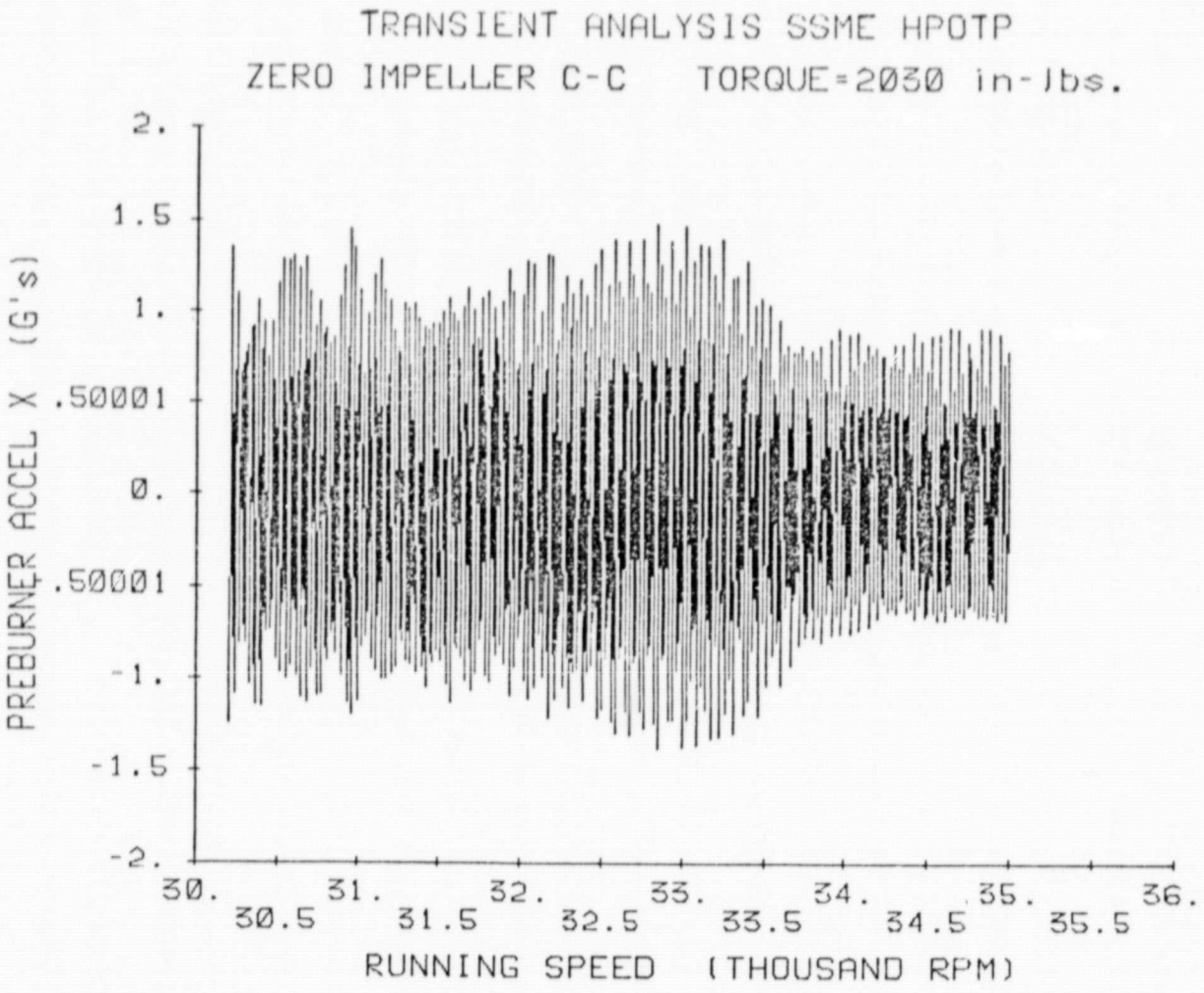

Figure 13(b). Preburner accelerometer amplitudes (g's) in the X-Z plane for an acceleration from 30,200 to 35,000 rpm with the bearing clearances of Eq.(11), no external bearing damping, and no destabilizing force at the main impeller.

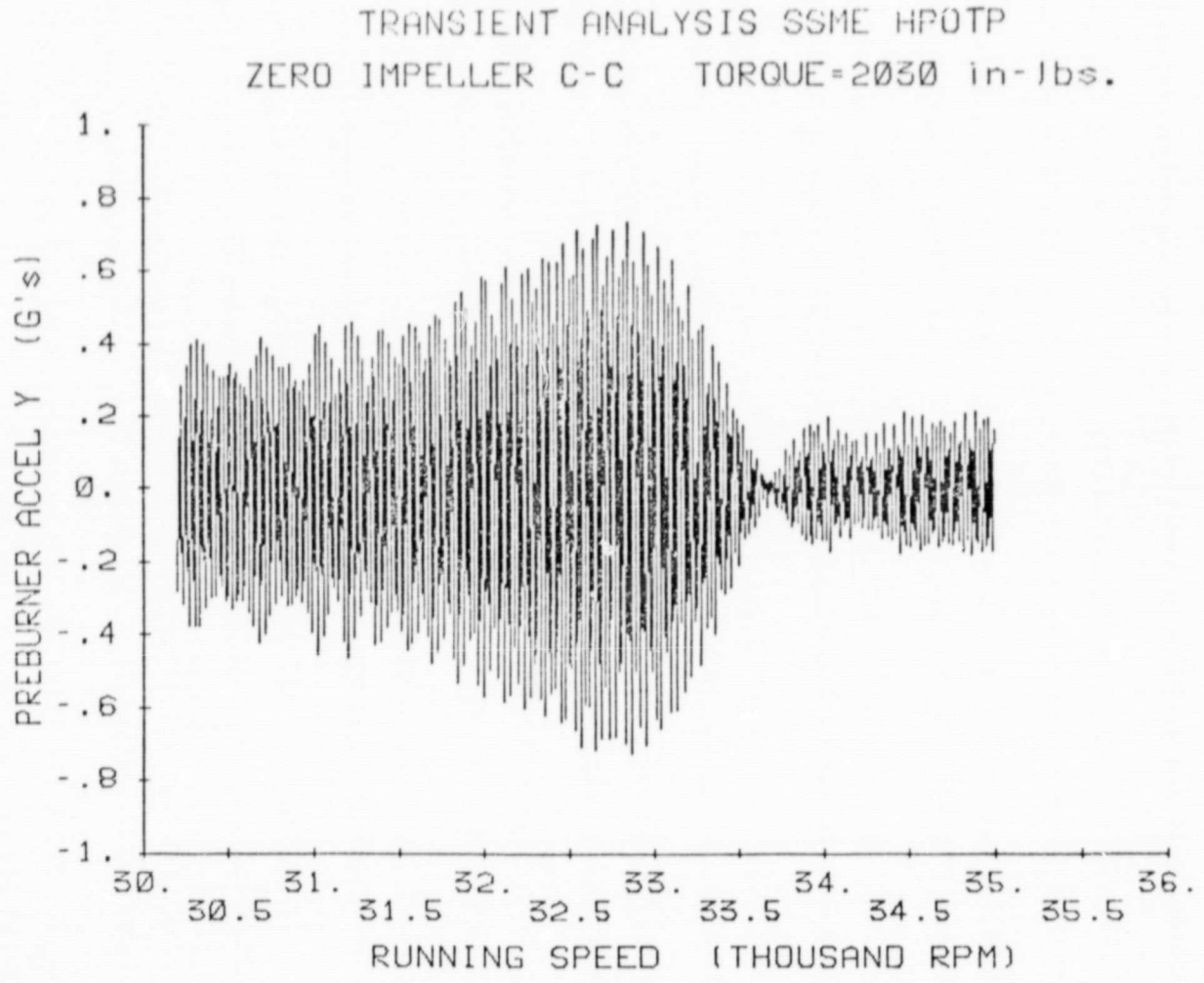

Figure 13(c). Preburner accelerometer amplitudes (g's) in the Y-Z plane for an acceleration from 30,200 to 35,000 rpm with the bearing clearances of Eq.(11), no external bearing damping, and no destabilizing force at the main impeller.

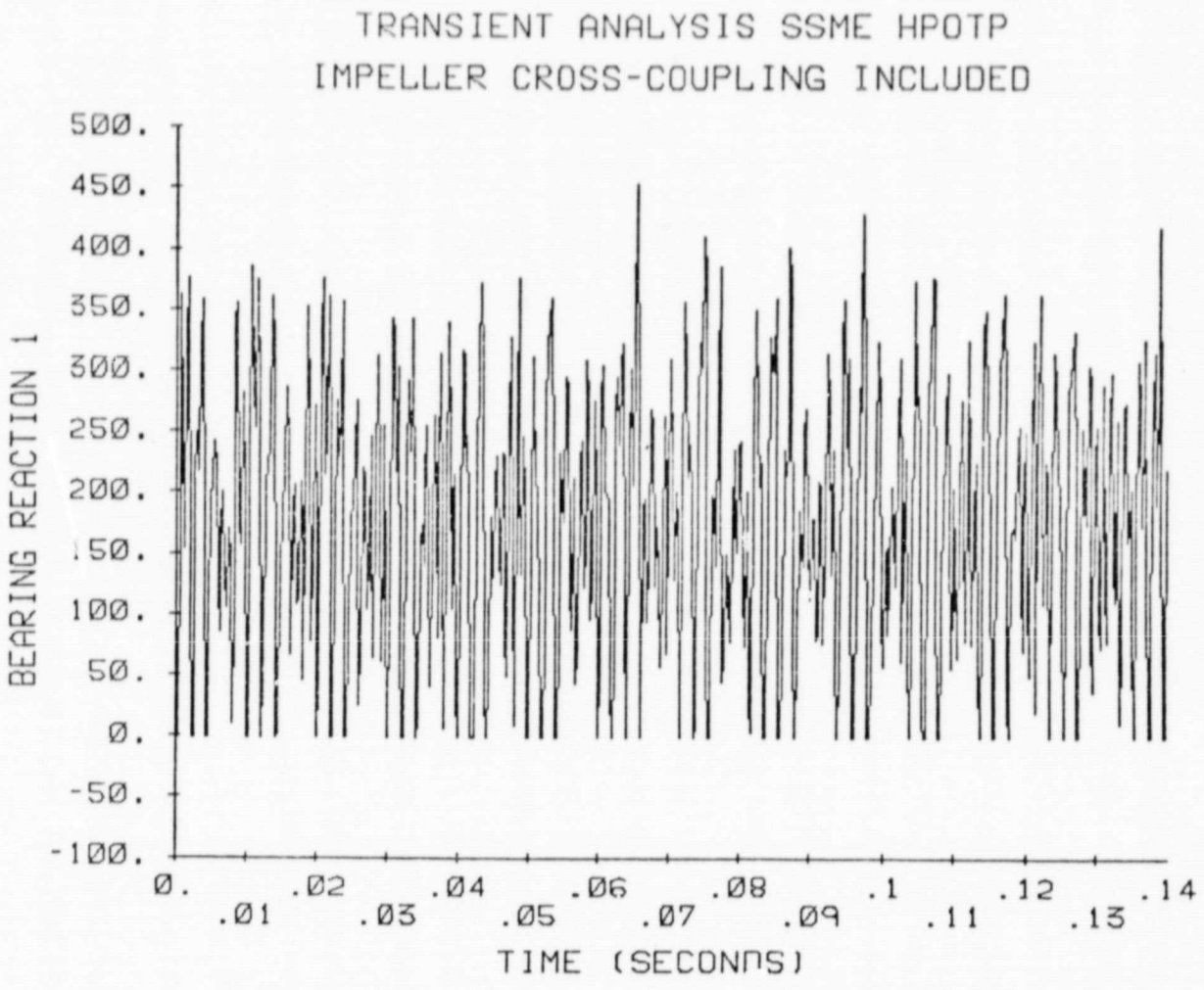

Figure 14(a). Bearing reaction 1 from the transient, nominal, nonlinear model for a simulation of 30,000 rpm running speed.

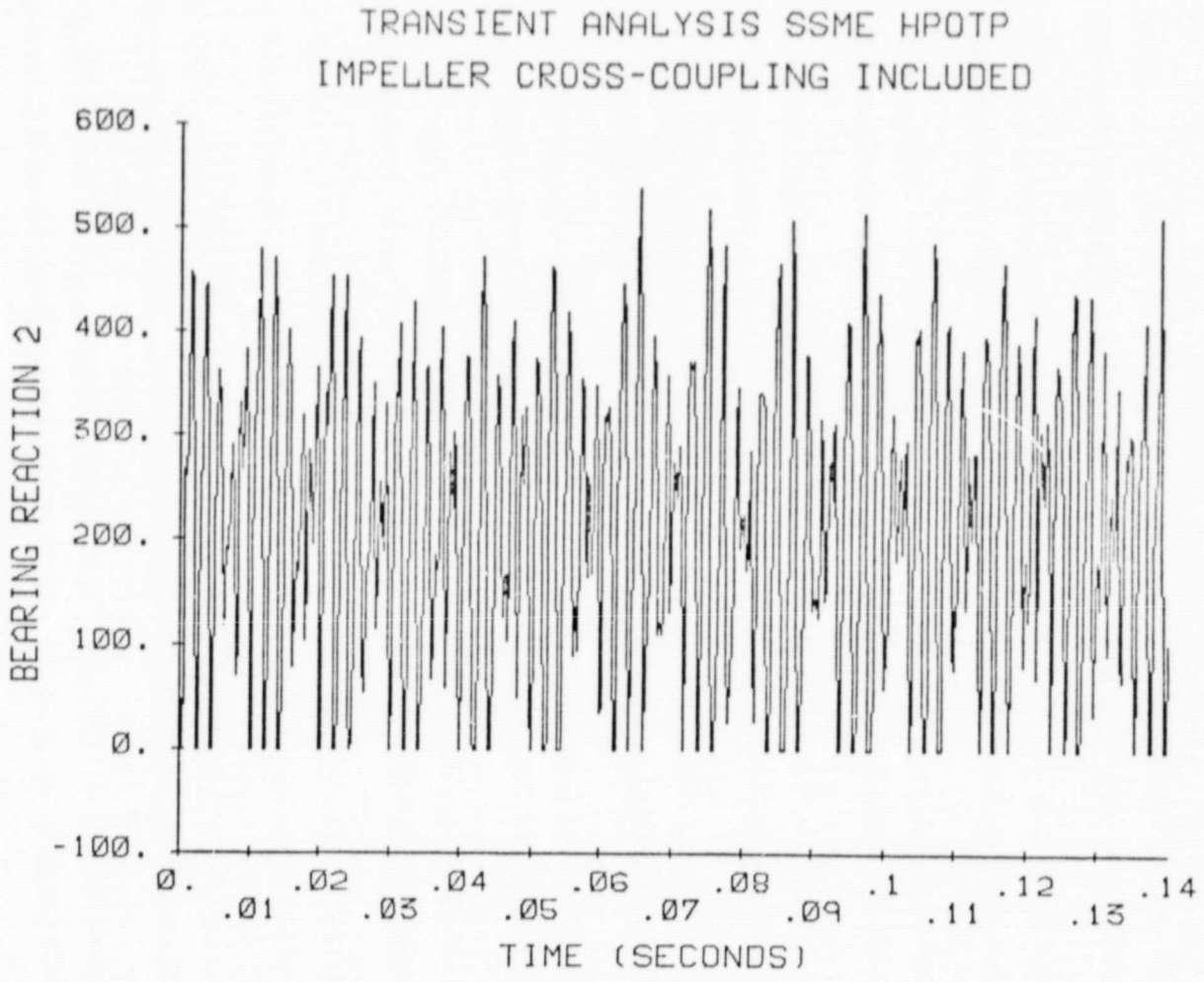

Figure 14(b). Bearing reaction 2 from the transient, nominal, nonlinear model for a simulation of 30,000 rpm running speed.

Figures 14(c) and (d) show the more frequent unloading of bearings 3 and 4. The preburner and turbine accelerometer magnitudes of Figures 14(e) through 14(h) illustrate a "beating" type motion which could be generated by a nonsynchronous frequency near the 30,000 rpm running speed.

Increasing the impeller-cross-coupling coefficients by a factor of 1.29 and 1.57, respectively, causes the following changes in the nominal solution:

(a) Bearing-reaction magnitudes for bearings 1 and 2 are increased, and the frequency at which they become unloaded increases.

(b) Bearing-reaction magnitudes for bearings 3 and 4 are largely unchanged.

(c) The preburner accelerometer magnitudes are relatively unchanged in magnitude; however, the "regular" beating of Figure 14(f) is replaced by the more erratic result of Figure 15(a). Similar results are demonstrated for the turbine accelerometer response illustrated in Figure 15(b).

The results of reducing the bearing stiffnesses by 80% while maintaining the remainder of the nominal model constant are illustrated in the following results of Figure 16:

(a) As illustrated in Figure 16(a), bearings 1 and 2 are no longer periodically unloaded.

(b) The nominal magnitude and variations of bearing reactions for bearings 3 and 4 are reduced as illustrated in Figure 16(b).

(c) The "beating" in the accelerometer levels are largely eliminated as illustrated in Figure 16(c).

The results of the simulations performed above support the expected conclusions with respect to stability and synchronous response amplitudes; however, they do not explain the observed experimental results; specifically, the occurrence of subsynchronous vibrations which track running speed. A more lengthy study, involving extensive simulation runs and spectrum analyses, would be required to advance an explanation. This type of study is beyond the scope-of-work for the present investigation.

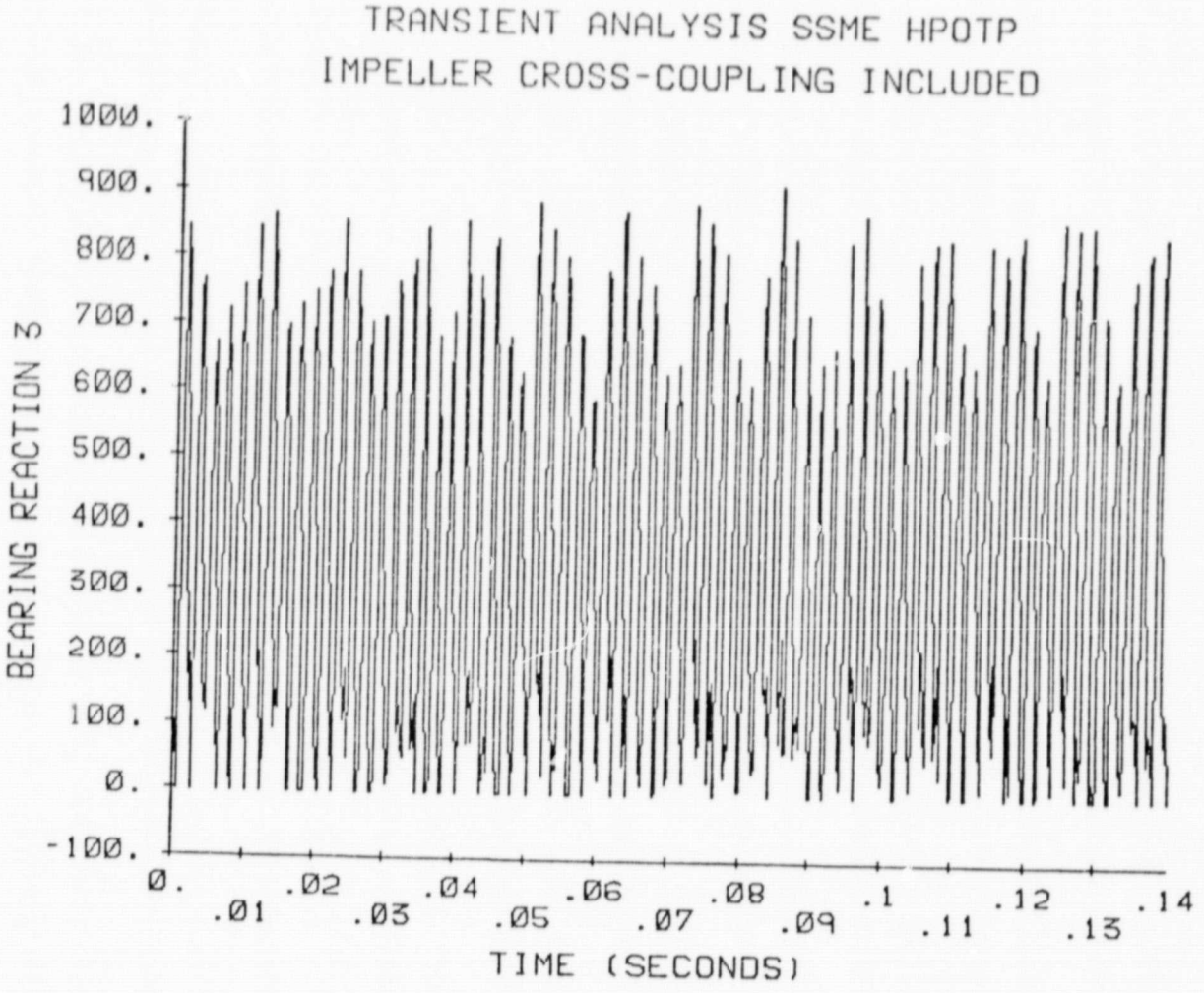

Figure 14(c). Bearing reaction 3 from the transient, nominal, nonlinear model for a simulation of 30,000 rpm running speed.

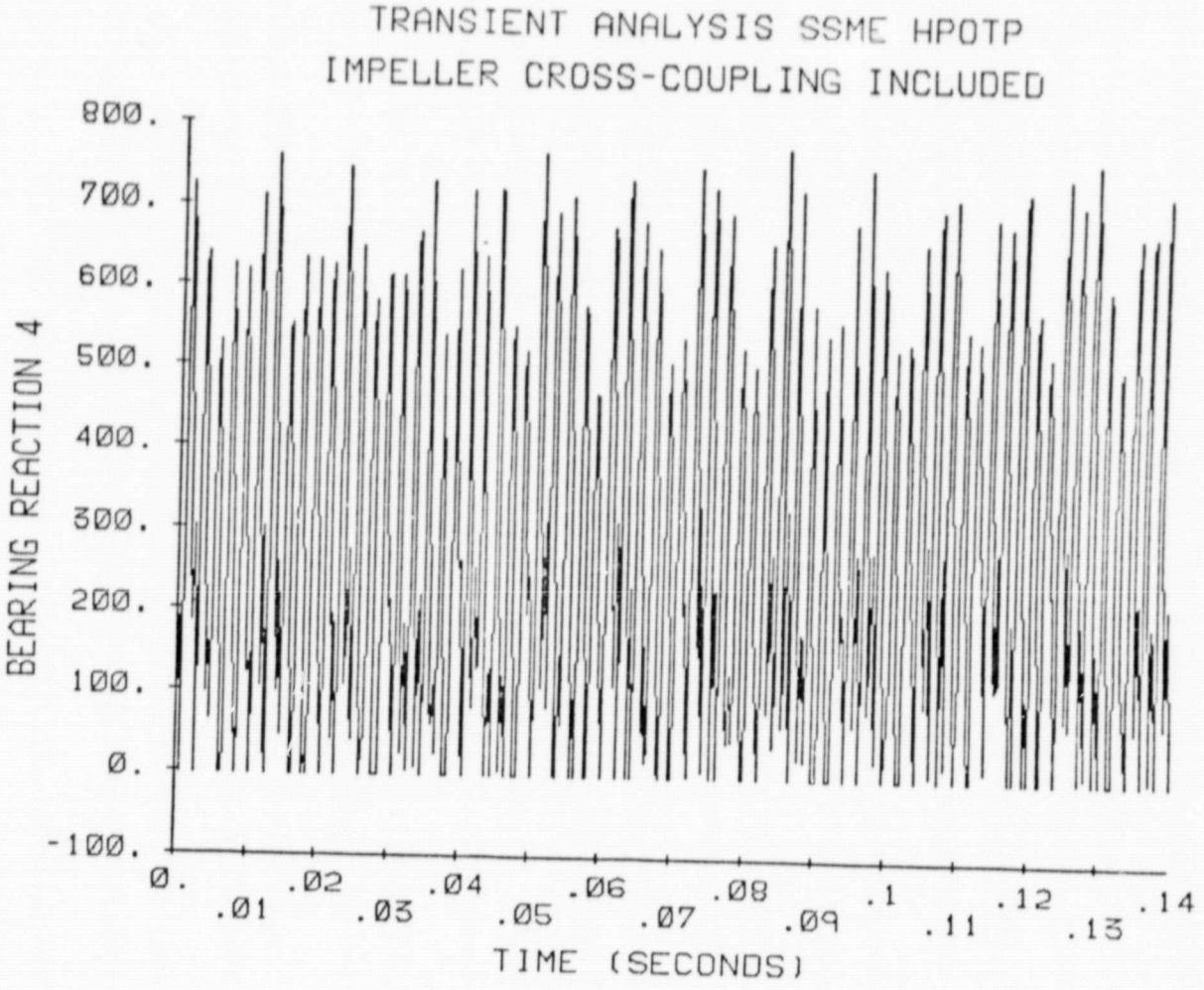

Figure 14(d). Bearing reaction 4 from the transient, nominal, nonlinear model for a simulation of 30,000 rpm running speed.

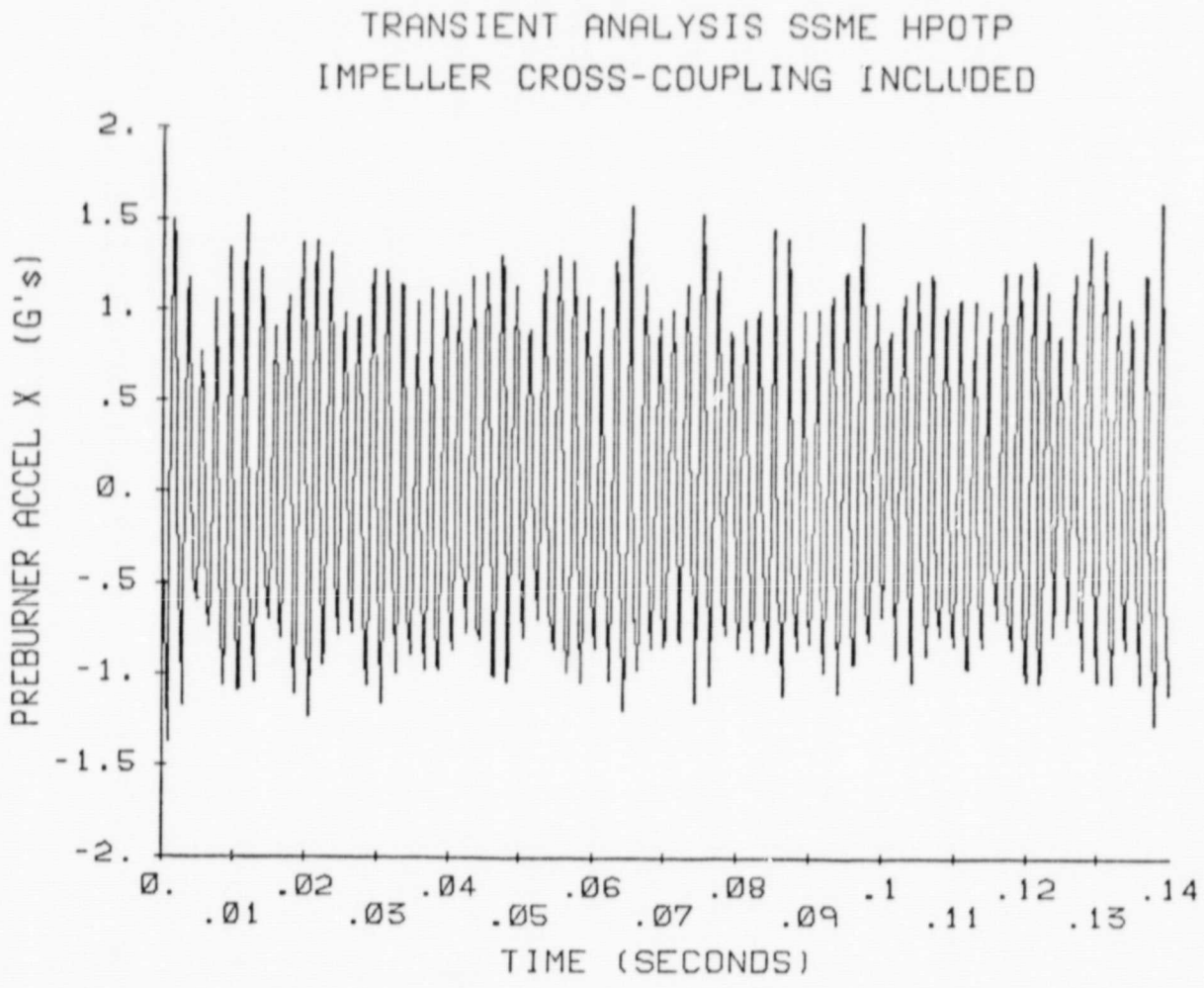

Figure 14(e). Preburner accelerometer in the X-Z plane from the transient, nominal, nonlinear model for a simulation of 30,000 rpm running speed.

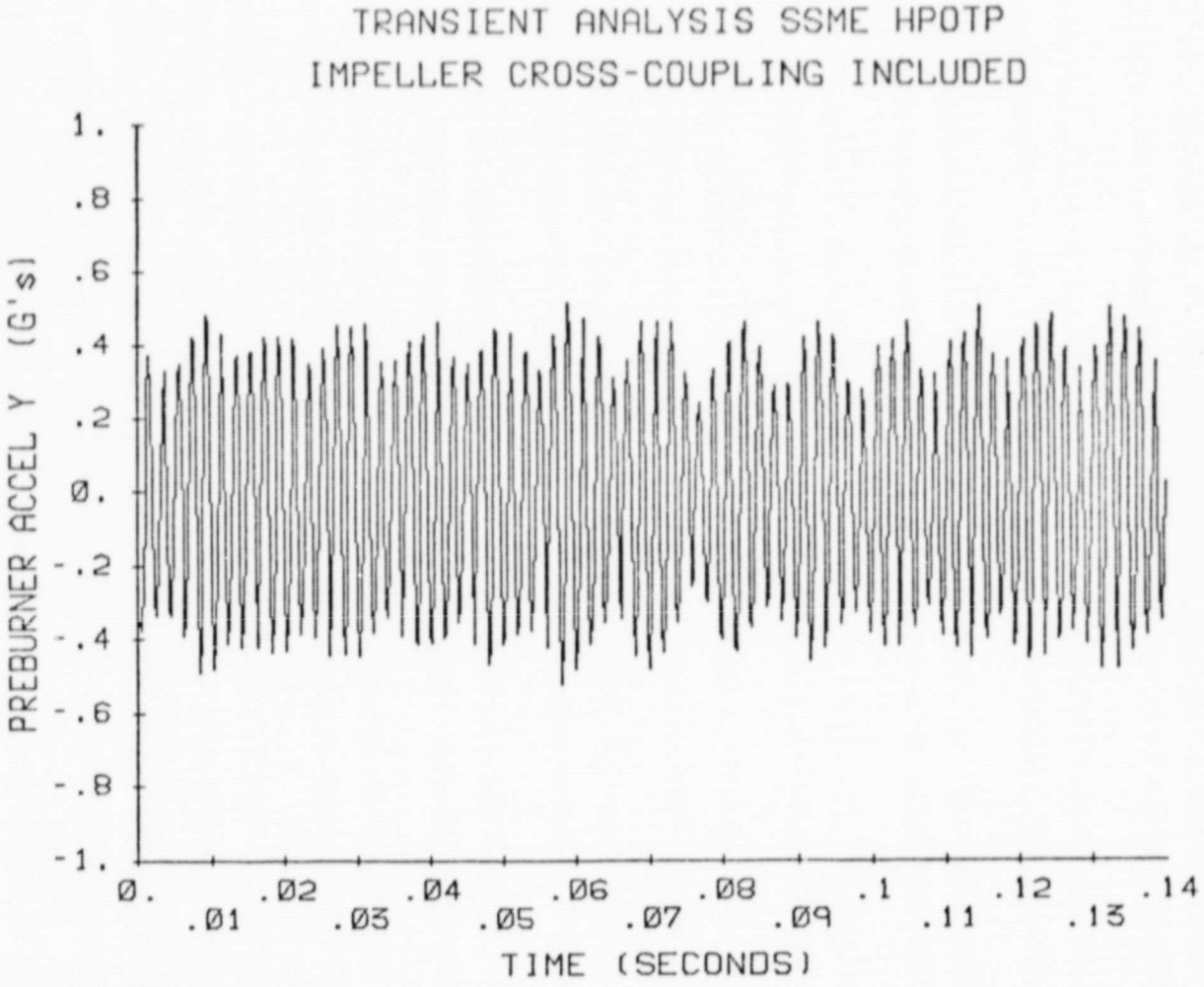

Figure 14(f). Preburner accelerometer in the Y-Z plane from the transient, nominal, nonlinear model for a simulation of 30,000 rpm running speed.

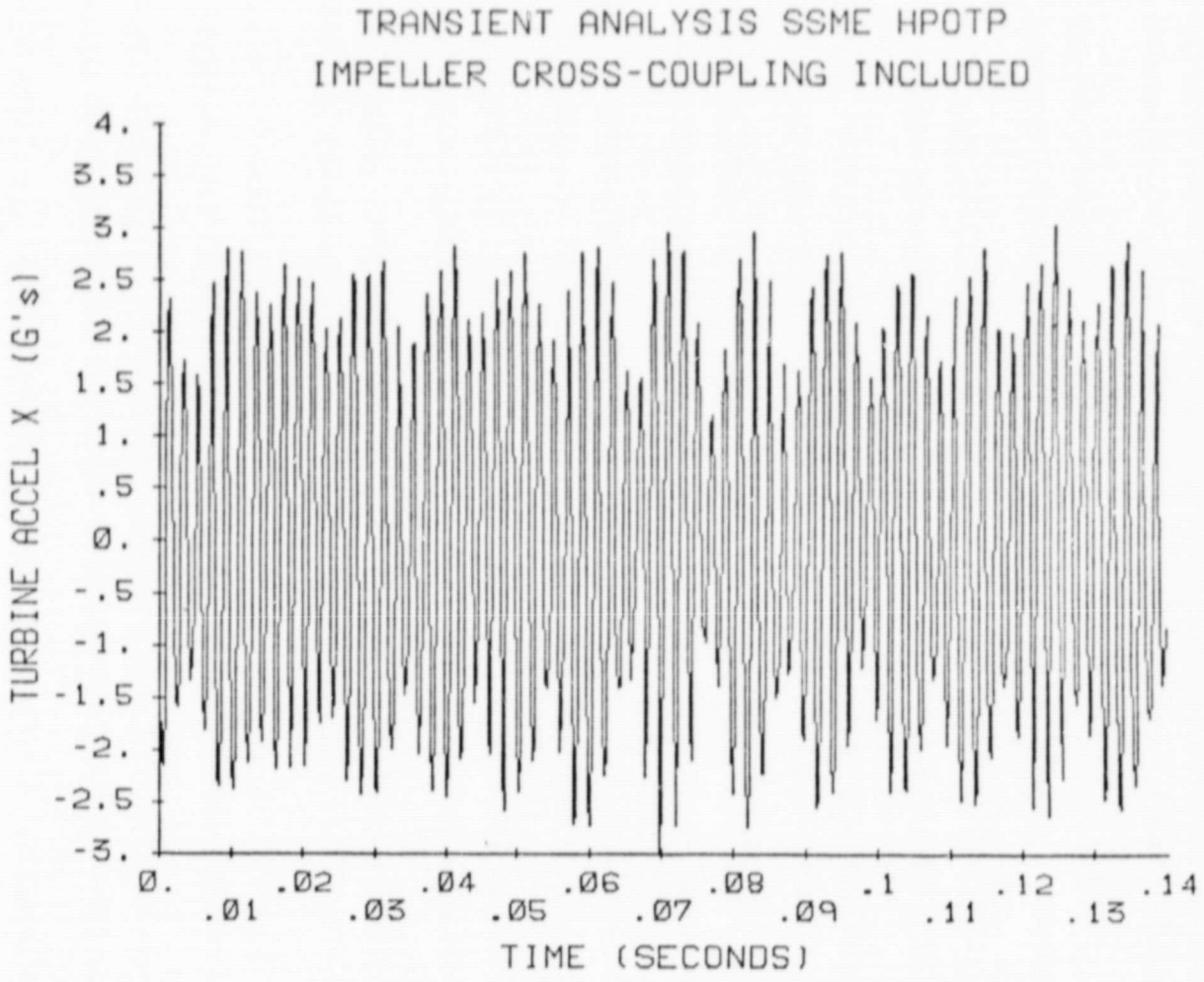

Figure 14(g). Turbine accelerometer in the X-Z plane from the transient, nominal, nonlinear model for a simulation of 30,000 rpm running speed.

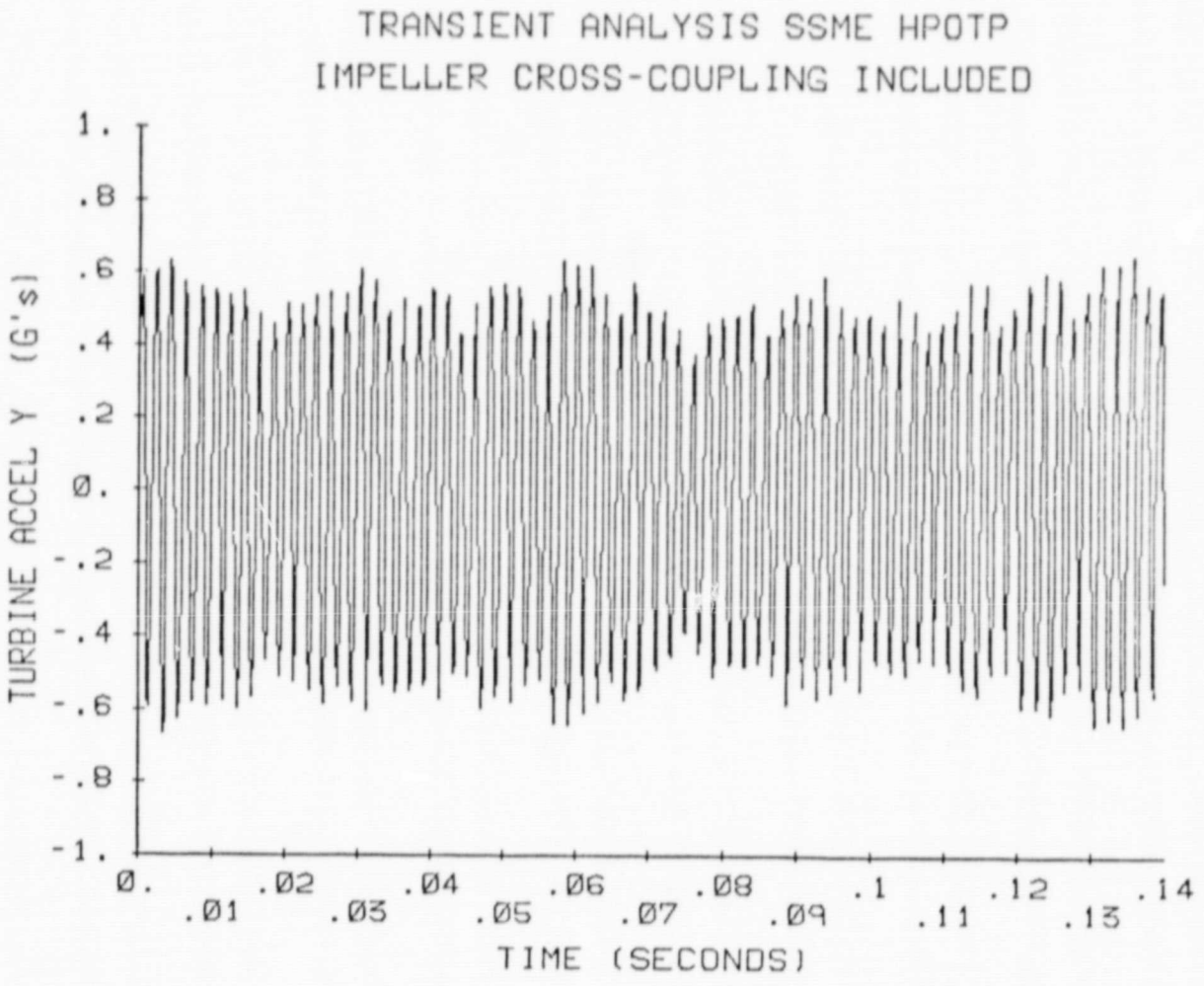

Figure 14(h). Turbine accelerometer in the Y-Z plane from the transient, nominal, nonlinear model for a simulation of 30,000 rpm running speed.

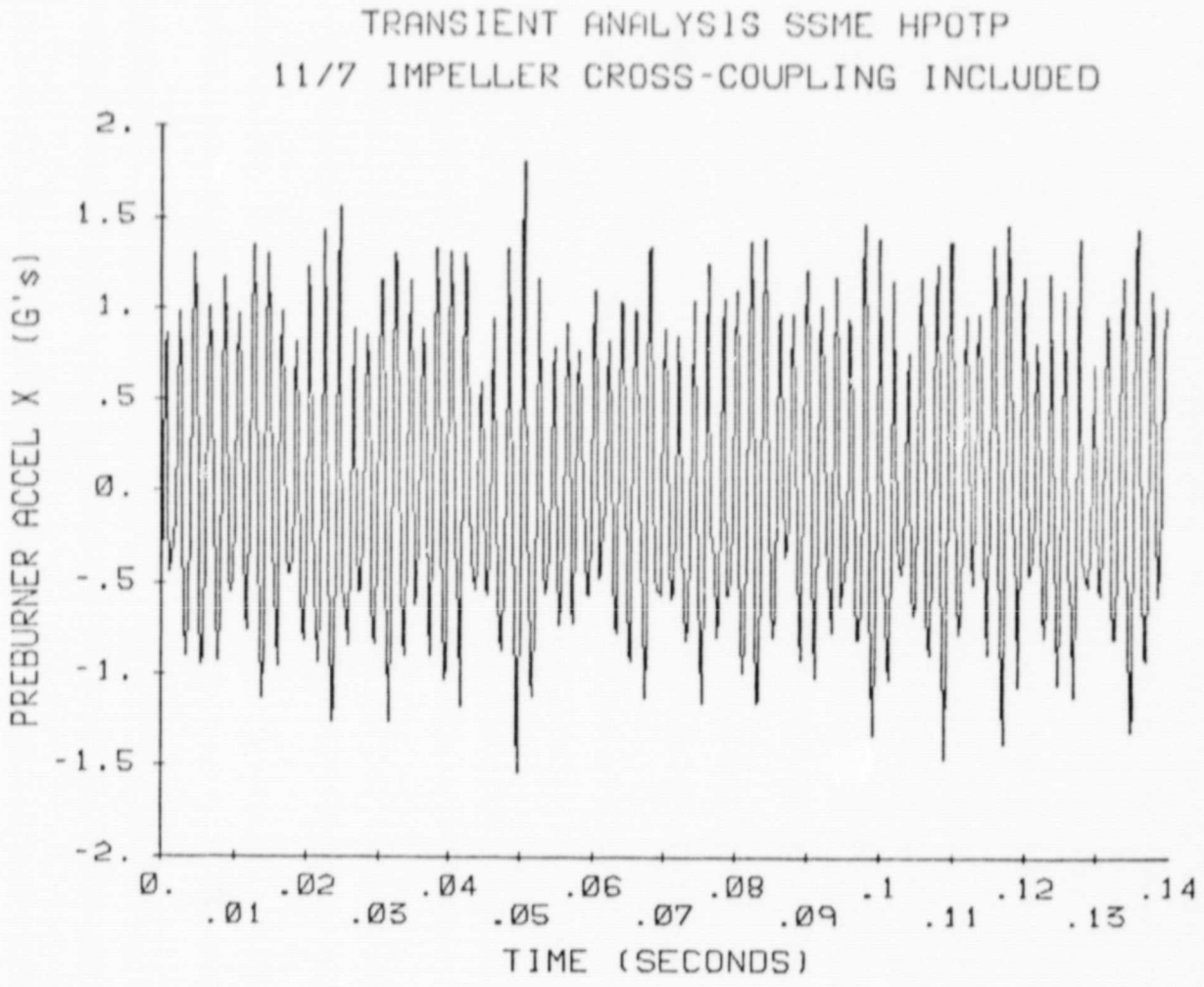

Figure 15(a). Preburner accelerometer levels in the X-Z plane from the transient, nominal, nonlinear model at 30,000 rpm for an increase in the main impeller cross-coupling coefficient by the factor 1.57.

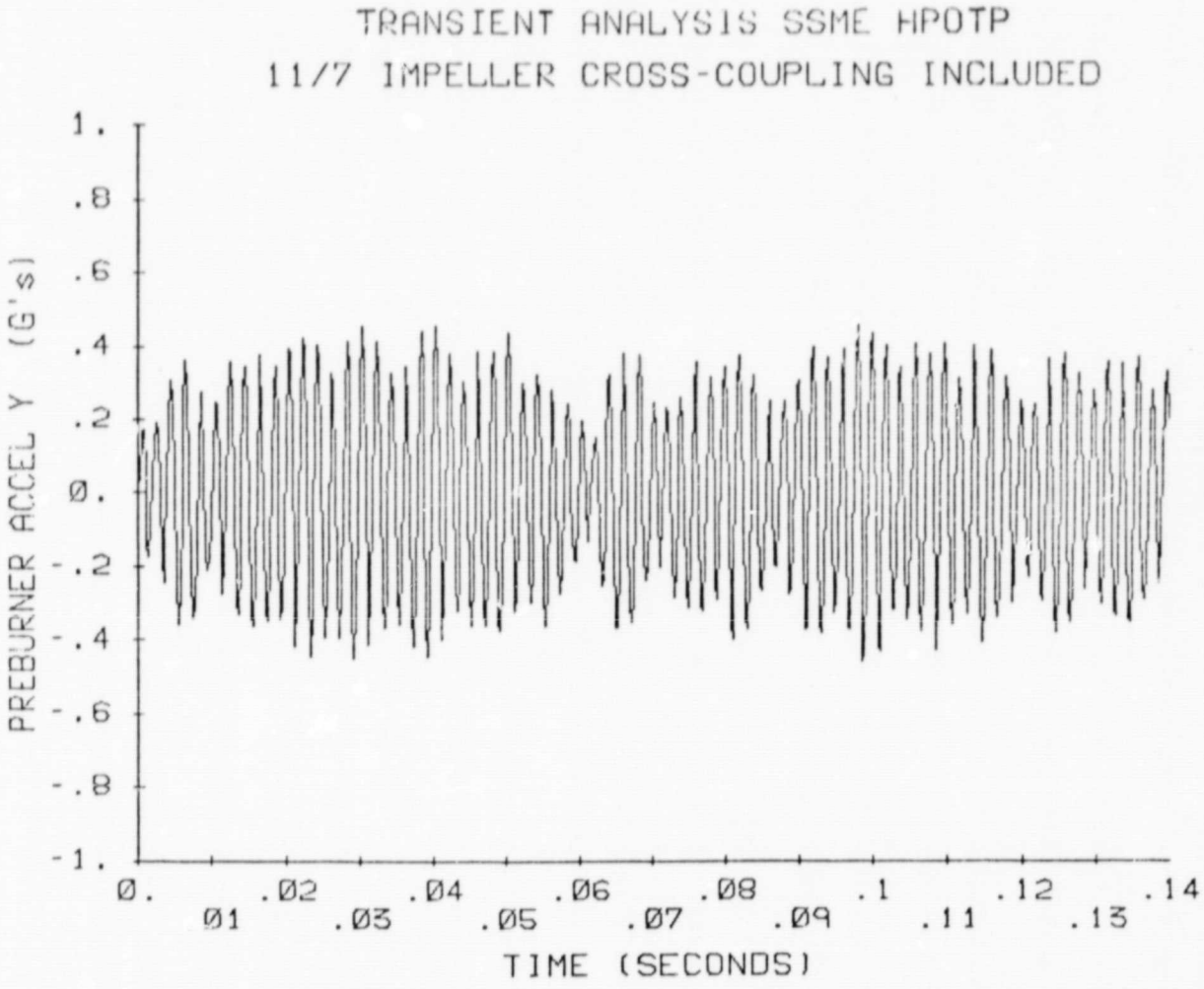

Figure 15(b). Preburner accelerometer levels in the Y-Z plane from the transient, nominal, nonlinear model at 30,000 rpm for an increase in the main impeller cross-coupling coefficient by the factor 1.57.

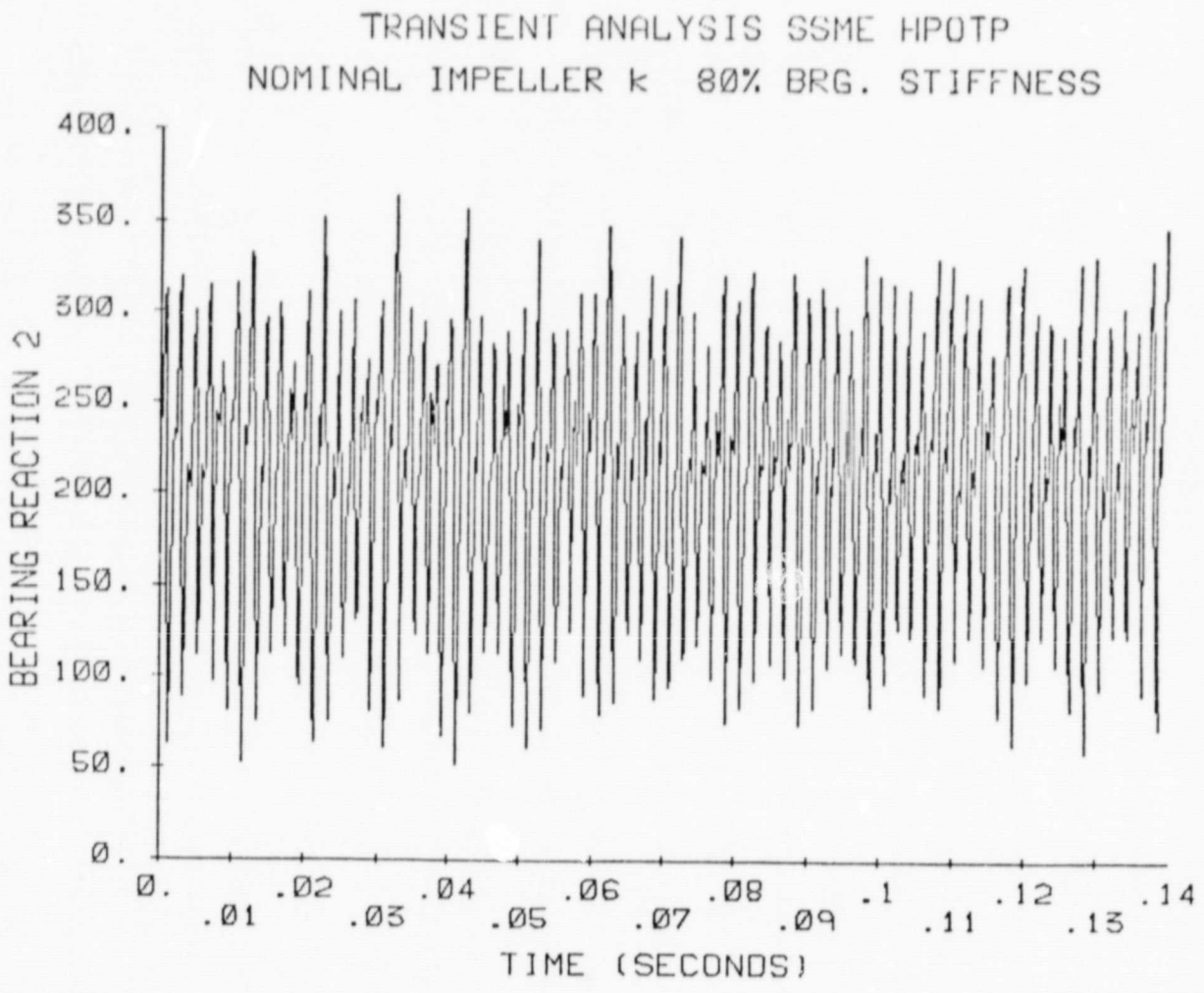

Figure 16(a). Bearing 2 reaction magnitude for the nominal model with all bearing stiffnesses reduced by 80%.

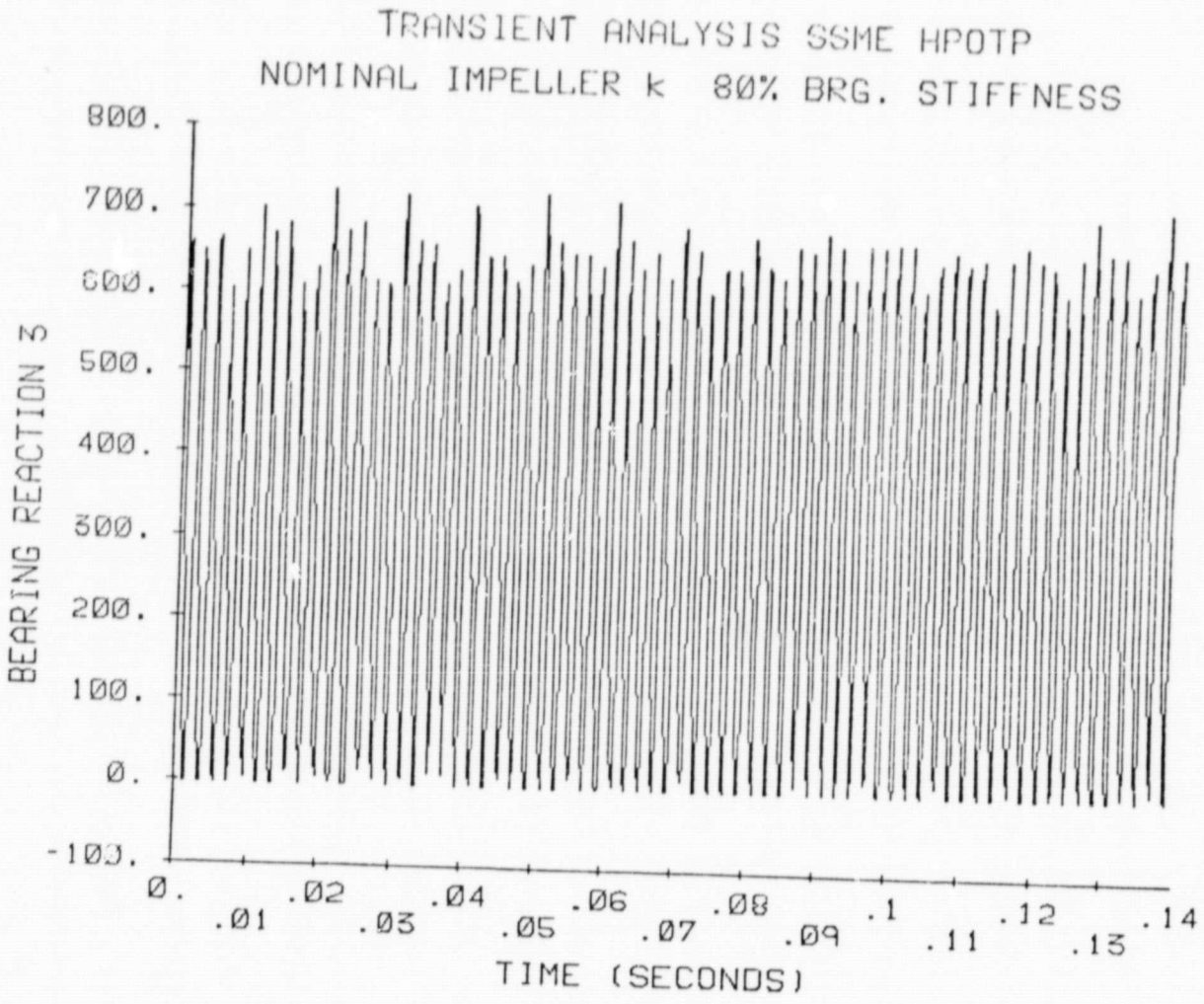

Figure 16(b). Bearing 3 reaction magnitude for the nominal model with all bearing stiffnesses reduced by 80%.

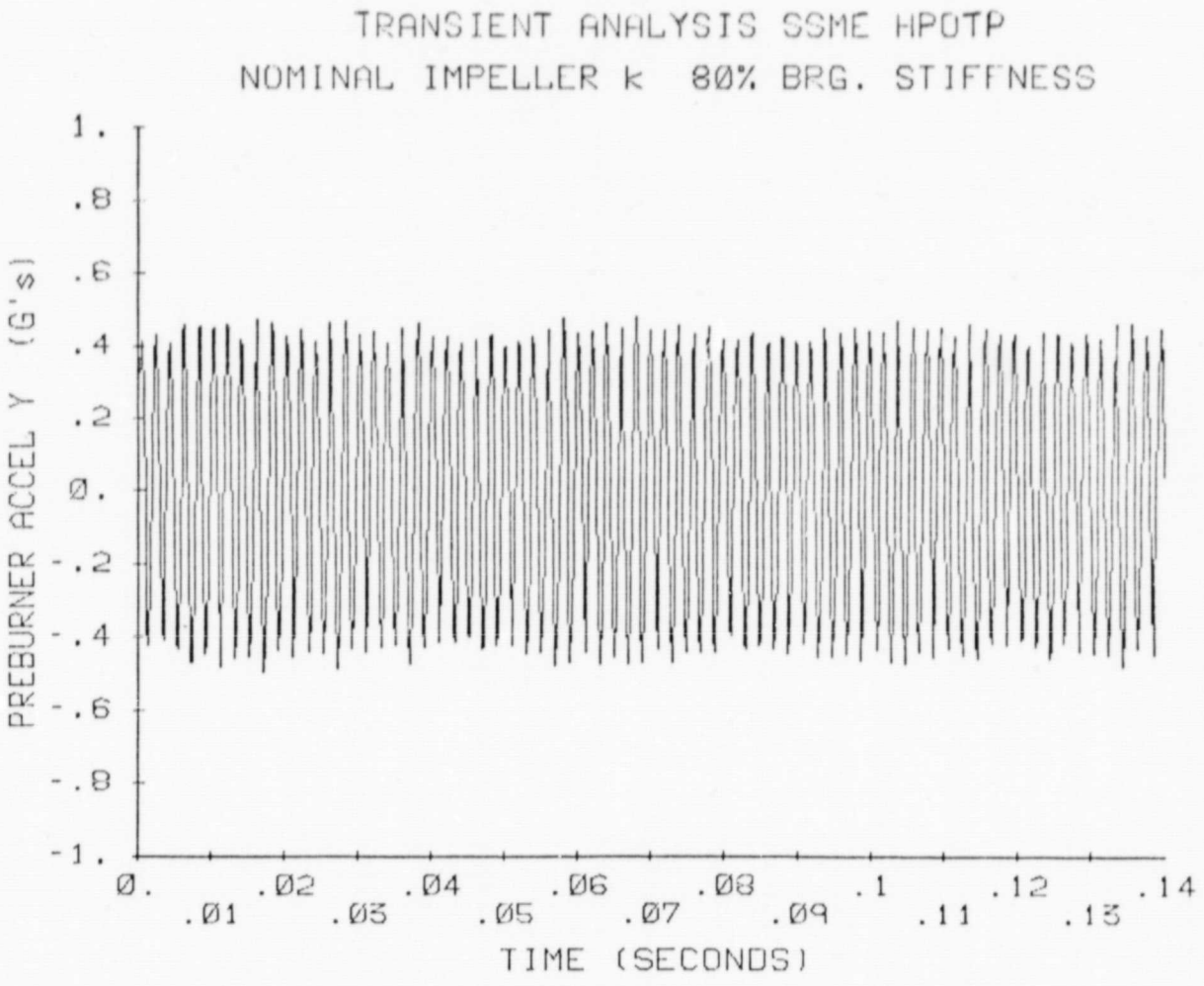

Figure 16(c). Preburner accelerometer magnitude in the Y-Z plane for the nominal model with all bearing stiffnesses reduced by 80%.

I. Summary and Conclusions for the HPOTP

The rotordynamic characteristics of the HPOTP involve problems with both subsynchronous motion associated with the second critical speed and synchronous response amplitudes due to operation near the second critical speed. The pertinent linear results are summarized in Table 2, and support the following general conclusions:

(a) Both synchronous-response and OSI characteristics are sensitive to bearing stiffnesses. Generally speaking, the situation would be improved by increasing the bearing stiffness; however, no feasible approach is available to further increase the bearing stiffnesses.

(b) Loss of stiffness in bearing will generate critical speeds within the speed range which could explain some of the subsynchronous frequencies observed in practice. Very large bearing reactions are predicted if the second critical speed drops into the operating range.

(c) Replacement of the current labyrinth configuration for the inlet seal of the boost impeller by either a smooth constant clearance seal or a damper seal will elevate the OSI by approximately 14% and reduce the bearing loads by approximately 25%. These are feasible options in the HPOTP.

(d) Replacing the current labyrinth configuration for the discharge seal of the preburner impeller elevates the OSI by 37% and reduces the bearing reactions by approximately 50%. Unfortunately, due to bearing-lubricant flow limitations, this does not seem to be a viable option.

(e) Introducing shrouded inducers with seals eliminates subsynchronous vibration problems associated with the second critical speed. Bearing

Configuration	Frequency Results			Bearing Reaction Results (N)				
	Second Critical Speed(rpm)	OSI (rpm)	Whirl Frequency (Hz.)	Reference Speed(rpm) for Calculation	Brg.1	Brg.2	Brg.3	Brg.4
1. Nominal	32,500	30,430	540	30,500	2,527	2,835	2,780	2,433
2. 50% Bearing Stiffnesses	25,020	21,950	417	25,020	22,820	23,950	18,281	15,150
3. 150% Bearing Stiffnesses	38,750	25,300	646	30,500	934	1,090	867	506
4. Bearing 2 - Zero Bearing Stiffness	26,420 27,890 29,370	32,640	444	26,420	15,710	0.0	10,680	88.20
5. Preburner Impeller Seals								
a. Smooth Inlet	33,000	34,580	550	30,500	1,780	2,120	2,410	1,950
b. Damper Inlet	32,900	34,980	550	30,500	1,830	2,160	2,430	1,970
c. Smooth Discharge	34,500	41,640	575	30,500	1,130	1,430	1,780	1,400
6. Inducer Seals	eliminated	>>40,000	eliminated	30,500	518	540	410	410
7. Inducer Seals plus Preburner Inlet Damper Seal	eliminated	>>40,000	eliminated	30,500	406	464	410	398

Table 2. Summary of linear analysis results for HPOTP configurations.

loads are reduced by a factor of 5~6 by this modification. On a linear basis, shrouded inducer seals are the only proposed change which absolutely eliminates the current problems.

(f) Changes in either the clearance-excitation forces or the turbine-interstage seal coefficients have little or no effect on either synchronous or subsynchronous motion associated with the second critical speed. They do have a significant influence on motion associated with the first critical speed.

(g) The bearing clearances investigated have a pronounced influence on both synchronous and subsynchronous amplitudes associated with the second critical speed. Specifically, they sharply reduce the bearing-reaction amplitudes which would be obtained for zero-bearing clearances. Further, in combination with the fixed-direction side loads acting on the turbopump rotor, they substantially enhance rotor stability.

III. ANALYSIS RESULTS FOR THE HPFTP

A. Introduction

The principal rotordynamic difficulties which have been experienced with the HPFTP involve a conventional rotordynamic instability problem associated with the first or lowest critical speed [2]. This instability problem arose because of the following factors:

(a) A softly-supported bearing design yielded a first-critical speed at 10,000 rpm as compared to the FPL (Full Power Level) running speed of 37,360 rpm.

(b) The unshrouded turbines yield relatively large predictions of destabilizing forces, and the original turbopump design provided no significant sources of damping.

This problem was remedied by stiffening the bearing supports and eliminating grooves in the interstage seals. Stiffening the bearing supports elevates the undamped critical speeds of the rotor-housing system, and eliminating the interstage seal grooving markedly increases the stiffness and damping forces due to relative motion between the rotor and housing. The initial interstage seal modification eliminated the grooving in the original seal design but retained the stepped configuration, yielding a "smooth-stepped" configuration. Subsequently, a seal having the same general dimensions but with a convergent-taper geometry has been employed. The taper angle in this configuration is relatively small and is provided to restrict any two-phase flow condition to the seal exit. Despite the taper, this configuration has generally been referred to as a "smooth-straight" configuration. The current flight hardware employs the "straight-smooth" seal configuration.

The principal changes which have arisen since the last examination of HPFTP rotordynamics [4] involve (a) replacement of the "smooth-stepped"

interstage configuration with the "smooth-straight", and (b) development of extensive test data for both configurations from a test program at Texas A&M University [9]. This chapter examines the influence of changes in the interstage seal rotordynamic coefficients on the rotordynamic characteristics of the HPFTP, and also considers reasonable variations [1]. of other parameters of importance.

Only linear analysis procedures are used in the current investigation of HPFTP rotordynamics. The influence of nonlinear effects due to "dead-band" bearing clearances are considered for the HPOTP in Chapter II. They were examined in reference [4] for the HPFTP, and are notably less important for the HPFTP than the HPOTP because of the following factors:

(a) the clearances are smaller for the HPFTP; 6.35 μm versus 25.4 μm, and

(b) the spring constants of the interstage seals reduce the degree of discontinuity experienced when moving through the "dead band". More specifically, the seal stiffnesses are comparable to the bearing stiffness, and are not influenced by motion through the bearing clearances; hence, there is never a complete loss in radial stiffness between the rotor and housing.

B. The Nominal Model

The nominal model is based on best estimates of parameters for the current flight hardware. The fixed data cited in Chapter I define the basic structure of the nominal model. The remaining data used to define the nominal model are discussed below:

Bearing Stiffnesses

The four bearings are identified numberically, proceeding from the pump inlet to the turbine. The nominal bearing stiffnesses used are

$$K_{bi} = 8.76 \times 10^7 \text{ N/m } (.5 \times 10^6 \text{ lb/in}); \; i = 1,2,3,4 \qquad (12)$$

Impeller Cross-Coupling Coefficients

Table A.6 defines the nominal coefficients.

Clearance Excitation Forces

The nominal clearance-excitation force coefficient is based on the data of Table A.7.

Seal Coefficients

The nominal rotor model accounts for seal configurations used in the current flight hardware; in particular, the nominal model uses the smooth-straight seal coefficients of Table A.5(b).

Damping

No damping was used in the rotor model at the bearings or elsewhere.

Imbalance Distribution

An imbalance of .1524 gm-m (6 gm in) between the main impeller was used for all cases. This imbalance distribution provides adequate excitation for all modes.

C. The Influence of Changes in Bearing Stiffnesses

Introduction

The principal direct influence of a change in bearing stiffnesses is a change in the location of critical speeds. Results are presented in this section for the dynamic characteristics of the following configurations:

(a) nominal model,

(b) nominal model with bearing stiffnesses reduced 50%, and

(c) nominal model with bearing stiffnesses increased by 50%.

Nominal Model

Figure 1 illustrates the local coordinate system used for definition of HPFTP rotor and housing motion. The frames of Figure 17 illustrate the synchronous response characteristics of the nominal model. Recall that the nominal model uses $K_{bi} = 8.76 \times 10^7$ N/m ($.5 \times 10^6$ lbs/in) for the

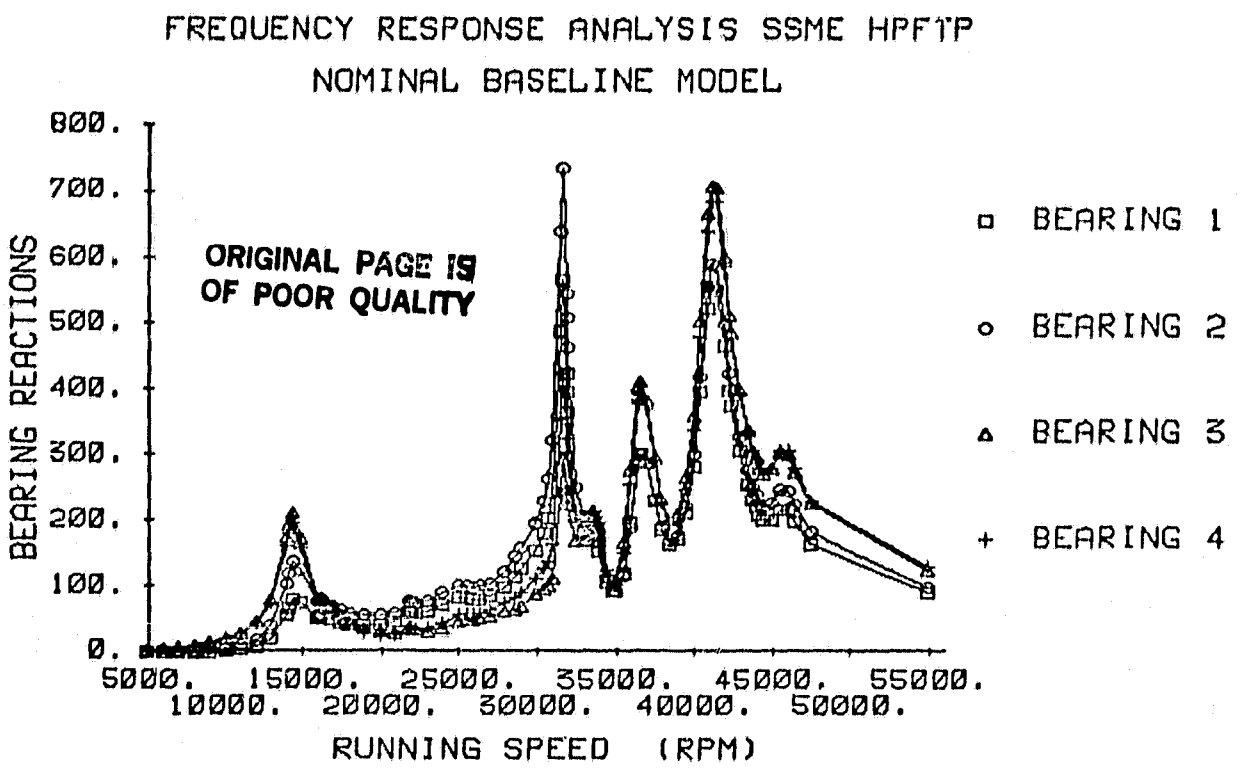

Figure 17(a). Synchronous response solutions for bearing reactions of the nominal HPFTP model.

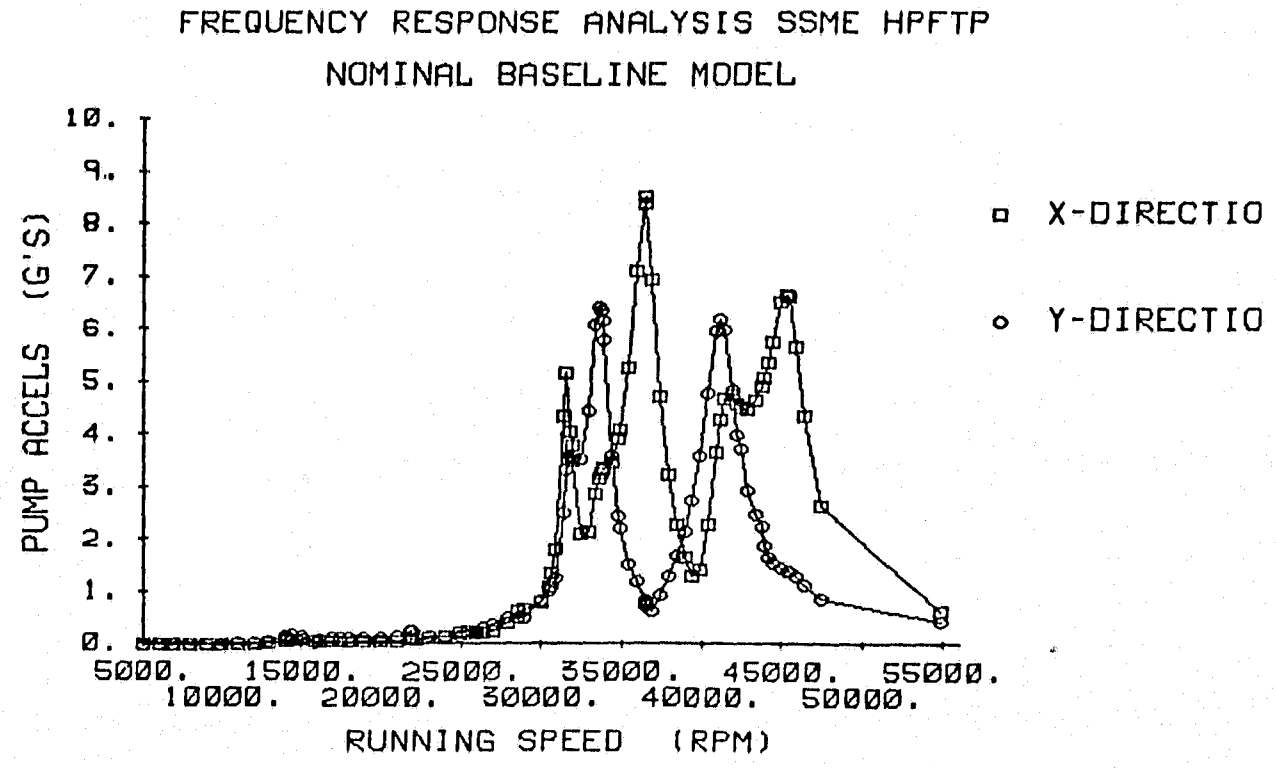

Figure 17(b). Synchronous response solutions for preburner accelerometer magnitudes of the nominal HPFTP model.

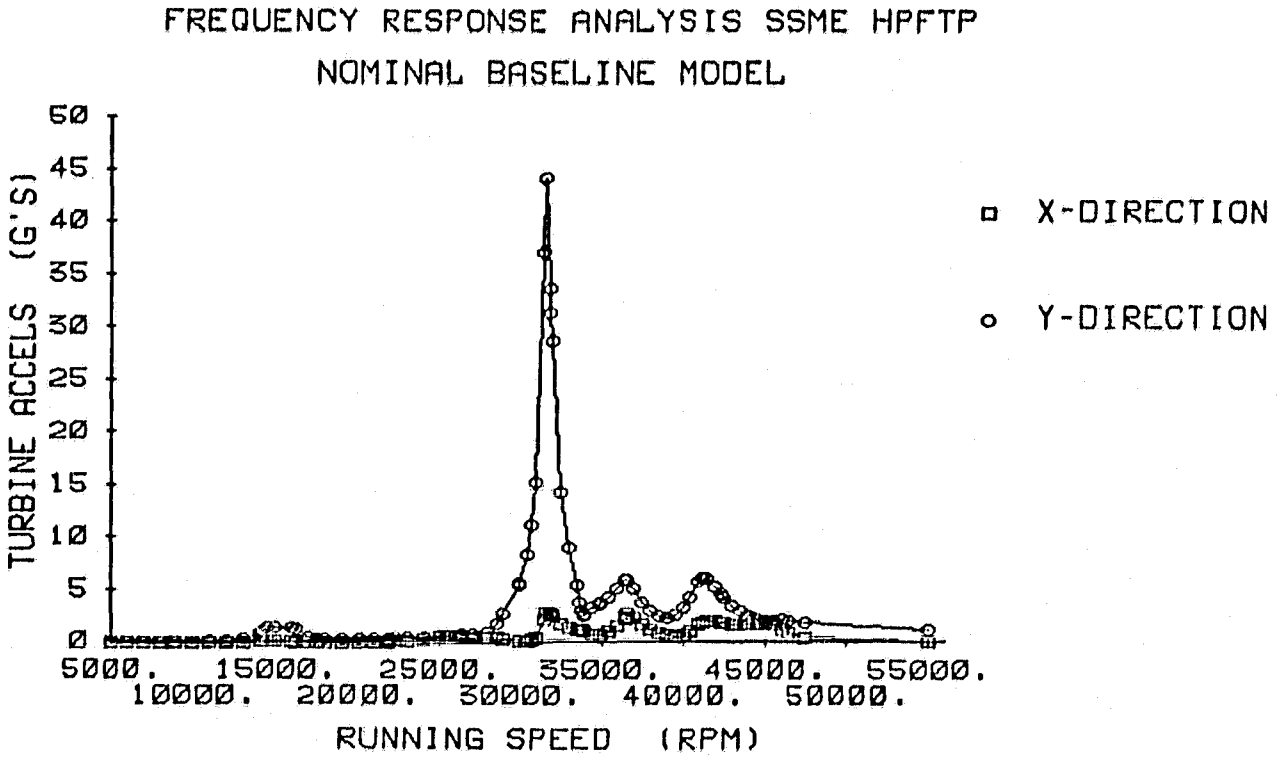

Figure 17(c). Synchronous response solutions for turbine accelerometer magnitudes of the nominal HPFTP model.

bearing stiffnesses and the rotordynamic coefficients for the "smooth-straight" seal. The MPL (Minimum Power Level), RPL, (Rated Power Level) and FPL (Full Power Level) running speeds are 23,700, 35,000, and 37,400 rpm, respectively. Hence, the second and third rotor-housing critical speeds at 31,600 and 36,600 rpm are of primary concern from a bearing-reaction viewpoint.

By comparison to Figure 2, the HPFTP nominal model is seen to display a higher degree of assymmetry. This is particularly notable in the turbine accelerometer results of Figure 17(c) which shows very high g levels in the Y-Z plane and minimal response in the X-Z plane associated with the critical speed located at 31,600 rpm. Similarly Figure 17(b) shows alternate peaks in the X and Y directions as the speed increases.

Figure 18 illustrates the coupled rotor-housing modes which are primarily responsible for the first critical speeds around 14,450 rpm. The modes in the X-Z and Y-Z planes have approxiamately equal eigenvalues and very similar mode shapes. The mode shapes would predict substantially larger bearing reactions for bearings 3 and 4 than bearings 1 and 2. Further, the large amplitudes in the center of the rotor would explain the effectiveness of the interstage seals in providing effective damping for the first critical speed.

Figure 19 illustrates the Y-Z plane mode shape which is responsible for the sharp critical speed near 31,600 rpm. This is a closely-coupled rotor-housing mode with comparatively small relative deflections between the rotor and housing at the interstage seal locations. This might account for the very sharp peak evidenced in Figures 17(a) and 17(c). The rotor mode shape is Figure 19 resembles the first bending modes of Figure 18.

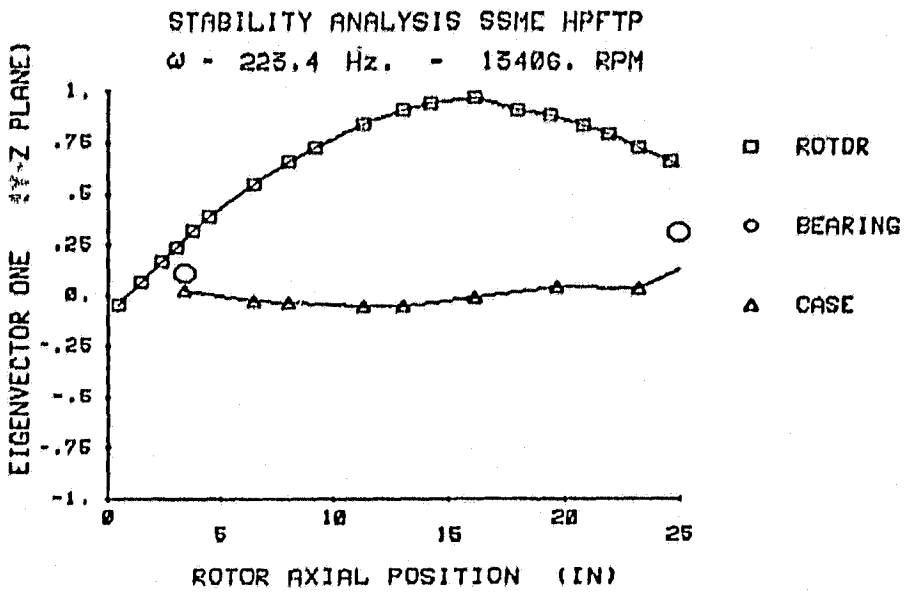

Figure 18(a). Coupled rotor-housing mode in the X-Z plane which is associated with the first HPFTP critical speed.

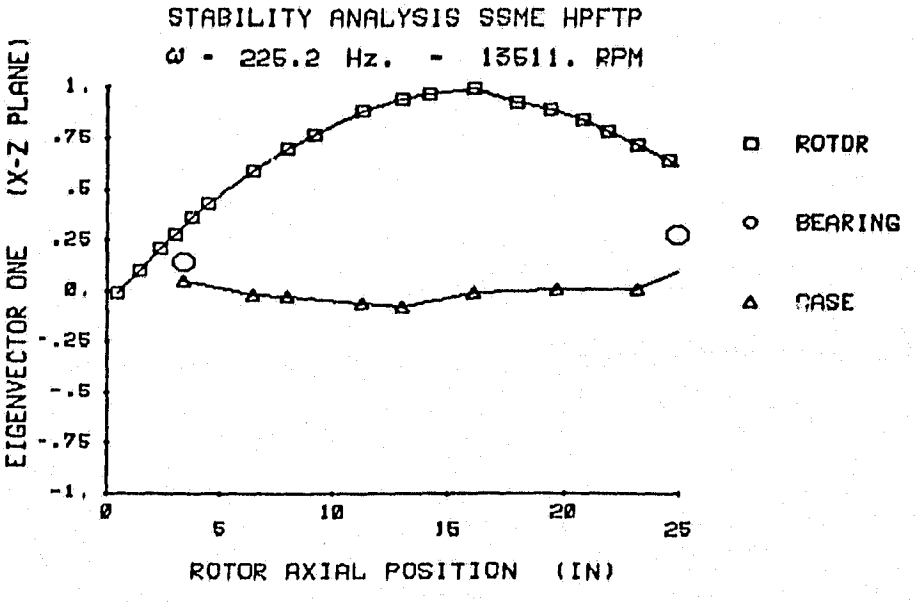

Figure 18(b). Coupled rotor-housing mode in the Y-Z plane which is associated with the first HPFTP critical speed.

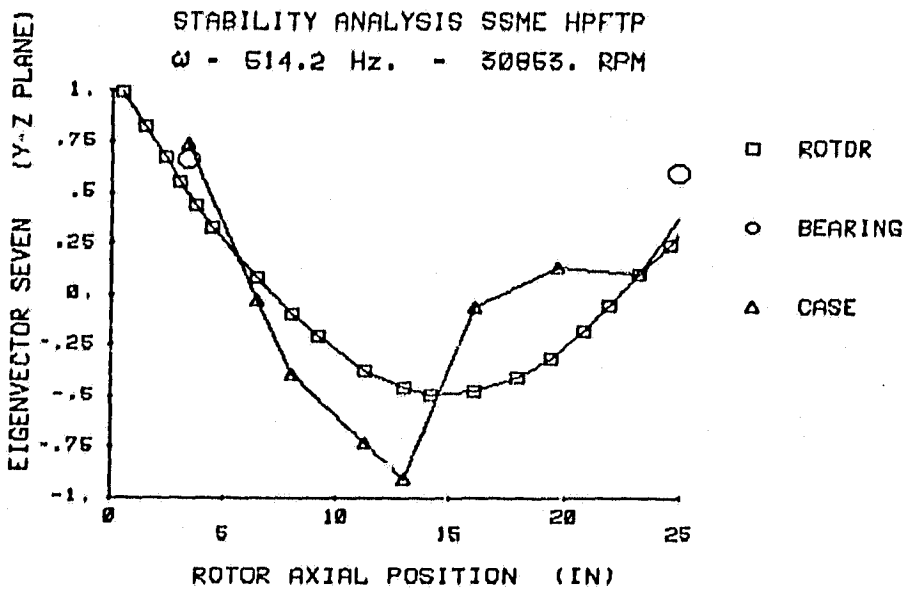

Figure 19. HPFTP coupled rotor-housing mode in the Y-Z plane which is associated with the critical speed at 31,600 rpm.

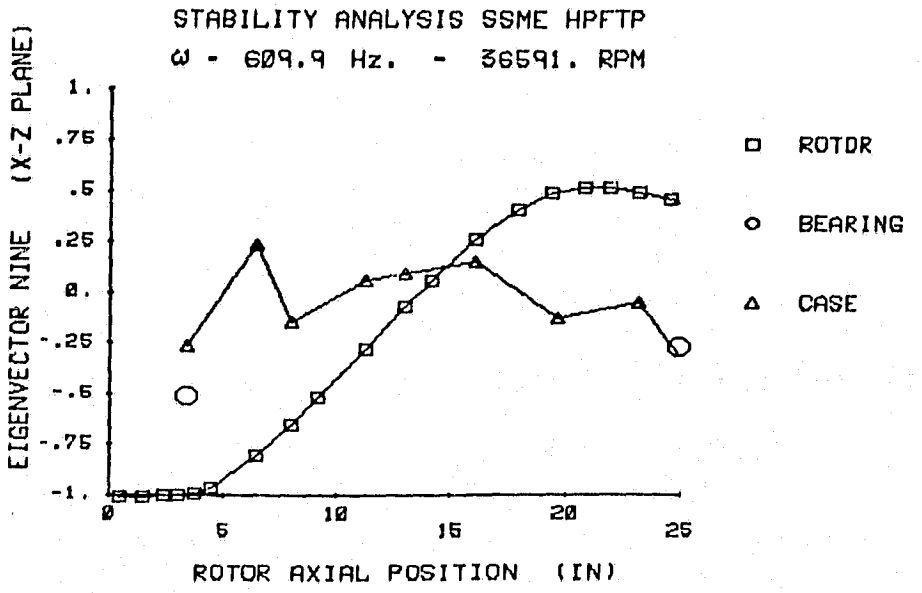

Figure 20. HPFTP coupled rotor-housing mode in the X-Z plane which is associated with the nominal-model critical speed at 36,600 rpm.

Figure 20 illustrates the rotor-housing mode which is primarily responsible for the critical speed at 36,600 rpm. Note that the rotor mode shape resembles a second-critical speed mode shape for a beam supported by bearings with zero motion of the housing. The comparatively small displacement at the midspan of the rotor would suggest that the damping and stiffness provided by interstage seals should have a minimal influence on this mode.

The nominal model predicts an OSI of 66,000 rpm with an associated whirl frequency of 360 Hz. At FPL, the mode which is eventually predicted to become unstable has 3.78% of critical damping. The peak bearing reactions occur at 31,600 rpm and are

$$R_1 = 2{,}520 \text{ N } (566 \text{ lbs}), \quad R_2 = 3{,}280 \text{ N } (738 \text{ lbs})$$
$$R_3 = 1{,}300 \text{ N } (294 \text{ lbs}), \quad R_4 = 1{,}890 \text{ N } (424 \text{ lbs}) \tag{13}$$

Soft Bearings

Figure 21 illustrates the synchronous bearing reactions for a 50% reduction in the nominal bearing stiffnesses. The critical speeds within the operating range are now located at 14,000, 31,000 and 35,500 rpm as compared to 14,450, 31,160 and 36,600 rpm for the nominal-bearing-stiffness results. Peak bearing reactions occur at 31,000 rpm and are

$$R_1 = 1{,}085 \text{ N } (244 \text{ lbs}), \quad R_2 = 1{,}370 \text{ N } (308 \text{ lbs})$$
$$R_3 = \phantom{1{,}}712 \text{ N } (160 \text{ lbs}), \quad R_4 = \phantom{1{,}}912 \text{ N } (205 \text{ lbs}) \tag{14}$$

The bearing reactions are reduced by approximately a factor of 2.0 due to a 50% reduction in bearing stiffnesses.

The predicted OSI is 59,945 rpm with a whirl frequency of 361 Hz. At FPL the mode which is eventually predicted to become unstable has 3.46 % of critical damping.

Stiff Bearings

Figure 22 illustrates the synchronous bearing reactions associated with a 150% increase in bearing stiffnesses. The rotor-housing critical speeds are now located at 15,040, 31,900, 33,900 and 38,100 rpm. Peak bearing reactions occur for bearings 1 and 2 at 31,900 rpm, while peak bearing reactions occur at 33,900 rpm for bearings 3 and 4. At 31,900 rpm the bearing reactions are

$$R_1 = 2335 \text{ N } (525 \text{ lbs}), \quad R_2 = 3090 \text{ N } (695 \text{ lbs})$$
$$R_3 = 1050 \text{ N } (237 \text{ lbs}), \quad R_4 = 1610 \text{ N } (361 \text{ lbs}) \tag{15}$$

while at 33,900 rpm they are

$$R_1 = 1590 \text{ N } (358 \text{ lbs}), \quad R_2 = 1730 \text{ N } (387 \text{ lbs})$$
$$R_3 = 1580 \text{ N } (355 \text{ lbs}), \quad R_4 = 1780 \text{ N } (400 \text{ lbs}) \tag{16}$$

By comparison to Eq.(13), the peak bearing reactions occurring for the stiff bearings are comparable to those for the nominal bearing stiffnesses.

The predicted OSI is 82,740 rpm with an associated whirl frequency of 360 Hz. Increasing the bearing stiffness increases the damping factor from 3.78 to 9.74 percent of critical damping.

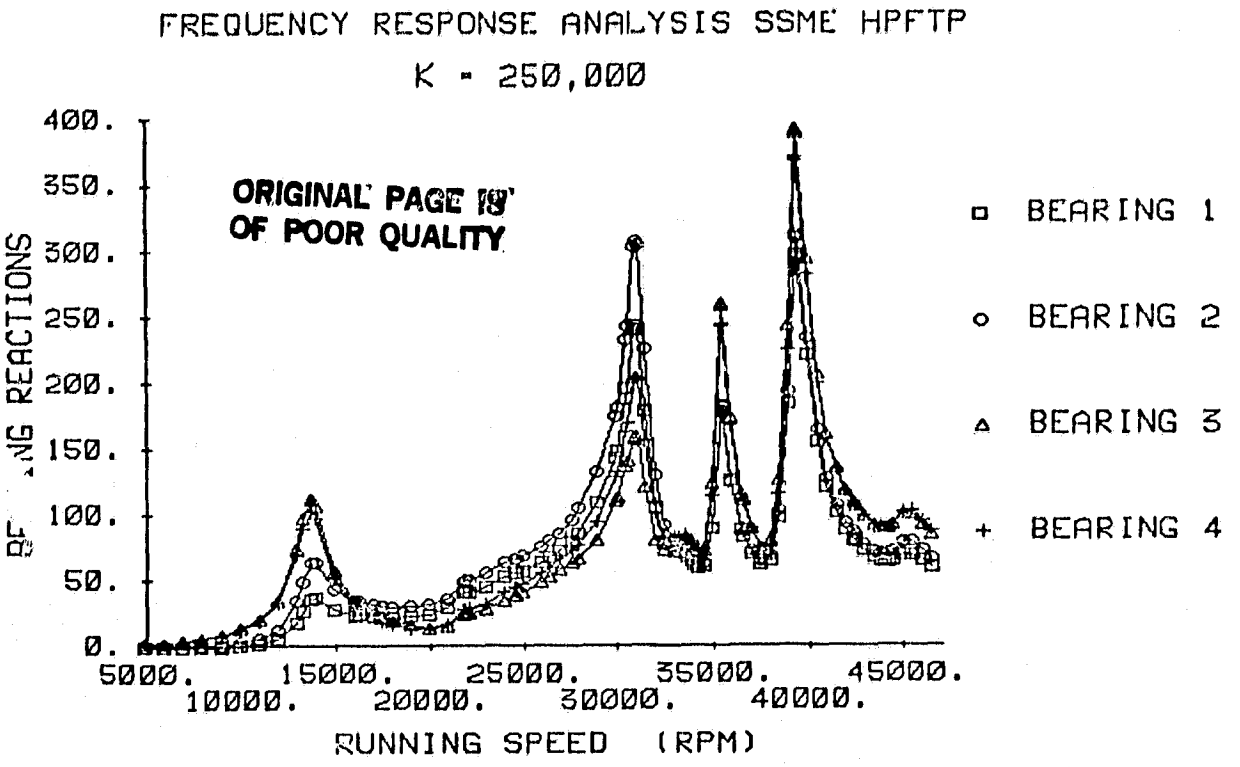

Figure 21. Synchronous response solutions for bearing reactions of the nominal HPFTP model with soft bearing stiffnesses; K_{bi} = 4.38 x 10^7 N/m (.25 x 10^6 lbs/in).

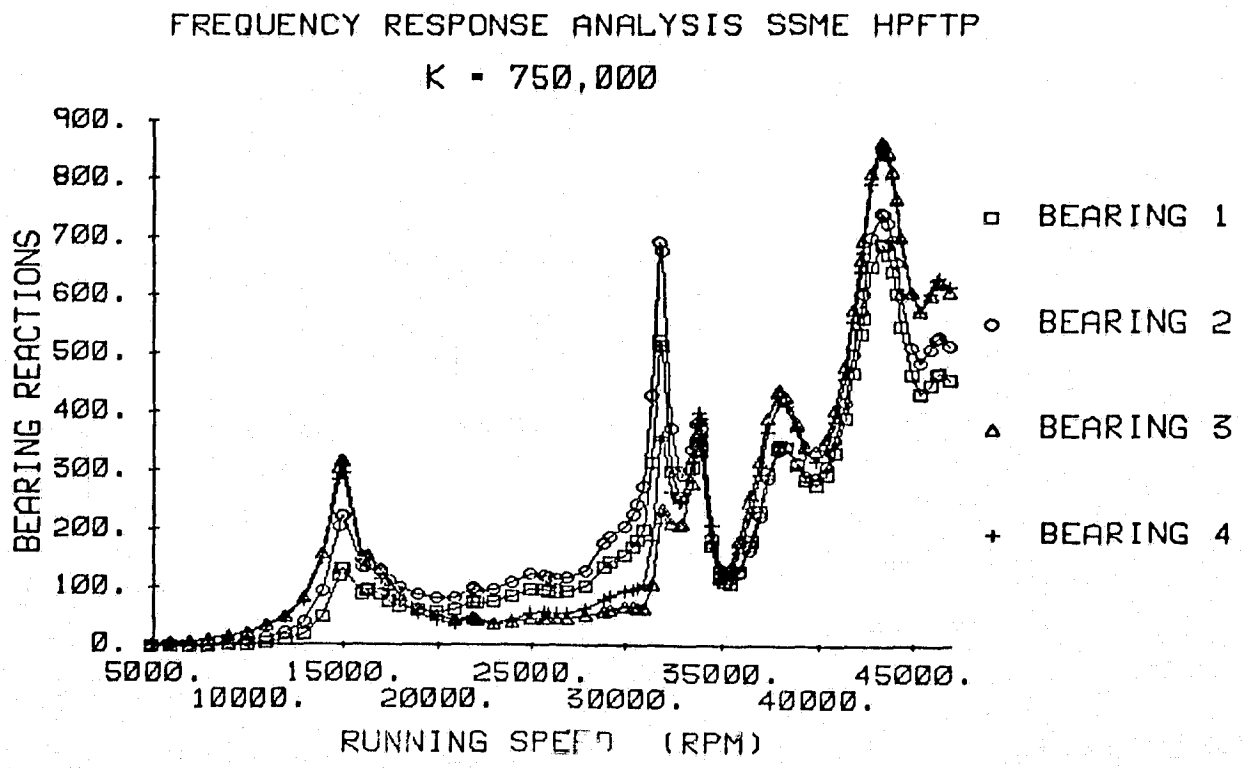

Figure 22. Synchronous response solutions for bearing reactions of the nominal HPFTP model with stiffer bearings; K_{bi} = 1.31 x 10^8 N/m (.75 x 10^6 lbs/in).

D. The Influence of Changes in Interstage Seals

Figure 23 illustrates the synchronous-response bearing reactions that result when the smooth-straight interstage seals are replaced with smooth-stepped seals. The critical speed locations are now at 14,100, 31,600, and 36,750 as compared to 14,450, 31,600, and 36,600 rpm. The following maximum bearing reactions occur at 31,600 rpm:

$$R_1 = 4130 \text{ N } (927 \text{ lbs}), \quad R_2 = 5220 \text{ N } (1170 \text{ lbs})$$
$$R_3 = 2510 \text{ N } (564 \text{ lbs}), \quad R_4 = 3374 \text{ N } (758 \text{ lbs}) \qquad (17)$$

By comparison to Eq.(13), bearing reactions 1 and 2 are increased by a factor of approximately 1.6, while bearing reactions 3 and 4 are increased by a factor of approximately 1.8. Clearly, the seal forces provide a substantial amount of damping for the mode whose critical speed occurs at 31,600 rpm. However, since the critical speed location is not shifted by a change in interstage seals, the direct-stiffness coefficients of these seals has a minimal influence on this mode.

A change to the smooth-stepped interstage seals yields the predicted onset speed of instability at 58,336 rpm with a whirl frequency of 337 Hz. At FPL, the mode which is predicted to become unstable has 2.3% of critical damping.

E. The Influence of Changes in Clearance Excitation Forces

As defined by Eq.(A.10), the clearance-excitation force coefficient is proportional to the factor β which is defined by Alford [10] to be the "change in thermodynamic coefficiency per unit of rotor displacement, expressed as a function of blade height." For unshrouded turbine blades, Alford predicts β's on the order of 1~1.5; however, Urlich's measurements [11] yield estimates on the order of 4~5.

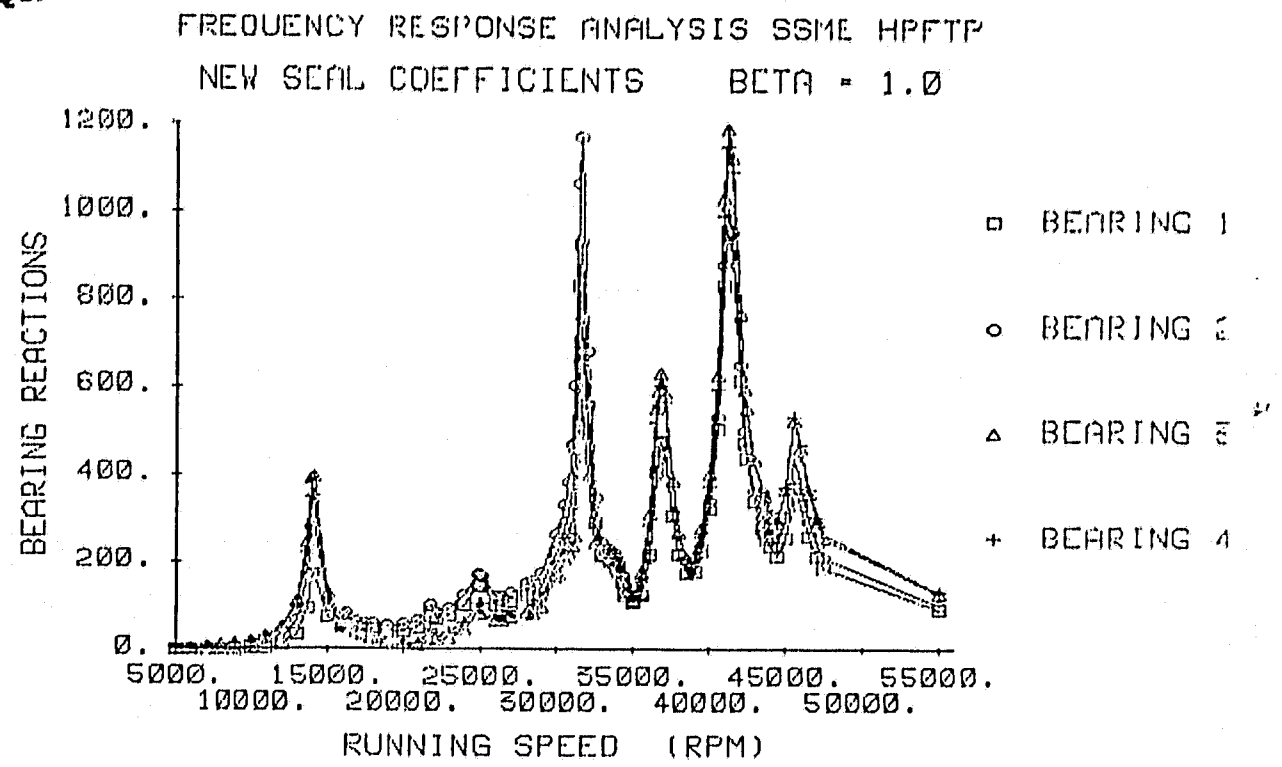

Figure 23. Synchronous response solutions for bearing reactions of the nominal HPFTP model with rotordynamic coefficients for the "smooth-stepped" seal of Table A.4(b).

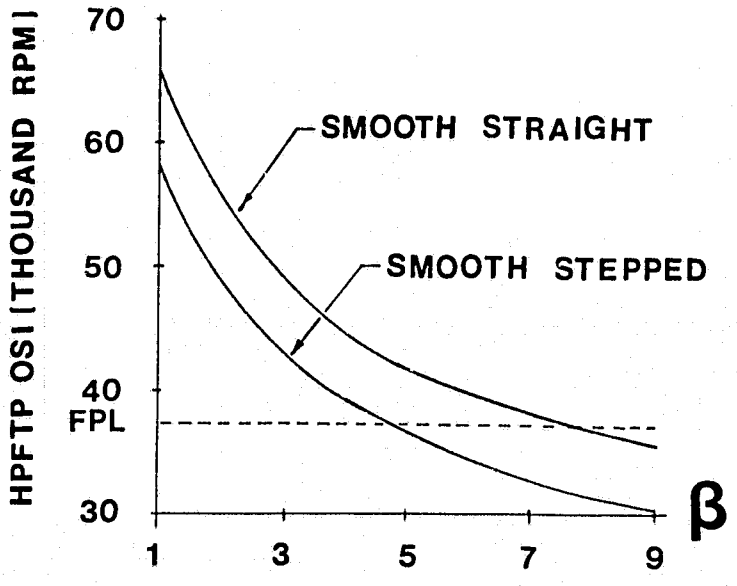

Figure 24. Onset speeds of instability for the HPFTP versus the clearance-excitation force coefficient of Eq.(A.10) for (a) smooth-straight interstage seals, and (b) smooth-stepped interstage seals.

Figure 24 illustrates the predicted OSI for the nominal model with smooth-straight and stepped-smooth seals. Values of β which are required to reduce the OSI to FPL are approximately 7.3 and 5, respectively, for the smooth-straight and smooth-stepped configurations, respectively.

F. The Influence of Changes in Impeller Diffuser Forces

The impeller cross-coupling force coefficients of Table A.6 are notably small in comparison to the direct and cross-coupled stiffness coefficients for the interstage seals which are provided in Tables 4(b) and 5(b). These coefficients are accounted for in the nominal model which yields an OSI prediction of 66,000 rpm. Removing the coefficients increases the OSI prediction to 70,590 rpm. This roughly 7% increase in OSI is not surprising in view of the comparatively small coefficients, and supports the conventional view that impeller-diffuser cross-coupling forces are negligible in the HPFTP due to the low density of hydrogen.

G. The Influence of Changes in the Turbine Interstage Seal

As noted in the preceding chapter, changing the turbine interstage seal from a stepped-labyrinth to a straight-honeycomb configuration significantly improves the stability and response characteristics of the motion associated with the first critical speed of the HPOTP. The question that arises is, "Would a comparable improvement in stability and response result for the same type of change in the HPFTP?" Figure 25 illustrates the bearing reactions which result if the HPOTP honeycomb turbine interstage coefficients are used for the HPFTP interstage. The use of HPOTP coefficients is justified based on comparable dimensions, pressure differentials, and fluid properties. No appreciable reduction in bearing reactions is predicted by the results of Figure 25. The

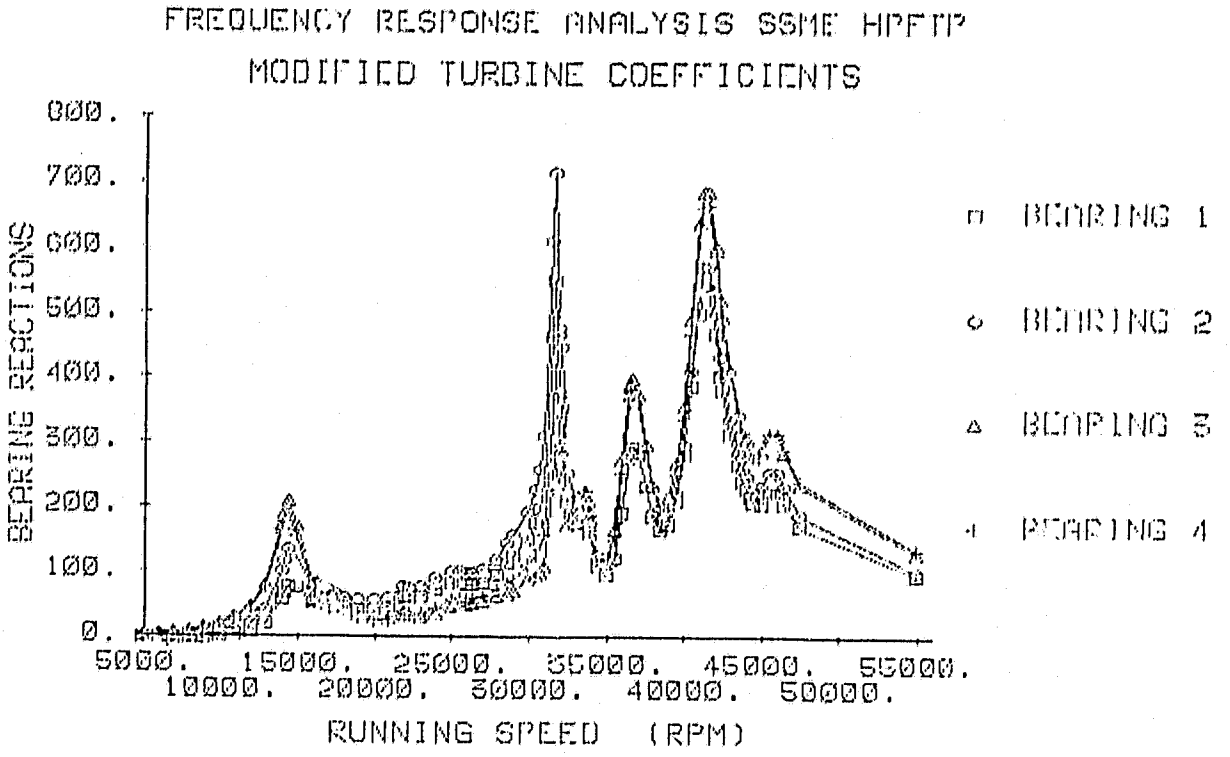

Figure 25. Synchronous response solutions for bearing reactions of the nominal HPFTP model using HPOTP rotordynamic coefficients for the turbine interstage seals.

following peak bearing reactions occur at 31,660 rpm:

$$R_1 = 2450 \text{ N } (551 \text{ lbs}), \quad R_2 = 3190 \text{ N } (717 \text{ lbs})$$
$$R_3 = 1284 \text{ N } (289 \text{ lbs}), \quad R_4 = 1850 \text{ N } (415 \text{ lbs}) \tag{18}$$

A comparison to Eq.(13) indicates a reduction in bearing reactions on the order of 2~3%.

The OSI which results for these turbine interstage seal coefficients is 87,100 rpm with an associated whirl frequency of 664 Hz. The mode which is predicted to become unstable has 2.1% of critical damping at FPL. These results represent a 32% increase in OSI as compared to the results for the nominal model. The fact that the turbine-interstage seals act basically at the same location as the clearance-excitation forces of the turbine wheels accounts for this significant improvement. Introducing the larger turbine-interstage-seal coefficients increases the percent of critical damping from 3.78% to 3.9% for the 360 Hz. mode at FPL.

H. Summary and Conclusions for the HPFTP

The current HPFTP configuration which incorporates stiff bearing supports and smooth-straight seals has a comfortable predicted margin of stability. As illustrated in Figure 24, it is able to withstand a very sizable clearance-excitation force increase without becoming unstable; hence, the initial over-riding concern for the stability of this unit has substantially been eliminated. The remaining dominant concern deals with the bearing reactions at critical speeds and at FPL (Full Power Level). Table 3 summarizes the results of this section and supports the following general conclusions:

(a) The synchronous response and OSI characteristics are sensitive to changes in bearing stiffnesses. Generally speaking, an increase in bearing stiffnesses improves the stability margin while increasing the bearing reactions. Decreasing the bearing stiffnesses decreases both the stability margin and the bearing reactions.

(b) A comparison of the results for configuration 1 (nominal model using smooth-straight interstage seals) and configuration 4 (nominal model using smooth-stepped interstage seals) demonstrates the clear superiority of the smooth-straight configuration. This superiority is valid for both stability margins and bearing reactions.

(c) The onset speed of instability is only modestly improved by removing the impeller-diffuser forces, and the bearing reactions are substantially unchanged.

(d) Changes in the turbine interstage seals from the current coefficients to those of the HPOTP turbine interstage seals (honeycomb) yields a substantial increase in the predicted OSI with a minimal change in bearing reactions.

Configuration	Frequency Results				Bearing Reaction Results (N)				
	Critical Speeds (rpm)	OSI (rpm)	Whirl Frequency (Hz.)	% Critical Damping at FPL	Reference Speed(rpm) for Calculation	Brg.1	Brg.2	Brg.3	Brg.4
1. Nominal	14,450 31,640 36,620	66,026	362	3.78	31,640 36,620 37,400	2520 1350 1080	3280 1320 1090	1300 1830 1390	1890 1740 1360
2. 50% Bearing Stiffnesses	14,000 31,000 35,500	59,945	361	3.46	31,000 35,500 37,400	1085 814 282	1370 797 293	712 1160 347	912 1090 350
3. 150% Bearing Stiffnesses	15,040 31,900 33,900 38,100	82,740	360	9.74	31,920 33,900 37,400	2335 1590 1266	3090 1730 1235	1050 1580 1684	1610 1780 1583
4. Nominal with Stepped Interstage Seals	14,100 31,600 36,600	58,336	337	2.30	31,600 36,750 37,400	4130 2130 1510	5220 2110 1520	2510 2810 1900	3374 2700 1870
5. Nominal without Impeller-Diffuser Force Coefficients	14,450 31,640 36,620	70,590	340	3.79	31,656 36,638 37,400	2401 1304 1090	3026 1296 1096	1165 1789 1405	1695 1700 1370
6. Nominal with HPOTP Turbine Interstage Seal Coefficients	14,460 31,660 36,630	87,100	664 360	2.10 3.76	31,660 36,630 37,400	2450 1300 1080	3190 1280 1088	1284 1770 1395	1850 1680 [illegible]2

Table 3. Summary of linear analysis results for HPFTP configurations.

IV. SUMMARY AND CONCLUSIONS

The present study has examined the influence of variations in forces which are known to act on rotors and influence their rotordynamic characteristics. The magnitude of variations which have been considered are based on the Task A report [1] and current estimates of force coefficients. Both the HPFTP and HPOTP units have been examined and variations in the design and dynamic characteristics of these two units have lead, in some cases, to quite different results. In general terms, the relative importance of changes in force coefficients can be summarized as follows:

Force Element	HPOTP	HPFTP
Bearing Stiffness	Very important	Very important
Clearance Excitation Force	Important for first mode	Very important as principal destabilizing element
Liquid Seals	Potentially very important if introduced in shrouded inducer	Interstage seals are very important
Gas Seals	Turbine interstage seal is very important	Potentially significant if a honeycomb seal should be introduced for the turbine interstage seal
Impeller-Diffuser Force	Very important for second mode instability	Minimal importance
Bearing "Dead-band" Clearances	Very important	Moderately important

These results are consistent with earlier studies and reveal no "new" force element or new action of an old force element. The absence of a "new" finding is not surprising in view of (a) the past extensive studies which have been carried out on both the HPFTP and HPOTP, and (b) the nature of the study which has first established reasonable variations in the parameters of known force elements and then examined the influence of these parameter changes. The author feels that a great deal of uncertainty remains concerning the identity of "new" elements which may have a significant influence on the rotordynamics of turbomachinery. For example, the inducers of the HPOTP main impeller probably have a significant influence on rotordynamic characteristics, but no test data are available to quantify or describe the forces developed by these elements. The forces developed by the fluid in the annuli at bearing clearances represents a potentially significant source of damping in turbopumps. Again, no test data are available to estimate or bracket the forces developed by these elements. Additional insight concerning the influence of these and other force elements awaits additional test data.

V. REFERENCES

1. D.W. Childs, "Definition of Forces on Turbomachinery Rotors - Task A Report," Turbomachinery Laboratories, Mechanical Engineering Department, Texas A&M University, February 1983.

2. D.W. Childs, "The Space Shuttle Main Engine High-Pressure Fuel Turbopump Rotordynamic Instability Problem," ASME Trans. J. of Engineering for Power, pp. 48-57, January 1978.

3. D.W. Childs, "Rotordynamics Analysis for the HPOTP (High Pressure Oxygen Turbopump) of the SSME (Space Shuttle Main Engine)," an Interim Progress Report for NASA Contract NAS8-31233, Speed Scientific School, The University of Louisville, Louisville, Ky., 15 September 1979.

4. D.W. Childs, "Rotordynamics Analysis for the HPFTP (High Pressure Fuel Turbopump) of the SSME (Space Shuttle Main Engine)," an Interim Progress Report for NASA Contract NAS8-31233, Speed Scientific School, The University of Louisville, Louisville, Ky., 30 July 1980.

5. B. Jery and R. Franz, "Stiffness Matrices for the Rocketdyne Diffuser Volute," Report No. E249.1, California Institute of Technology, October 1982.

6. D.S. Chamieh, A.J. Acosta, C.E. Brennen, T.K. Caughey, and R. Franz, "Experimental Measurements of Hydrodynamic Stiffness Matrices for a Centrifugal Pump Impeller," Proceedings, Rotordynamic Instability Problems in High-Performance Turbomachinery--1982, NASA Conference 2250, pp. 382-398, 1982.

7. L. Hauck, "Measurement and Evaluation of Swirl-Type Flow in Labyrinth Seals of Conventional Turbine Stages," NASA Conference Publication 2250, Proceedings, 2nd "Workshop on Rotordynamic Instability Problems in Turbomachinery," pp.242-259, May 1982.

8. T. Yamamoto, "On the Critical Speeds of a Shaft," Memoirs of the Faculty of Engineering, Nagoga University, Vol. 6, No. 2, 1954.

9. D.W. Childs, "SSME HPFTP Interstage Seals: Analysis and Experiments for Leakage and Reaction-Force Coefficients," Progress Report-NASA Contract NAS8-33716, Turbomachinery Laboratories Report, Texas A&M University, SEAL-1-83, February 1983.

10. J. Alford, "Protecting Turbomachinery from Self-Excited Rotor Whirl, ASME Trans. J. of Engineering for Power, pp.333-334, October 1965.

11. K. Urlichs, "Die Spaltstrommüng bei Therimischen Turbo-Machinen als Ursache für die Enstehung Schwingungsanfacher Querkrafte," Ingenieur Archic, Vol. 45, No. 3, 1976, pp. 195-208, also available in English Translation, "Leakage Flow in Thermal Turbo-Machines as the Origin of Vibration-Exciting Lateral Forces," NASA-TT-1709, March 1977.

12. Y. Yamada, "Resistance of Flow through an Annulus with an Inner Rotating Cylinder," Bull. J. S. ME, Vol.5, No. 18, pp.302-310, 1962.

13. P.E. Allaire, C.C. Lee, and E.J. Gunter, "Dynamics of Short Eccentric Plain Seals with High Axial Reynolds Number," AIAA J. Spacecraft and Rockets, Vol. 15, No. 6, pp. 341-347, December 1978.

14. C.F. Colebrook, "Turbulent Flow in Pipes with Particular Reference to the Transition Region between the Smooth and Rough Pipe Laws," J. of the Institute of Civil Engineering, (London), Vol. 11, pp.133-156, 1938-1939.

15. D.W. Childs, "Finite-Length Solutions for Rotordynamic Coefficients of Turbulent Annular Seals," ASME Paper 82-Lub-42, ASME-ASLE Joint Lubrication Conference, October 1982.

16. D.W. Childs, "Dynamic Analysis of Turbulent Annular Seals Based on Hirs' Lubrication Equation," ASME Paper 82-Lub-41, ASME-ASLE Joint Lubrication Conference, October 1982.

17. D.P. Fleming, "Stiffness of Straight and Tapered Annular Gas Seals," ASME Paper No. 78-Lub-18, ASME-ASLE Joint Lubrication Conference, Minneapolis, Minn., 24-26 October 1978.

18. D.P. Fleming, "Damping in Ring Seals for Compressible Fluids," NASA-CP-2133, Rotordynamic Instability Problems in High-Performance Turbomachinery, Proceedings of a Workshop held at Texas A&M University, pp. 169-188, 12-14 May 1980.

19. W. Chen, "SSME HPOTP Preburner Pump Impeller Front Seal Performance," Rocketdyne Internal Letter, RIH-2173-4333.

20. L. Hauck, "Measurement and Evaluation of Swirl-Type Flow in Labyrinth Seals," 2nd Workshop on Rotordynamic Instability Problems in High Performance Turbomachinery, held at Texas A&M University; College Station, Texas, 10-12 May 1982.

21. S. Winder, "Data Input HPOTP Computer Simulation Model," ED14-05-78, NASA MSFC, 17 February 1978.

APPENDIX A

INPUT DATA FOR THE HPFTP ROTORDYNAMICS MODEL

The fixed data used to define the HPFTP rotordynamics model are provided in this appendix. SI units are used throughout.

Rotor Eigenvalues

The rotor eigenvalues and eigenvectors used here are based on a structural-dynamic model by B. Rowan. The free-free eigenvalues used are listed below:

$\lambda_1 = 0$ $\qquad$ $\lambda_5 = 2048.6$ Hz

$\lambda_2 = 0$ $\qquad$ $\lambda_6 = 2622.7$ Hz

$\lambda_3 = 632.72$ Hz $\qquad$ $\lambda_7 = 3155.4$ Hz

$\lambda_4 = 1397.2$ Hz $\qquad$ $\lambda_8 = 3784.7$ Hz

One-half percent of critical damping was used for all bending modes.

Case Eigenvalues and Damping Factors

The case eigenvalues and eigenvectors are based on a 1980 MSFC structural dynamic model. The eigenvalues used in this study are:

$\lambda_{c1} = 271.04$ Hz $\qquad$ $\lambda_{c6} = 561.79$ Hz

$\lambda_{c2} = 370.11$ Hz $\qquad$ $\lambda_{c7} = 564.99$ Hz

$\lambda_{c3} = 440.28$ Hz $\qquad$ $\lambda_{c8} = 609.84$ Hz

$\lambda_{c4} = 500.54$ Hz $\qquad$ $\lambda_{c9} = 706.10$ Hz

$\lambda_{c5} = 512.59$ Hz $\qquad$ $\lambda_{c10} = 730.64$ Hz

One-half percent of critical damping was used for all modes.

Seal Rotordynamic Coefficients

Stepped-Seal Configuration

The only seals of importance to the rotordynamic response of the HPFTP are the interstage seals. The original flight configuration used a "stepped" configuration consisting of three annular segments separated by two steps. The steps introduce a radius reduction in the direction of flow. The seal segment dimensions consisting of radius, length, and radial clearance are listed below:

i	R_i(cm)	L_i(cm)	C_{ri}(mm)
1	4.039	1.199	.2667
2	3.988	1.219	.2159
3	3.937	1.438	.1778

Table A.1 Dimensions of "stepped" HPFTP interstage seal.

Seal coefficients are to be calculated for FPL, RPL, and MPL conditions defined by the following data:

	ω(rpm)	ΔP(bar)	ρ(Kg/m^3)	μ(Ns/m^2)
FPL	37,360	136.5	70.9	1.1623×10^{-5}
RPL	35,014	119.9	69.2	1.1012×10^{-5}
MPL	23,710	56.0	53.0	0.7560×10^{-5}

Table A.2 HPFTP seal operating conditions and fluid properties.

Seal leakage depends on the entrance-loss coefficients at each step and the wall friction along each annular segment. Yamada's formula [12] for seal leakage can be stated

$$\Delta P = \frac{\rho V^2}{2} (1 + \xi + 2\sigma) \qquad (A.1)$$

where ΔP is the pressure differential, ρ is the density, and V is the leakage velocity. The quantity $(1 + \xi)$ accounts for an inlet pressure drop due to (a) the acceleration of the fluid from a velocity near zero to V, and (b) additional entrance losses within the seal until a fully-developed flow field is established. The term $\sigma\rho V^2$ is the pressure drop due to wall friction, where σ is defined in terms of the friction factor, length, and radial clearance by

$$\sigma = \lambda L/C \tag{A.2}$$

Yamada's definition for λ is

$$\lambda = no\ R_{ao}^{mo}[1 + (R_{co}/R_{ao})^2]^{\frac{1+mo}{2}} \tag{A.3}$$

where no and mo are empirical constants, and (R_{ao},R_{co}) are the nominal axial and circumferential Reynolds numbers defined by

$$R_{ao} = \frac{2CV\rho}{\mu} \quad , \quad R_{co} = \frac{CR\omega\rho}{\mu} \tag{A.4}$$

The constants (mo,no) depend on the surface roughness of the particular seal of interest. Yamada's test results yielded the numbers mo = 0.079, no = -0.25. The friction-factor formula employed by Allaire et al. [13] directly accounts for changes in surface roughness. Their formulas are adopted from Colebrook's rough-pipe formula [14] and provide the following definition for the friction factor

$$\begin{aligned} 4\lambda &= a + bR_{ao}^{-c} \\ a &= 0.094\delta^{0.225} + 0.53\delta \\ b &= 88\delta^{0.44} \\ c &= 1.62\delta^{0.134} \end{aligned} \tag{A.5}$$

where δ is the relative roughness, and is defined in terms of the surface roughness ε and the radial clearance C_r by

$$\delta = \varepsilon/C_r \qquad (A.6)$$

Measured test results at TAMU (Texas A&M University) [9] under contract NAS8-33716 yielded the following values for the stepped-seal entrance-loss and relative roughness coefficients:

i	ξ_i	δ_i
1	0.129	$.309 \times 10^{-9}$
2	-0.566	$.309 \times 10^{-9}$
3	-0.538	$.309 \times 10^{-9}$

Table A.3 Entrance loss and relative-roughness coefficients for stepped seal.

These numbers were obtained form static zero-eccentricity flow data, and yield reasonable correlation with leakage-ΔP results.

The seal rotordynamic-coefficient model used in current seal analyses are

$$-\begin{Bmatrix} F_X \\ F_Y \end{Bmatrix} = \begin{bmatrix} K & k \\ -k & K \end{bmatrix} \begin{Bmatrix} X \\ Y \end{Bmatrix} + \begin{bmatrix} C & c \\ -c & C \end{bmatrix} \begin{Bmatrix} \dot{X} \\ \dot{Y} \end{Bmatrix} + \begin{bmatrix} M & m \\ -m & M \end{bmatrix} \begin{Bmatrix} \ddot{X} \\ \ddot{Y} \end{Bmatrix} \qquad (A.7)$$

where (X,Y) are the components of the seal displacement vector, and (F_X, F_Y) are the reaction-force components.

Calculated coefficients for the stepped-seal configuration are provided below:

	FPL	RPL	MPL
K	$.2193 \times 10^8$	$.1927 \times 10^8$	$.9014 \times 10^7$
k	$.1863 \times 10^7$	$.1617 \times 10^7$	$.6522 \times 10^6$
C	3675.	3395.	2001.
c	12.22	10.34	.8538
M	-.01853	-.01809	-.01465
m	-.02928	-.02818	-.01873

Table A.4(a) Calculated dynamic seal coefficients for HPFTP stepped interstage seals; v_o = -0.5 initial swirl.

These results are based on an improved short-seal solution by Childs [15], and use a summation of the segment coefficients.

The TAMU test program measures radial and tangential force components on an eccentrically-precessing seal. The test results show reasonable agreement between theory and prediction for the phase angle between the radial and tangential components; however, measured force amplitudes are approximately twice as large as predictions. Hence, the nominal seal coefficients used in the present study are obtained by doubling the coefficients of Table 4(a) to obtain the following results.

	FPL	RPL	MPL
K	$.4386 \times 10^8$	$.3854 \times 10^8$	$.1803 \times 10^8$
k	$.3726 \times 10^7$	$.3234 \times 10^7$	$.1304 \times 10^7$
C	7350.	6790.	4002.

Table A.4(b) Nominal dynamic seal coefficients for HPFTP stepped interstage seals; v_o = -0.5 initial swirl.

Straight Seal Configuration

The dimensions for the constant-clearance seal which replaced the stepped seal are

$$R = 4.039\text{cm} \quad , \quad L = 4.57\text{cm} \quad , \quad C_r = .2184\text{mm}$$

Using the entrance-loss coefficient $\xi = 0.1$ and the data of Table 2 yields the calculated predictions

	FPL	RPL	MPL
K	$.6883 \times 10^8$	$.6046 \times 10^8$	$.2772 \times 10^8$
k	$.8568 \times 10^7$	$.7452 \times 10^7$	$.3029 \times 10^7$
C	16,310	15,080	8,866
c	370.3	338.7	174.2
M	.3390	.3313	.2548
m	-.0370	-.0353	-.0226

Table A.5(a) Calculated rotordynamic seal coefficients for HPFTP constant-clearance interstage seals; v_o = -0.5 initial swirl.

These results are based on an improved short-seal solution by Childs [15]. Experience has shown that k and C are reasonably well predicted by the theory but that K is underpredicted by approximately 20%. Hence, the nominal seal parameters used in this study are given in Table 5(b).

	FPL	RPL	MPL
K	$.7021 \times 10^8$	$.6167 \times 10^8$	$.2827 \times 10^8$
k	$.8568 \times 10^7$	$.7452 \times 10^7$	$.3029 \times 10^7$
C	16,310	15, 080	8,866

Table A.5(b) Nominal rotordynamic seal coefficients for HPFTP constant-clearance interstage seals; v_o = -0.5 initial swirl.

Impeller-Diffuser Forces

Jery et al. [5] have reported the results of force measurments on impellers in volutes, and have also recently conducted tests on impeller forces within vaned diffusers. Their tests yield the following nondimensional model for impeller-diffuser forces

$$-\frac{1}{\rho A_2 V_2^2}\begin{Bmatrix}F_X\\F_y\end{Bmatrix}=\begin{bmatrix}K^* & k^*\\-k^* & K^*\end{bmatrix}\begin{Bmatrix}X/R_2\\Y/R_2\end{Bmatrix}=\begin{bmatrix}-2.0 & 0.7\\-0.7 & -2.0\end{bmatrix}\begin{Bmatrix}X/R_2\\Y/R_2\end{Bmatrix} \qquad (A.8)$$

where R_2 is the impeller radius, ρ is the fluid density, $V_2 = R_2\omega$ is the impeller tip velocity and $A_2 = 2\pi R_2 b_2$ is the exit flow area. Note that the direct-stiffness coefficient in Eq.(A.8) is negative, i.e., the impeller-diffuser force causes a net loss in system stiffness. From Eq.(A.8), the dimensional impeller-diffuser coefficients are defined by

$$\overline{K} = K^*\frac{\rho A_2 V_2^2}{2R_2} = K^*(\pi\rho b_2 R_2^2)\omega^2$$

$$\overline{k} = k^*(\pi\rho b_2 R_2^2)\omega^2 \qquad (A.9)$$

The dimensions of the HPFTP main impellers are

$R_2 = 14.99\text{cm}$, $b_2 = 1.27\text{cm}$

The density and calculated coefficients for the HPFTP impellers are given below:

	FPL	RPL	MPL
RPM	37,361	35,014	23,710
ρ	75.3	72.1	64.1
$\overline{K}$	$-.2055 \times 10^8$	$-.1735 \times 10^8$	$-.7073 \times 10^8$
$\overline{k}$	$.7222 \times 10^7$	$.6073 \times 10^7$	$.2476 \times 10^7$

Table A.6 Impeller-diffuser force coefficients for HPFTP impellers.

By comparison to Tables 4(b) and 5(b), $|\overline{K}|$ is approximately 5% and 3%, respectively, of the stepped and constant-clearance predictions for the direct stiffness coefficient K. Further, $\overline{k}$ is approximately 20% and 8%, respectively, of the stepped and constant-clearance predictions for the cross-coupled stiffness coefficient k.

Clearance-Excitation Forces

Clearance-excitation forces are developed at turbines due to the dependency of local efficiency on local clearances. This destabilizing force is modeled by

$$\begin{Bmatrix} F_X \\ F_Y \end{Bmatrix} = \begin{bmatrix} 0 & k_T \\ -k_T & 0 \end{bmatrix} \begin{Bmatrix} X \\ Y \end{Bmatrix} \quad ; \quad k_T = \frac{\beta T}{D_p H} \qquad (A.10)$$

where T is the turbine torque, D_p is the average pitch diameter of the turbine blades, H is the average height, and β is the "change of thermodynamic efficiency per unit of rotor displacement, expressed as a function of blade height." Alford [10] states that β is on the order of 1~1.5, while Urlich's measurments [11] yield estimates on the order of 4~5.

The dimensions of the HPFTP turbines are

$$D_p = 25.8\text{cm} \quad , \quad H = 2.217\text{cm}$$

The torque and clearance-excitation coefficient (β=1) are listed below:

	ω(rpm)	T(N/m) x 10^{-4}	k_T(N/m) x 10^{-6}
FPL	37,361	1.456	2.544
RPL	35,015	1.266	2.212
MPL	23,710	.5123	0.8954

Table A.7 Combined clearance-excitation coefficients for both HPFTP turbine stages with β = 1.

Balance-Piston Stiffness and Damping Coefficients

The balance-piston stiffness and damping coefficients are

$$KZ = 4.553 \times 10^8 \text{ N/m}$$

$$CZ = 7.882 \times 10^4 \text{ N/m}$$

Bearing & Bearing Carrier Stiffness

The following nominal bearing stiffness is used for all bearings

$$K_b = 8.756 \times 10^7 \text{ N/m}$$

The bearing support stiffness used is

$$K_s = 4.640 \times 10^8 \text{ N/m}$$

APPENDIX B

DATA INPUT FOR THE HPOTP ROTORDYNAMICS MODEL

The fixed data used to define the HPOTP rotordynamics model are provided in this appendix. Explanations for the parameters and models are provided in Appendix A.

Rotor Eigenvalues

The rotor eigenvalues and eigenvectors used here are based on a model by B. Rowan. The free-free eigenvalues used are listed below.

$\lambda_1 = 0$	$\lambda_7 = 3723.6$ Hz
$\lambda_2 = 0$	$\lambda_8 = 4388.7$ Hz
$\lambda_3 = 426.2$ Hz	$\lambda_9 = 6599.5$ Hz
$\lambda_4 = 969.6$ Hz	$\lambda_{10} = 7396.7$ Hz
$\lambda_5 = 1560.9$ Hz	$\lambda_{11} = 10396.0$ Hz
$\lambda_6 = 2698.0$ Hz	$\lambda_{12} = 11916.0$ Hz

One-half percent of critical damping was used for modes three through twelve. Zero damping was used for modes 1 and 2.

Case Eigenvalues and Damping Factors

The case eigenvalues and eigenvectors are based on a 1982 Rocketdyne structural-dynamic model. The eigenvalues used in the study are

$\lambda_{c1} = 45.21$ Hz	$\lambda_{c6} = 351.35$ Hz
$\lambda_{c2} = 85.67$ Hz	$\lambda_{c7} = 431.90$ Hz
$\lambda_{c3} = 111.47$ Hz	$\lambda_{c8} = 468.48$ Hz
$\lambda_{c4} = 300.52$ Hz	$\lambda_{c9} = 487.91$ Hz
$\lambda_{c5} = 310.11$ Hz	$\lambda_{c10} = 542.45$ Hz

One-half percent of critical damping was used for all housing modes.

Seal Rotordynamic Coefficients

Nominal seal rotordynamic coefficients at FPL and MPL are given in Tables B.1(a) and (b). These coefficients were calculated by Rocketdyne personnel in 1977. Experience has shown that the high pressure turbine seal and the turbine interstage seals are important in the current configuration. Forces developed at the remaining seals are comparatively small. Both of the "important" seals in the current configuration are gas seals, sealing hydrogen-rich steam. The Mach number in the turbine interstage seal is on the order of 0.3, and incompressible analyses [15,16] are appropriate. However, flow in the high pressure turbine seal is choked, and Fleming's analyses [17,18] must be used. The numbers used for the convergent-tapered seal with anti-vortex seals were calculated by W. Chen at Rocketdyne, and correspond to entry and exit clearances of .38/.25 mm (.015/.010 in) with an assumed inlet tangential velocity that is (Rω/2)/4, i.e., one fourth of the predicted asymptotic velocity within the seal.

Table B.1(a) Calculated seal stiffness and damping coefficients at FPL; ω = 30,965 rpm.

	K	k	C	c
Preburner Wear Ring	4.574×10^5	3.080×10^5	190.0	1.014
Preburner Discharge	4.849×10^6	2.650×10^6	1634.0	22.96
High Pressure Turbine	3.714×10^7	7.984×10^5	492.4	1.243
Second Stage Turbine Tip Seal	1.087×10^6	8.341×10^5	514.5	15.71
Turbine I.S. (Original)	6.765×10^6	3.038×10^6	1507.0	35.86
First Stage Turbine Tip Seal	1.005×10^6	8.124×10^5	501.0	16.27
Turbine I.S. (Convergent taper with anti-vortex ribs)	1.583×10^7	1.707×10^6	1400.0	

Table B.1(b) Calculated seal stiffness and damping coefficients at MPL; ω = 19,841 rpm.

	K	k	C	c
Preburner Wear Ring	2.112×10^5	1.296×10^5	124.7	.7765
Preburner Discharge	1.750×10^5	9.582×10^5	922.5	11.10
High Pressure Turbine	1.418×10^6	2.052×10^5	197.5	.3341
Second Stage Turbine Tip Seal	2.541×10^5	1.360×10^5	129.2	3.898
Turbine I.S. (Original)	1.791×10^6	8.266×10^5	504.9	9.964
First Stage Turbine Tip Seal	1.396×10^5	9.954×10^4	95.81	3.557
Turbine I.S. (Convergent taper with anti-vortex ribs)	7.880×10^6	6.655×10^5	700.0	

C-2

At various times, proposals have been made to modify the current grooved and stepped preburner-discharge seal by one of the following two procedures:

(a) remove the grooves yielding a "smooth-stepped": configuration, or

(b) remove both the steps and the grooves yielding a smooth, constant-clearance configuration.

The dimensions for the proposed smooth-stepped seal and operating conditions are given in Tables B.2 and B.3.

i	R_i(cm)	L_i(cm)	C_{ri}(mm)
1	4.267	0.579	0.381
2	4.229	0.695	0.381
3	4.191	0.775	0.381

Table B.2 Dimensions for a proposed smooth stepped HPOTP boost-impeller discharge seal.

	ω(rpm)	ΔP(bar)	ρ(kg/m^3)	μ(Ns/m^2)
FPL	30,960	439	1068	1.4610×10^{-4}
MPL	19,841	205	1088	1.5224×10^{-4}

Table B.3 Operating conditions for preburner discharge seal.

Seal coefficients were calculated using the data of Tables 3, 9, and 10 using an improved short-seal solution [16] for $v_o = 0.0$, i.e., pre-rotated flow entering the seal. The results of these calculations are provided in Table B.4.

	FPL	MPL
K	$.6908 \times 10^7$	$.3354 \times 10^7$
k	$.6925 \times 10^7$	$.3026 \times 10^7$
C	4420.0	3002.0
c	-383.0	-246.9
M	-.1212	-.1216
m	-.0511	-.0484

Table B.4 Calculated rotordynamic coefficients for a smooth-stepped preburner discharge seal.

Based on the TAMU test results, the nominal coefficients used in the study are provided in Table B.5.

	FPL	MPL
K	1.3816×10^8	$.6708 \times 10^7$
k	1.3850×10^7	$.6052 \times 10^7$
C	8840	6004

Table B.5 Nominal rotordynamic coefficients for a smooth-stepped preburner discharge seal.

The proposed dimensions for a constant-clearance preburner discharge seal are

$L = 2.21cm$, $R = 4.267cm$, $C_r = 0.381mm$

Using the operating conditions of Table B.3, with zero inlet swirl and $\xi = 0.1$ yields the predicted coefficients of Table B.6.

	FPL	MPL
K	$.3569 \times 10^8$	$.1773 \times 10^8$
k	$.3125 \times 10^8$	$.1352 \times 10^8$
C	19,620	13,216
c	21.41	56.94
M	-2.337×10^{-4}	.02163
m	-0.1188	-.10671

Table B.6 Calculated rotordynamic coefficients for a smooth constant-clearance preburner discharge seal.

Based on the TAMU test experience, the nominal seal coefficients used in this study are provided in Table B.7.

	FPL	MPL
K	$.4283 \times 10^8$	$.2127 \times 10^8$
k	$.3750 \times 10^8$	$.1622 \times 10^8$
C	23,540	15,859

Table B.7 Nominal rotordynamic coefficients for a smooth, constant-clearance preburner pump discharge seal.

Recently, a proposal has been made to change the HPOTP boost-impeller inlet wear-ring seal from a stepped labyrinth configuration to a "damper" seal configuration employing a surface-roughened stator and a smooth rotor. This proposed seal has the dimensions

$$L = 1.27 \text{ cm}, \quad D = 7.34 \text{ cm}, \quad L/D = 0.173$$

The clearance depends on the running speed as follows

	C_r	C_r/R
FPL	.127 mm	3.46×10^{-3}
RPL	.152 mm	4.14×10^{-3}

For specified surface-roughness magnitudes of .203 μm and 20.3 μm for the rotor and housing, respectively, W. Chen [19] has made the following predictions for the seal dynamic coefficients

	K N/m	k N/m	C Nsec/m	c Nsec/m
FPL	$.220 \times 10^6$	$.167 \times 10^5$	6080	317
MPL	$.957 \times 10^5$	$.616 \times 10^4$	3770	193

Table B.8 Nominal rotordynamic coefficients for a "damper" seal configuration to be used for the preburner inlet wear-ring seal.

An alternative configuration which has been proposed for this seal would use the same geometry with a smooth stator. For this configuration, W. Chen [19] predicts the following seal coefficients.

	K	k	C	c
	N/m	N/m	Nsec/m	Nsec/m
FPL	$.268 \times 10^7$	$.173 \times 10^6$	10,900	2510
MPL	$.108 \times 10^7$	$.710 \times 10^5$	6,680	1500

Table B.9 Nominal rotordynamic coefficients for a smooth seal configuration to be used for the preburner inlet wear-ring seal.

The proposal has been made to replace the current unshrouded inducers for the main impeller with shrouded inducers. Calculated coefficients for the sealing, surfaces formed at the outside of the shrouded inducers are provided in Table B.10.

	K	k	C
	N/m	N/m	Nsec/m
FPL	2.70×10^7	2.88×10^7	2.91×10^4
MPL	1.09×10^7	1.14×10^7	1.72×10^4

Table B.10 Nominal rotordynamic coefficients for shrouded-inducer seals.

Impeller-Diffuser Forces

The model of Eq.(A.8) is used to define impeller-diffuser forces for the main and boost impellers. The dimensions of the two impellers are provided below:

Main Impeller: $R_2 = 8.51cm$, $b_2 = 2.54cm$

Boost Impeller: $R_2 = 6.60cm$, $b_2 = 0.686cm$

The impeller-diffuser coefficients for the two impellers are provided in Table B.11.

	Main Impeller		Boost Impeller	
	FPL	MPL	FPL	MPL
ω	30,960	19,841	30,960	19,841
ρ	1,137	1,137	1,114	1,109
$\overline{K}$	-1.381×10^7	-4.833×10^6	-2.200×10^6	-9.002×10^5
$\overline{k}$	5.670×10^6	1.984×10^6	9.034×10^5	3.150×10^5

Table B.11 Impeller-diffuser coefficients for the HPOTP main and boost impellers.

Clearance-Excitation Forces

The dimensions of the HPOTP turbines are

D_p = 24.3cm , H = 1.26cm

The torque and clearance-excitation coefficient (β = 1) are listed below.

	ω(rpm)	T(Nm)	k_T(N/m) x 10^{-6}
FPL	30,960	7,005	2.2870
MPL	19,841	2,803	.9155

Table B.12 Combined clearance-excitation coefficients for both HPOTP turbine stages with β = 1.

Measured values for β in shrouded turbine blades have yielded values on the order of 0.6, [20].

Balance-Piston Stiffness and Damping Coefficients

The balance-piston stiffness is modeled by the quadratic

$$K_Z = -431.97\ \omega + .3542\ \omega^2$$

where ω is the rotor running speed. However, K_Z is never allowed to fall below 200,000 lbs/in. The equation above fits Winder's graphical data [21]. Balance piston damping is held at 15% of critical for all speeds.

Hydrodynamic Side Loads

The hydrodynamic side loads used in this study were assumed to be proportional to speed squared. The proportionality constants employed are listed below.

	K(X-Z)	K(Y-Z)
Boost Impeller	-1.248×10^{-4}	2.200×10^{-5}
Main Impeller	3.243×10^{-4}	-2.721×10^{-4}
Turbine	0	1.058×10^{-4}

Local Case Stiffnesses

The local case stiffnesses at the bearings used in this study are

$$K_{c1} = 3.502 \times 10^8 \text{ N/m}$$
$$K_{c2} = 3.502 \times 10^8 \text{ N/m}$$
$$K_{c3} = 7.002 \times 10^8 \text{ N/m}$$
$$K_{c4} = 7.002 \times 10^8 \text{ N/m}$$

Bearing Stiffness and Damping

Nominal values for the bearing stiffness and damping coefficients are

$$K_b = 8.756 \times 10^7 \text{ N/m}$$

$$C_b = 0$$